Self-assembled liquid-gated Zinc oxide nanowire transistors: fabrication and sensing operation

THÈSE (2011)

PRÉSENTÉE A LA FACULTE SCIENCES DE BASE

Institut de physique des nanostructures

SECTION DE PHYSIQUE

ÈCOLE POLYTECHNIQUE FÉDÉRALE DE LAUSANNE

POUR L'OBTENTION DU GRADE DE DOCTEUR ÈS SCIENCES

PAR

Vivek Pachauri

M. Sc. Chemistry, Dr. B. R. Ambedkar University Agra, India

et de nationalité indienne

Acceptée sur proposition du jury:

Prof. Nadine Baluc (président)

Prof. Klaus Kern, (directeur)

Prof. Francesco Stellacci (rapporteur)

Prof. Alf Mews (rapporteur)

Prof. Alexander Bittner (rapporteur)

Lausanne EPFL

“ असतो मा सद्गमय, तमसो मा ज्योतिर्गमय, मृत्योर्मामृतं गमय ”

Contents

Abstract

This thesis aims at the site-specific realization of self-assembled field-effect transistors (FETs) based on semiconducting Zinc oxide NWs and their application towards chemical and bio-sensing in liquid medium.

At first, a solution based growth method for hierarchical ZnO nanostructures was devised in order to achieve synthesis of high quality ZnO NWs. This solution based growth method was then deployed for the growth of NWs from preferred sites on a substrate. In order to make a transistor, microelectrode pairs prewritten on a Si/SiO_2 chip (4mm×4mm) using standard photolithography procedure served as growth sites and also formed source and drain terminals. The NWs bridging these 'source' and 'drain' electrodes formed the transistor channel. The procedure here yields ZnO NWs in up to 100 percent of the positions available for growth.

The site-specific self-assembled fabrication of ZnO NW FETs was evaluated in terms of scalability and applications. The procedure was extended from 4mm×4mm silicon chips to large area silicon wafers (80mm×80mm) and flexible substrates of Kapton polyimide of the same size. On the large area substrates this procedure yields ZnO NWs in up to 80 percent of the positions available for growth, which can be bettered. Furthermore, the method was also employed to fabricate ZnO NW FETs in situ in a microfluidic channel. For this purpose the precursor solution was let to flow on to the microelectrode pairs with the help of microfluidic channels assembled on top of the substrate. The substrate was heated locally under the microelectrode pairs to stimulate the NW growth. Thus a solution-based self-assembled fabrication of NW FETs was achieved locally inside a microfluidic channel.

Microfluidic channels were made of silicon nitride (Si_3N_4) on top of Si/SiO_2 chips and facilitated the characterization of FETs in liquid medium. Alternatively, microfluidic channels made of polydimethylsiloxane (PDMS) were used for characterization of transistor devices in liquids. In order to deploy FETs in liquids, the back-gate is replaced by a reference electrode (Ag/AgCl) and the potential is applied through a liquid surrounding the transistor channel (ZnO NW). The liquid surrounding the ZnO NW creates an electrochemical double layer (EDL) on the NW surface which in turn gives rise to the gate capacitance. The resulting gating effect can be used to modulate the NW conductance depending on the voltage applied through the liquid. The ZnO NW transistors showed a current modulation of up to 6 orders of magnitude, high field-effect mobilities (around 1.85 cm^2/Vs) and sub-threshold slopes as low as 105 mV/decade. This is the first demonstration of liquid-gated FETs using ZnO NWs.

The liquid-gated FETs are used as a basic device for further sensing trials in liquids. For this purpose, the FETs were functionalized with receptor molecules. These so called ion-selective FETs (ISFETs) were demonstrated as functional pH sensors for liquids with pH values from 6 to 10. The NWs functionalized with analyte-sensitive molecules on their surface are influenced electrically by the presence of analytes in the surrounding liquid. Any change in the amount of analyte present in the surrounding liquid is thus reflected in the electrical transport characteristics of the FET. 3-aminopropyltriethoxysilane (3-APTES) molecules were used to functionalize the ZnO NWs in order to construct the pH sensors. Subsequently, the realization of a biosensor based on ZnO NW transistors is demonstrated. Label-free direct detection of urea molecules was carried out from a solution of urea in buffer. ZnO NWs were electrochemically functionalized with the enzyme urease incorporated into an electro-polymerized polypyrrole matrix. Urease molecules act as specific receptors for urea molecules and catalyze an enzymatic reaction. This reaction causes a pH change in the vicinity of NWs, which is reflected in the field-effect characteristics of transistor.

The performance of liquid-gated ZnO NW FETs used as chemical and biological sensor can be further improved by employing a metal gate in liquid medium. This was established by fabricating liquid gated metal-semiconductor FET (MESFET) based on ZnO NWs. ZnO NWs were decorated with metal nanoparticles (NPs) by using an electrochemical deposition method. The NPs were then used as metal gate and devices were characterized by applying a gate voltage on the NPs through the liquid. The realization of metal-semiconductor gate in liquids considerably improved the field-effect characteristics of liquid-gated FETs based on ZnO NWs.

The realization of high performance liquid-gated transistors based on ZnO NWs thus constitutes a suitable platform for label-free detection of biomolecules and shows promise for future applications in chemical analysis and medical diagnostics.

Keywords: ZnO nanowire, CBD growth, hierarchical, self-assembly, liquid-gating, dielectrophoresis, electrodeposition, pH sensor, MESFET.

Zusammenfassung

Diese Doktorarbeit untersucht das ortsselektive Wachstum von selbst-organisierten Feld-Effekt Transistoren (FETs) aus halbleitenden Zinkoxid Nanodrähten und ihre Anwendung als chemischer- und biologischer-Sensor in flüssigen Medien.

Zunächst wurde eine Wachstumsmethode in Lösung für die Synthese hierarchischer ZnO Nanostrukturen entwickelt um Nanodrähte hoher Qualität zu züchten. Diese Methode wurde dann eingesetzt für das gezielte Wachstum von Nanodrähten an gewünschten stellen auf dem Substrat. Um einen Transistor herzustellen wurden Paare von Mikroelektroden auf einem Si/SiO$_2$ Substrat (4x4mm) mittels optischer Lithographie definiert. Diese dienten zum einen als Wachstumskeime für die ZnO Nanodrähte und wurden gleichzeitig als elektrische Kontakte verwendet. Die Nanodrähte welche diese „source“ und „drain“ Kontakte verbinden formen den Transistor Kanal. Dieses Verfahren erlaubt es bis zu 100% der verfügbaren Mikroelektroden auf einem Substrat zu kontaktieren.

Die ortsspezifische, selbstorganisierte Herstellung von ZnO NW FETs wurde auf ihre Skalierbarkeit und ihre Anwendungsmöglichkeiten weiter evaluiert. Das Verfahren wurde von 4x4mm auf 80x80mm Silizium-Substrate und auf flexible Kapton Polyimide Substrate derselben Größe erweitert. Auf diesen größeren Substraten fand Wachstum auf bis zu 80% aller verfügbar Elektroden statt, was prinzipiell weiter verbessert werden kann. Außerdem wurde das Verfahren für die *in situ* Herstellung von ZnO NW-FETs in Mikrofluidik Kanälen eingesetzt. Für diese Anwendung wurden die notwendigen Precursor durch Mikrofluidik-Kanäle zu den Mikroelektroden geleitet. Das Substrat wurde lokal unter den Mikroelektroden erhitzt um das Wachstum zu ermöglichen. Auf diese Weise wurde ein lösungsbasiertes Verfahren für das lokale Wachstum von selbst-organisierten ZnO NW FETs in Mikrofluidik Kanälen realisiert.

Mikrofluidik Kanäle aus Siliziumnitrid (Si$_3$N$_4$) wurden auf Si/SiO$_2$ Substrate aufgebracht und erleichterten die Charakterisierung der FETs in flüssigen Medien. Alternativ wurden Mikrofluidik-Kanäle aus Polydimethylsiloxan (PDMS) verwendet. Um die FETs in Flüssigkeiten zu verwenden wurde das Backgate durch eine Referenzelektrode (Ag/AgCl) ersetzt, so dass das Potential über das flüssige Medium an dem Transistor Kanal (ZnO

Nanodraht) angelegt werden kann. Die flüssige Umgebung um den ZnO Nanodraht erzeugt eine elektrochemische Doppelschicht (EDL) auf der Nanodrahtoberfläche welche sich wie eine Gate-Kapazität verhält. Der daraus folgende Feld-Effekt ermöglicht es die Leitfähigkeit des Nanodrahtes durch die angelegte Spannung an das flüssige Medium zu steuern. Die ZnO-Nanodrähte zeigen eine Strommodulation von mehr als 6 Größenordnungen, hohe Feld-Effekt Mobilitäten (~ 1.85 cm^2/Vs) und eine geringe Steigung unterhalb der Schwellenspannung von 105 mV/Dekade.

Die flüssig-Gate FETs wurden für weitere Sensoranwendungen in Flüssigkeiten verwendet. Dafür wurden sie mit Rezeptor Molekülen funktionalisiert. Diese sogenannten ionen selektiven FETs (ISFETs) wurden als Sensoren in einem pH Bereich von 6 bis 10 verwendet. Nanodrähte welche mit einem Analyt sensitiven Molekül auf ihrer Oberfläche funktionalisiert wurden, werden elektrisch durch diese beeinflusst. Jegliche Änderung in der Menge des umgebenden Analytes führt somit zu einer Änderung in der elektrischen Transportcharakteristik des FETs. 3-Aminopropyltriethoxysilane (3-APTES) Moleküle wurden verwendet um ZnO Nanodrähte zu funktionalisieren die dann als pH Sensoren verwendet wurden. Darauf aufbauend wurde ein Biosensor basierend auf einem ZnO Nanodraht realisiert. Die markerfreie Detektion von Harnstoff Molekülen in einer Puffer Lösung wurde durchgeführt. ZnO nanodrähte wurden elektrochemisch mit dem Enzym Urease funktionalisiert welches in einer elektropolymerisierten Polypyrrol-Matrix eingebunden ist. Urease wirkt als ein spezifischer Rezeptor für Harnstoff und katalysiert eine enzymatische Reaktion. Diese Reaktion führt zu einer pH-Änderung in der Umgebung der Nanodrähte welche durch den Feld Effekt des Transistors messbar ist.

Die Eigenschaften eines flüssig-gate ZnO NW FETs für chemische und biologische Sensoren können durch die Verwendung eines Metall Gates im flüssigen Medium weiter verbessert werden. Dies wurde durch die Herstellung von flüssig gate Metall-Halbleiter FET (MESFET) realisiert. ZnO Nanodrähte wurden mittels einer elektrochemischen Depositionsmethode mit Metall-Nanopartickeln belegt. Diese Nanopartickel wurden im Weiteren als Metall Gate verwendet und durch Anlegen einer Spannung an die Nanopartickel über die Flüssigkeit konnten die FETs charakterisiert werden. Die Verwendung von Metall-Halbleiter Gate in Flüssigkeiten hat die Feld Effekt Charakteristik der ZnO basierenden flüssig-gate FETs wesentlich verbessert.

Die Verwendung von Flüssig Gate Transistoren basierend auf ZnO Nanodrähten stellen eine breite Platform für marker-freie Detektion von Biomolekülen zur Verfügung und zeigt zahlreiche weitere Einsatzmöglichkeiten in der chemischen Analytik und der medizinischen Diagnostik.

Schlüsselwörter: ZnO Nanodrähte, CBD Wachstum, hierarchischen, selbst-organisierten, flüssig-Gate, Dielektrophorese, galvanischen, pH Sensoren, MESFET

Chapter 1

Introduction

From the origin of life on earth, each and every living being has come under threat to their existence with many natural calamities and disasters. While many vanished to become as now known as ‘extinct’ owing to their inability to cope with environmental changes and diseases, humans have survived it all during the course of evolution. Humans have had an edge over others for their mental capabilities, ability to solve problems and abstract thinking. It has enabled them to manipulate nature to benefit them in survival and fight against deadly threats. The modern life as we live, is also composed of such manipulations of nature. Device and systems in transportation, electricity and telecommunications etc. helping us perform cumbersome tasks more easily are a few examples of such manipulations. Similarly biological systems have helped us providing food, medicine and cures against diseases like malaria, cholera, influenza and plague.

For instance science and technology have relentlessly progressed in the field of healthcare from the prehistoric era till the past century. Healthcare practices have seen radical developments in the recent times owing to our increased knowledge in the fields of chemistry, biology, physics and material science. Moreover, the advent of biotechnology enabled us examine smallest units of life like cells, nucleus and genetic materials in order to understand their anatomy and biochemical functions. Scientists have not only been able to unlock the mysteries of genetic materials with the help of technologies like genome sequencing but also get an insight of the molecular basis of many diseases such as cancer, tuberculosis and many genetic disorders.

The understanding of molecular mechanism for diseases and disorders is expected to open up avenues for new technologies for prevention and cure. Nanotechnology for example has been applied to discover new strategies of molecular detection. Nanoscale electronic devices have been recently used for molecular sensing and are expected to bring major breakthroughs in diagnostic practices [1-6]. The instant response of electrical detection methods and very low analyte concentration requirements are most advantageous for the use of nanoscale electronic devices in sensing. This has been recently demonstrated with high sensitivity carbon nanotube devices and many NW devices for sensing of DNA, ions, protein and viruses etc. [6-9]. While current medical diagnostic methods involve chemical and optical methods for analyte detection, disadvantages like large volumes of analyte required, long processing steps (such as polymerase chain reaction) and use of centralized labs are unavoidable. Moreover due to long processing steps the results often do not reflect the actual concentrations of analytes *in vitro*. Hence electrical sensing with nanoscale devices facilitates fundamental improvements over existing methods[10-12].

The electrical sensors used for molecular detection make use of either field-effect or electrochemical effect. Typical devices constructed for field-effect based sensing purposes employ metal oxide-semiconductor field-effect transistor (MOSFET) geometry as demonstrated in many reports [6]. The label free electrical detection of molecules is based on a 'lock and key model' where molecules functionalized on the transistor channel known as *receptor* interact with target molecules known as *analyte*. The receptor-analyte molecular interaction is very specific and mostly occurs by the formation of a chemical bond. These specific molecular interactions on the transistor channel (nanostructure surface) influence the density of charge carriers which is reflected in the transport characteristics of the device. Use of 1D and 2D nanostructures as transistor channel provide high surface to the volume ratio which is advantageous in order to functionalize maximum number of receptors and attain high sensitivities. The performance of a transistor is determined by the electrical properties of its channel and the efficiency of the gate [13]. Use of materials with high field-effect mobilities and the gate architecture engineering have been a matter of increased scientific attention in order to fabricate high performance FETs. Carbon nanotubes, silicon, cadmium sulphide, zinc oxide NW/nanobelts used as transistor channel in different gate geometries are few examples which have been studied recently and also demonstrated as chemical sensors [14-18].

The necessity to use semiconducting materials in order to make use of field-effect determines the choice of materials for future electrical sensors. The quest for high-performance materials for field effect operations has lead scientists to investigate many new materials. As a pertinent example graphene is being investigated for potential applications in electrical devices and sensors [19]. Methods and materials to make highly sensitive electronic sensors have been most sought and realized in a number of different kind FETs using semiconducting carbon nanotubes (CNTs)[20-23] and semiconducting NWs/nanobelts [24-30] etc. However for real applications of FETs, the fabrication techniques need an instant makeover. Scalable methods for device fabrication avoiding the use of bulky instruments for material synthesis and costly equipment are highly desired. Fabricating FETs with many materials such as CNTs, Si NWs and other semiconducting NWs generally involve high-temperature growth methods requiring heavy instrumental set-up and complicated equipment like e-beam lithography which are not possibly scalable. One of the biggest obstacles is the site-specific positioning of NWs over a large area substrate[31, 32]. While current methods of device fabrication with high-temperature grown materials pose a challenge for future application, it is of high interest to carry out investigations on 1D and 2D nanomaterial which can be grown at low temperatures with minimal set-up requirements. ZnO NWs are among the most studied 1D semiconducting nanomaterial and demonstrated in a number of prototype FETs [33, 34]. ZnO NWs are inherently semiconducting employable for transistor fabrication in scalable methods and can be grown site-specifically in solution growth. A number of different approaches have been proposed for large-scale assembly of ZnO NWs devices, which include trapping by AC dielectrophoresis[32] and lateral growth from locations pre-defined by patterning and lithography[35, 36]. The potential of ZnO NW based FETs for liquid sensing and advantages of using solution based growth methods in the fabrication process will be illustrated in the thesis.

The first part of the thesis deals with the challenges regarding synthesis of high-quality ZnO NWs for fabrication of transistors. ZnO nanostructure can be grown in a simple chemical bath deposition (CBD) method by heating their precursors in water. The morphology of ZnO nanostructure in such a method depends on many factors such as reaction temperature, precursor concentration, type of precursor, use of growth catalyst and even the substrates. The CBD method was revisited for the growth of hierarchical ZnO nanostructures. The experiments conducted here investigate various inherent factors affecting the reaction kinetics and its relation with the evolution of product morphology. A novel CBD method for self-assembly based synthesis of ZnO nanostructures is discussed in a template-free and shape-directing-reagent-free growth set-up. The CBD method for high quality ZnO NWs synthesis was applied for fabrication of ZnO NW based transistors. Drain source microelectrodes were written over Si/SiO_2 chips and Kapton foils using photolithography and ZnO NWs were site-specifically grown spanning the electrodes forming a transistor channel. Site-specific growth of ZnO NWs is achieved by selective deposition of nanoparticle seeds on microelectrode pairs. Gold and zinc oxide NPs were used as seed and deposited on microelectrodes from their colloids employing alternating current (AC) dielectrophoresis. The seeded Si/SiO_2 chips and Kapton foils are then put into precursor solution in a modified CBD growth and ZnO NW grow from seeded microelectrodes spanning the gap in between. The method was first developed on a local scale using 4 × 4 mm Si/SiO$_2$ chips consisting 8 microelectrode gap positions and yielded up to 100 percent fabrication rate. Subsequently the method was extended to large area substrates namely 4” silicon wafers and kapton foils (80 × 80 mm). Large area Si/SiO$_2$ wafers were written with 120 Ti/Pt microelectrode gap positions in a standard photolithography technique. The photolithography procedure to fabricate wafers on kapton foils required some optimizations because of hydrophobic nature of the kapton polyimide leading to poor adhesion of microelectrodes to the surface. A chemical route to modify the kapton surface provided robust adhesion between microelectrodes and surface. The large area wafers yielded up to 80 percent throughput. The technique accomplishes a clear advantage over other routes to fabricate devices where NWs are produced *exsitu* from various synthesis methods[37-42].

The ZnO NW based FETs thus fabricated in the CBD method, were used to develop chemical and biological sensors in this work. A wide range of sensors based on semiconducting NWs and semiconducting CNTs have used a transduction mechanism based on electric field-effect in a back-gated configuration[43]. However, deploying FETs as biosensors requires their functioning in liquid environments and the use of a reference electrode in spite of the back-gate is unavoidable. In liquids, the transduction mechanism has to be applied by an electrochemical (liquid) gate as demonstrated recently on CNT based sensors [44, 45]. An electrochemical gate is realized by the formation of an electrochemical double layer (EDL) in between the nanostructure (transistor channel) surface and the surrounding liquid. An electrochemical gate is more effective than a back-gate because of EDL size being comparable to and even smaller than the diameter of the transistor channels (1D nanostructure). The comparable sizes give rise to stronger gate capacitances and lead to very effective gating-effect in the transistor [46]. The stronger gating effects result in FETs showing very effective current modulation in liquids as will be shown for ZnO NW based transistor in this thesis. Until now, the potential of the electrochemical gating method remains largely unexplored for ZnO-NW-based FETs [47] and this work presents pioneering study to deploy ZnO NW based FETs as chemical and biosensors in liquid medium.

Liquid-gated FETs are also potential candidates for developing miniaturized total analytical systems (µTAS) based on electrical sensing platforms. In this regard, FETs based on CNT and Si NWs have been integrated with microfluidic channel and demonstrated as chemical and biological sensors [48-50]. Here, ZnO NW transistors were integrated with microfluidic systems for the first time and tested for operations in liquid environment. The liquid gating setup for field-effect operation of transistors in liquid involved a manual spotting method, open microfluidic channels carved into the silicon chips and polydimethylsiloxane (PDMS) based microfluidic channel.

Transistors deployed as chemical sensors in liquids were constructed in an ion-selective FET design [51, 52]. ZnO NWs were functionalized with receptor molecules to detect the pH variations of the liquid environment. 3-aminopropyltriethoxysilane (3-APTS) molecules were functionalized on ZnO NW FETs. 3-APTS functionalized on ZnO NWs have positively charged amino end-groups. The pH variation in the surrounding solution affects the positive charge density on the surface of NW working as transistor channel and is reflected in the transport characteristics of the device. The ZnO NW based transistors are demonstrated as pH sensor for solutions with pH values 6 to 10. The liquid-gated ZnO NW transistor used for pH sensing here demonstrated a high-performance pH sensor. The transistors showed the sensor response comparable to their counterpart silicon FETs[6, 53], while the transconductance bettered the highest values reported for ZnO NW transistors [54, 55].

The liquid-gated ZnO NW FETs were further employed as electrical biosensor for urea detection. In order to construct a sensor, ZnO NW FETs were electrochemically functionalized with enzyme urease acting as receptors for urea molecules. The enzymatic interaction between enzyme urease and urea forms ammonia[56] which affects the pH values in the vicinity of NW surface which is reflected in the field-effect characteristics of the transistor. The method demonstrated for the detection of urea molecules can be applied to many biomolecule-enzyme systems and soars promise for fast electrical detection techniques for diagnostic applications such as blood urea nitrogen (BUN)[57], creatinine[58] etc.

With the emerging applications of FET based sensors in liquids, it is important to optimize suitable FET designs for operations in liquid. The liquid-gated FETs demonstrated for sensing purposes in liquids till now require operating voltages which are considerably harmful for real biological samples. Transistors which can generate a high field-effect on critically low voltages are thus highly desired and critical for real biological sensing purposes. While FETs with many semiconducting NWs demonstrate considerable field-effect characteristics on voltages even below 1 volt, it seems unlikely that FETs with CNTs and other high field-effect mobilities make suitable choice for liquid based sensors. A novel method to improve the performance of liquid-gated FETs is discussed as concluding part of this thesis. The ZnO NW transistors were decorated with gold and palladium NPs forming a Schottky contact. The metal NPs were now employed as a metal gate and the device functions as metal-semiconductor field-effect transistors (MESFET). The ZnO NW based MESFETs thus constructed were characterized in a liquid-gated configuration similar to ISFET. The gate voltage was applied on the metal NPs using a reference electrode through the surrounding liquid medium. The use of NPs as metal gate improved the field-effect characteristics of the transistors even on low operating voltages. The improved performance of ZnO NW transistors is also reflected in the high field-effect mobilities values around 1400 cm^2/V.s as compared to ZnO NW based ISFET values typically around 1.85 cm^2/V.s. Further, the ZnO NW based MESFET were demonstrated as a functional chemical sensor in liquid medium.

The demonstration of ZnO NW based FETs in liquid sensing applications open up avenues for their application in real chemical and biological sensing platforms. The work conducted during this thesis also suggests the potential of self-assembly based growth of nanomaterials in future applications in devices. Fabrication of ZnO NWs transistors on flexible substrates and integration into microfluidics sets a stage for application in future lab-on-chip systems with electrical sensing. The improvement of liquid-gated FETs performance with the use of metal NPs as gate is advantageous for high sensitivities of devices. The NW MESFET with nanoparticle gate also provides a novel platform for exploring specific interactions related with the properties of NPs.

Chapter 2

Synthesis of zinc oxide NWs

Zinc oxide NWs used for transistor fabrication in the thesis were exclusively synthesized in a solution based growth method. After giving an overview of the different methods used for the ZnO NW synthesis, this chapter illustrates a novel solution based chemical bath deposition (CBD) method for self-assembly of ZnO NWs and other hierarchical structures. The self-assembled formation of NWs and other structures is investigated by studying the effect of different growth parameters on reaction kinetics.

2.1. Background

Zinc oxide is a wide band gap semiconductor material with an energy band gap of around 3.4 eV[59]. ZnO crystallizes in two forms named rocksalt and wurtzite. The material can be synthesized in many nanostructure morphologies from 0D to 3D such as NPs, NWs, nanobelts (NBs), nanotubes (NTs), thin films and many other constructions. The synthesis methods to grow ZnO nanostructure exist in different forms such as vapor phase, hydrothermal, electrochemical and solution based growth. Following will be an overview of different growth methods employed for ZnO NW synthesis.

2.1.1. Vapor-phase growth method

Vapor phase growth methods include techniques that involve evaporation of precursor materials in to vapor phase at elevated temperatures. The precursor vapors are subsequently condensed under certain conditions (temperature, pressure, atmosphere, substrate and catalyst etc.) to form a desired product. The methods for nanostructure growth usually involve the precursor material's vapors being exposed to catalyst NPs (seeds) in order to initiate the nucleation process and to control the morphology of the product. The nanoparticle (seed) layer condenses the vaporized precursor material on its surface leading to super saturation. The precursor molecules on the nanoparticle surface then solidify and grow outwards from the catalyst in certain morphology. Chemical Vapor Deposition (CVD) and metal-organic CVD (MOCVD) are the principal techniques based on this mechanism and employed for the growth of ZnO nanomaterials[60-63]. The processes are carried out in tube-furnaces equipped with pressure regulators, different gas-flow kits for providing specific environment inside furnace and other controllers. A typical CVD growth set-up is shown in the schematic representation in **figure 2.1**. The method provides a good quality but lacks in the adaptability to be used for scalable synthesis of material due to special atmospheric requirements and thus being expensive in terms of equipment set-up.

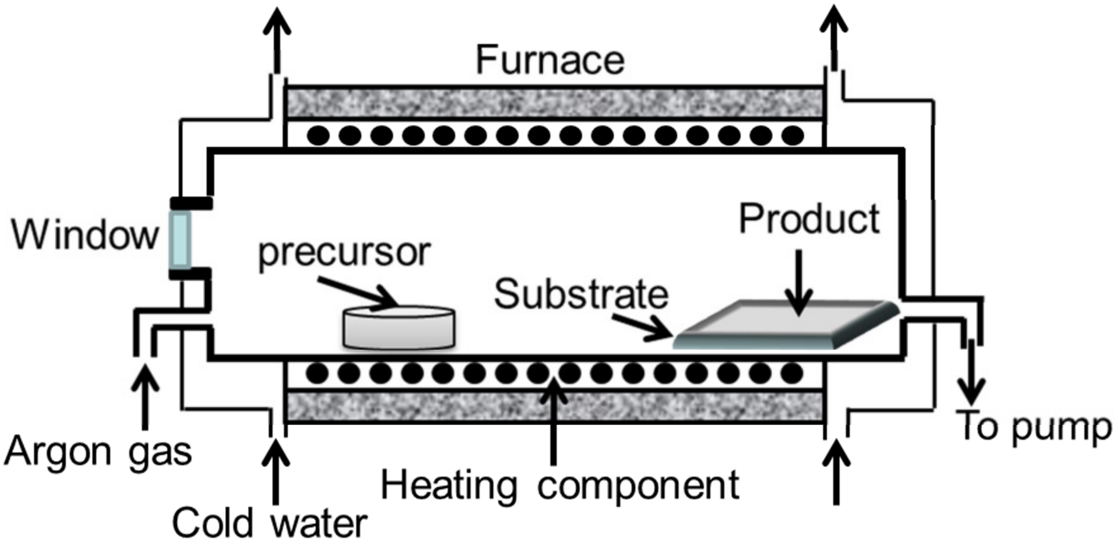

Figure 2.1: Schematic of a horizontal furnace used for the Vapor phase growth method for oxide nanostructures.

2.1.2 Hydrothermal growth

Hydrothermal growth techniques for the synthesis of nanomaterials involve the crystallization of products from their precursor's aqueous solutions at high temperatures and pressure environments. This method is mostly used in the synthesis of pure single crystals and nanostructures since it provides an easy route to synthesize materials from their liquid solutions. For example synthesis of ZnO nanostructures from its water soluble salts. The growth is generally performed in a steel or Teflon vessel called a*utoclave* as shown in **figure 2.2**. The autoclave also contains the substrates for the material growth. The vessel filled with precursor solution is kept in a special chamber to maintain a temperature gradient between its center and the ends. The ends are usually hotter than the central part. The hotter ends help to dissolves the precursor while cooler part helps the nucleation of the growth. Hydrothermal growth methods are widely used as cheaper production method for nanomaterials than other high temperature growth methods [64, 65].

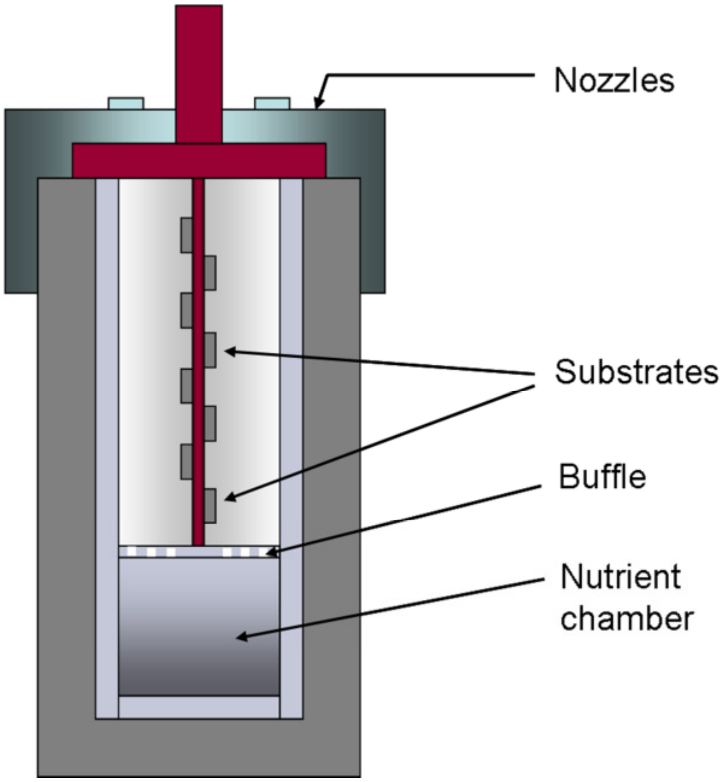

Figure 2.2: Schematic representation of “Autoclave”. A set-up designed for hydrothermal growth.

2.1.3 Electrochemical deposition

Electrochemical deposition of metal-oxide structures is known for long but rather less established as a method for the synthesis of ZnO nanostructures. However the method has been explored in recent years and ZnO nanostructure in various forms e.g. nanocolumn, nanorods and thin films have been synthesized[66,67]. ZnO nanostructure on different substrates grown from aqueous precursor solutions has been reported by different groups. The morphology of the nanostructures has been shown to depend on the current density, deposition time and bath temperatures. The growth set-up comprises an electrochemical cell employing one electrode as a substrate and another as a counter electrode as shown in **figure 2.3**. Here activation energy to form the product is provided by the electrical energy. The setup may follow two process- (i) The metal species in the solution is oxidized at the electrode (in this case substrate makes an anode) or (ii) the redox process at the electrodes bring changes in the local pH value of the solution and the metal precipitates out of solution as the hydroxide/oxide phase[41, 68-71].

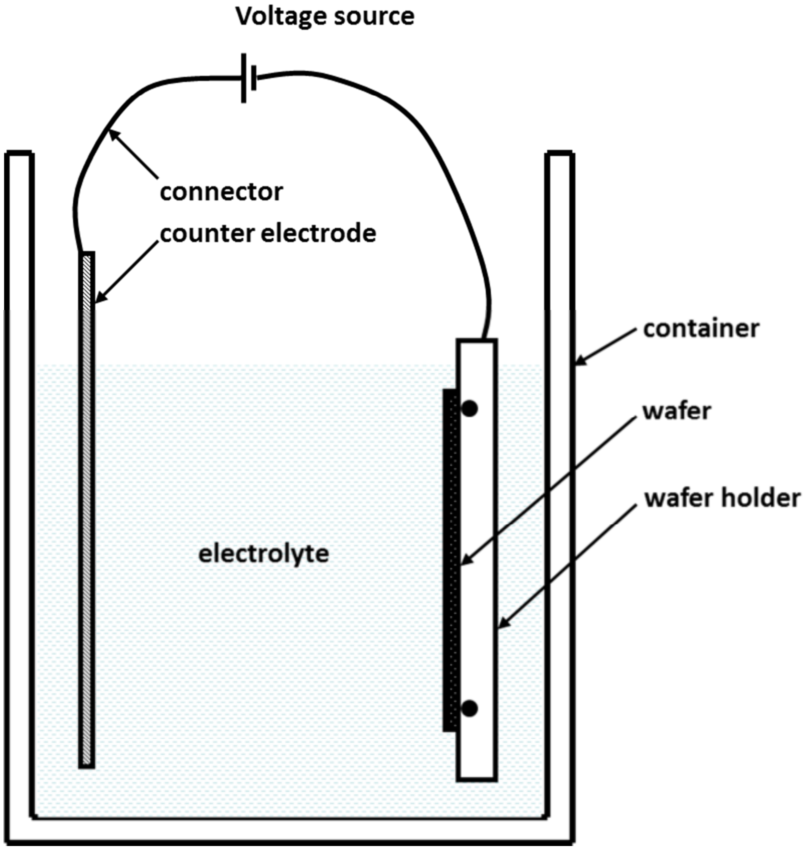

Figure 2.3: Schematic representation of a set-up designed for electrochemical deposition of ZnO.

2.1.4 Chemical bath deposition (CBD) method

Solution based growth of ZnO nanostructures in a chemical bath represents a method requiring minimal amount of set-up. This method involves preparing an aqueous precursor solution and heating to provide the precursor molecules with the activation energy to initiate the reaction. ZnO nanostructures can be produced typically by heating a precursor solution made of Zinc salts and a reducing agent. The method offers the possibility to carry out the material growth at very low temperatures and normal convection ovens are usually well suited. Typically, seeded substrates (substrates with catalyst NPs) are placed inside a container (e.g. glass beaker) filled with the precursor solution and kept for growth in the oven at ambient pressure and at a controlled temperature. Such solution based growth methods for synthesis using minimal growth set-up have gross advantages for large scale production of nanomaterials.

The aqueous CBD growth method was reported first time in 1990 by Andre-verges[72] to synthesize ZnO micro-crystals/microstructures. In this paper the authors proposed synthesis of divalent metal oxides from their salts solutions in basic medium. The use of basic medium for the metal oxides is required as the metal salts in low oxidation states tend not to hydrolyze in acidic medium. A controlled release of hydroxyl ions or metallic ions to a basic medium is the most suitable method to prepare metal-oxides in a (forced) hydrolysis method. In this classical work, they performed synthesis of microstructures by the hydrolysis of zinc nitrate and zinc chloride salts with controlled release of hydroxyl ions using hexamethylenetetramine (HMT). The authors studied the production ZnO nanostructures under the influence of different factors such as the nature of anions, reactant concentrations, pH, and temperature etc. on the morphology of the product. **Figure 2.4** shows some SEM images of the microcrystals obtained by Verges et. al.

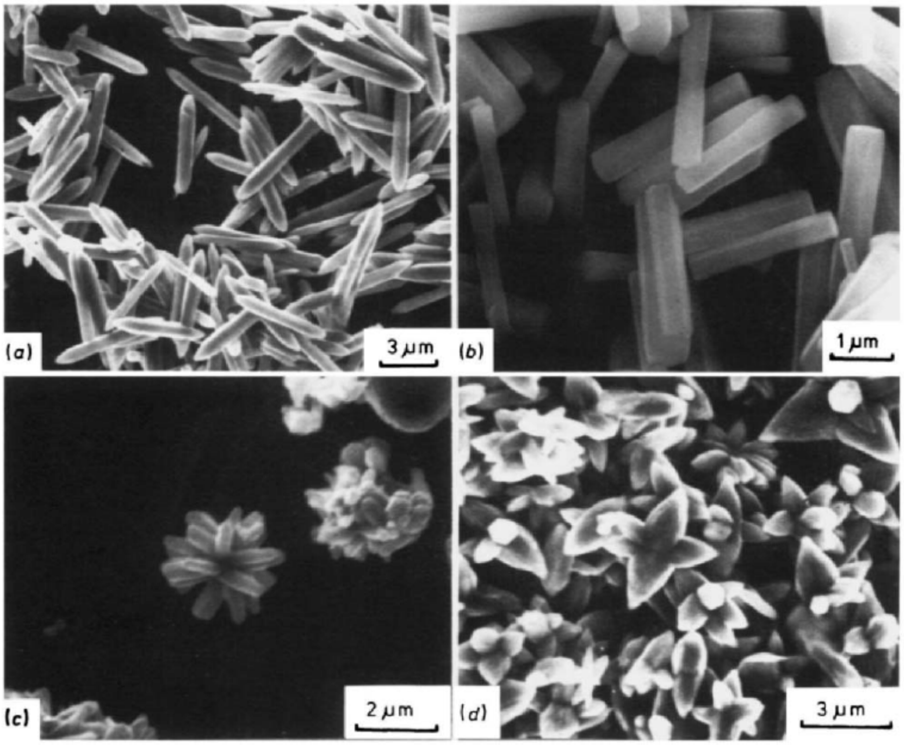

Figure 2.4: ZnO microcrystals obtained at 100^{0}C by controlled hydrolysis of Zinc nitrate at different concentrations[72]

Thereafter, understanding of the solution growth method to grow ZnO and other metal oxide microstructures/nanostructures has developed both theoretically and experimentally. The processes require low temperatures and can be carried out with minimal complications. Many reports in recent years have shown synthesis of ZnO nanostructures from one dimensional (1D) to three dimensional (3D) constructions by varying the reaction materials, physical parameters and some additive growth directing agents.

The fundamental growth process of ZnO from its precursor solutions shall be discussed here in order to understand the factors effecting the growth and morphology. The formation of metal oxides from their salts by hydrolysis method has been known since long [73]. In the case of metal salt solutions, the metal ions form a complex cation (aqua ions) depicted generally with a formula $M(H_2O)^{m+}$ (where M is the metal ion and m+ is charge on the metal ion) which undergo hydrolysis as follows-

$M(H_2O)_n^{m+} + H_2O \leftrightarrow M(H_2O)_{n-1}(OH)^{(m-1)+} + H_3O^+$ 2.1

The dissociation constant of the reaction is a linear relation of the charge-to-mass ratio of metal ions [74]. So ions with low charges behave as very weak acids e.g. Na^+ and difficult to hydrolyse. Larger divalent ions such as Ca^{2+}, Zn^{2+}, Sn^{2+} and Pb^{2+} have their dissociation constants around 6 and undergo mild hydrolysis while small divalent ions like Be^{2+} which have large charge-to-size ratio undergo extensive hydrolysis and are noticeably acidic. Thus the hydrolysis is favored or suppressed by increasing basicity or increasing acidity respectively in a solution.

The hydrolysis of a common Zinc salt for example Zinc nitrate $[Zn(NO_3)_2.6H_2O]$ can be shown as-

$Zn^{2+} + 4OH^- \leftrightarrow Zn(OH)_4^{2-}$..2.2

$Zn(OH)_4^{2-} \leftrightarrow ZnO + H_2O + 2OH^-$..2.3

Here OH^- ions are supplied from the dissociation of water molecules. ZnO is obtained as a precipitate in the solution.

(i) Crystal growth and self-assembly

A crystal is made of atom, molecule or ion constituents arranged in a repeating pattern. Zinc oxide can be found in single crystalline or polycrystalline form depending on the growth methods. ZnO crystals grown in solution based method are generally polycrystalline. ZnO can crystallize in two phases- (i) rock salt type cubic phases and (ii) hexagonal zincite phase. The hexagonal zincite phase with wurtzite structure is thermodynamically more stable and haspolar and non-polar planes in its crystal. The polar plane is either Zn terminated [the $(000\bar{1})$ face] or O terminated [the (0001) faces] while the non-polar surface includes (1120) and (1010) faces. Under thermodynamic equilibrium of a crystal, the small planes exhibit large surface energy and vice versa. Such planes also exist in a ZnO crystal and {0001} plane corresponds to high surface energy facet and is more active resulting in preferred growth of the crystal in c-axis. On the other hand crystal planes {0110} and {2110} exhibit low surface energy and are less reactive. Anisotropy of growth is therefore a special feature of ZnO nanostructures. The surface energy of crystal planes can be influenced by controlling the growth kinetics, and it is thus possible to control the growth behavior of ZnO crystals in different dimensions. For example one dimensional structures of ZnO reported in different synthesis processes consisting of nanorods, NWs, nanotubes and nanobelts etc are the result of c-axis preferred growth of a ZnO crystal [75].

From a general point of view, crystal growth can be divided in to homogeneous and heterogeneous growth processes depending on the nucleation and mechanism of growth.

Homogeneous nucleation takes place when all the reactants belong to one phase. The reaction does not involve any foreign agents such as catalyst which can act as nuclei for the growth. The metal ions react with the hydroxyl ions and form a primary metal oxide active complex. This complex serves as an embryo nucleus for further attachment of M^+ and O^- ions into the lattice and forms a crystalloid. Further growth of this crystalloid is a consequence of the followed influx of the constituent atoms from the solution towards the active sites of the crystalloid (i.e. thermodynamically less stable facets). The reason for the influx of constituent atoms towards the active sites is believed to be the ion super saturation in the solution. This crystalloid formation followed by the further diffusion of constituent ions on to the active planes results in the growth of nanostructure. This whole process may or may not be assisted with the Ostwald's ripening processes.

The nucleus formation in homogeneous processes creates an interface between the newly formed phase (solid) and solution phase. This happens if the vapor pressure of the newly formed (solid) phase is less than the vapor pressure of the solution phase itself. The formation of a new solid phase then releases some energy in the creation of interface and brings a difference in the free energy of the solution per unit volume or Gibb's free energy (G_v). The nucleation will be favored if the overall change in the Free energy is negative during these processes[76]. Here we will discuss the process of nucleation from a thermodynamics point-of-view and how it is affected in a solution phase. For example, a spherical cluster forming in homogeneous nucleation would generate free energy $-G_v$ Joules/cm^3 and consume t Joules/cm^2 to form the interface with the surroundings. The free energy needed to form the cluster here can be given with the following equation-

$\Delta G = 4/3\pi r^3 G_v + 4\pi r^2 t$……………………………………………………………….2.4

where the first term on right side (volume excess free energy G_v) refers to energy gain in creating new volume and is a negative quantity. The second term (surface excess free energy G_s) refers to the energy loss from surface tension on the new interface and represents a positive quantity. The free energy ΔG is maximized for the formation of nucleus of a critical radius r^* of value - $2t/G_v$. The evolution of both G_v and G_s during a growth process is depicted in figure 2.5A where the free energy change (ΔG) gains a maximum at the point of the formation of clusters of a critical radius (r^*).

$d\Delta G/dr = 8\pi rt + 4\pi r^2 \Delta G_v = 0$………………………………………………………… 2.5

ΔG_v is called volume excess free energy.

The free energy of critical nucleus formation $\Delta G^* = 4\pi t r^{*2}/3$………………………….2.6

At constant temperature and pressure, parts of the growth solution with high free energy favor the nucleation process depending on the other factors e.g. supersaturation of constituent atoms/ions and their supply towards the nucleating structure. The rate of the nucleation (J) can be given by the following relation based on the Arhenius reaction velocity equation for thermally activated process-

$J = A \exp(-\Delta G/kT)$…………………………………………………………………....2.7

where A is a constant, k is Boltzmann constant and T is temperature. The supersaturation in a solution is represented by the Gibbs-Thomson relationship as-

$\ln S = 2\, t\, v/kTr$

where v is molar volume and T is temperature.

or, $kT\ln S/V = 2T/r = -\Delta G_v$

from eq. 2.6,

$-\Delta G^* = 16\pi t^3 v^2/3(kT\ln S)$……………………………………………………………..2.8

Now, from eq. 2.7 and 2.8, the rate of nucleation J can be written as variable of-

(i) Temperature, (ii) Supersaturation and (iii) the Interfacial tension as can be shown in the following equation-

$J = \mathrm{A}\ \exp\ (-16\pi\ t^3\mathrm{v}^2/3\mathrm{k}^3\mathrm{T}^3\ln S^3)$.

The three variables of the solution based nucleation process have a decisive effect on the product morphology which will be illustrated in the experimental section.

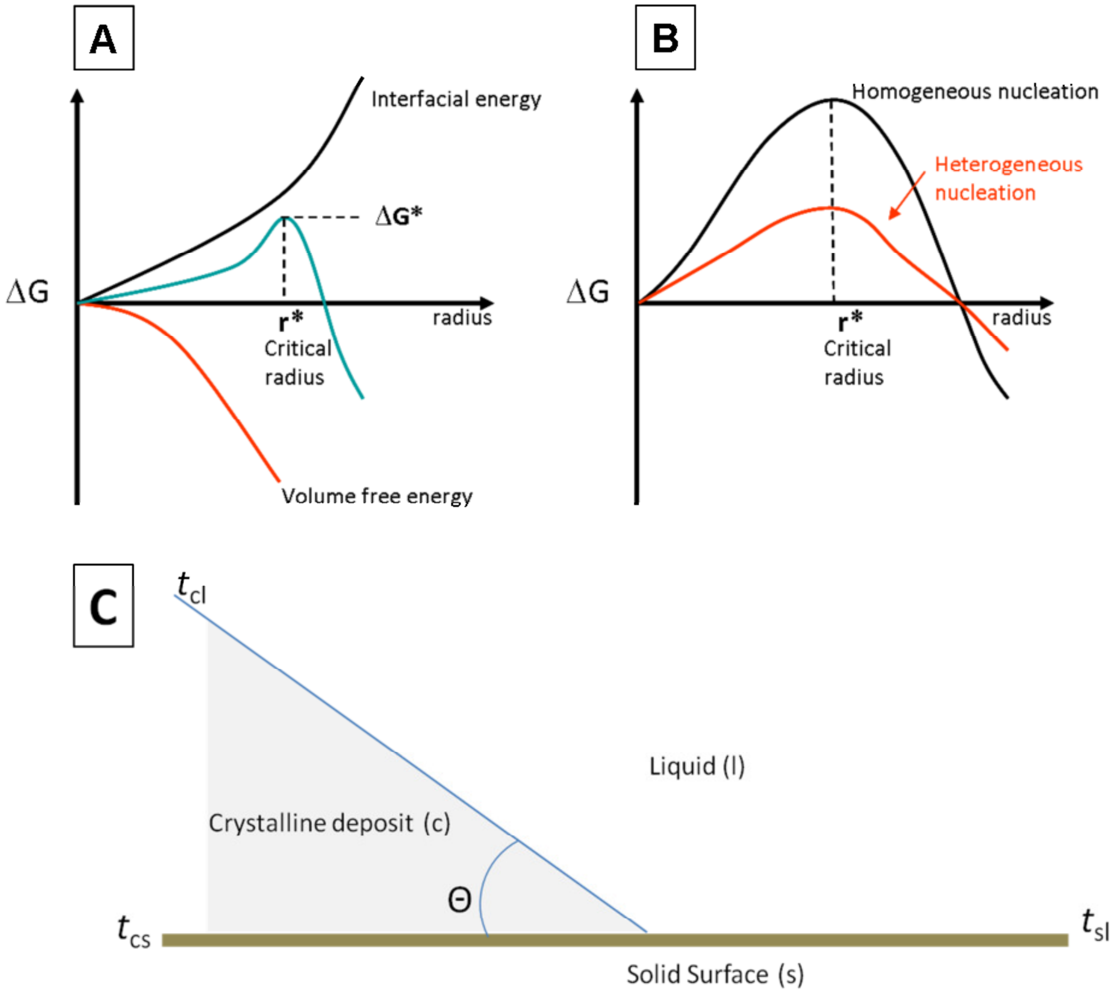

Figure 2.5: (A) Evolution of free energy during the formation of clusters, also showing the two terms Interfacial energy and Volume free energy Comparison of the evolution of free energy during homogeneous and (B) heterogeneous nucleation[72] and (C) different interfaces in the heterogeneous nucleation and the wetting angle.

The heterogeneous nucleation processes on the other hand involve a catalyst present in the reaction medium existing in a different phase from that of the reactants. The catalyst may be present in the solution or on some substrates. The catalyst serves as a seed for the nucleation as it contains chemically active and thermodynamically unstable lattice planes which react with the metal ions and anions in the solution. These interactions incorporate ions onto the lattice sites and initiate the crystal growth. From a thermodynamics point of view, this is mainly due to the decrease of effective surface energy contributions to the work of critical clusters formation. The thermodynamic barriers (free energy needed for nucleation) in heterogeneous and homogeneous nucleation are shown in **figure 2.5B**. The thermodynamic barrier of nucleation for condensation on planar interfaces can be given as-

$\Delta G^*_{heter} = \Phi \,.\, \Delta G^*$ ………………………………………………………………..2.9

Φ is a factor depending on the interfacial tension between solid surface, catalyst and the solution phases (figure 2.5C). For positive catalysis, the value of Φ is always less than unity.

$\Phi = (2 + \cos\theta)(1 - \cos\theta)^2/4$…………………………………………… ……………2.10

Here θ is the wetting angle on the interface between solid phase and the solution as shown in **figure 2.5C**. From eq. 2.10 it is understood that the free energy needed for heterogeneous nucleation is equal to the product of homogeneous nucleation free energy and a function of the contact angle. The ease of nucleation is determined by the wetting angle. Since $\cos\theta < 1$, nucleation is favored.

On the cluster, the activity of different crystal planes, change in diffusion rate of ions depending on the concentration of the reactants and other thermodynamic constraints affect the growth of crystals in different directions in 3D, thus altering the final morphology and size of the grown product.

2.2 Experimental

An aqueous CBD method was used for the growth of NWs and hierarchical structures of ZnO. The set up used for the growth of ZnO nanostructures is shown in **figure 2.4**. The set up consisted of a convection oven and glass beakers as containers for the precursor solutions (shown in inset of figure 2.4). An aqueous solution composed of zinc nitrate and either methyl amine (MA) or hexamethylenetetramine (HMT) was used for the synthesis. The precursor solution (~200 ml) was filled in 400 ml glass beakers and substrates/chips (seeded/unseeded) were dipped in the growth solution before/after putting the beakers in a hot air oven depending on the growth procedure (see **Table 1**). Zinc nitrate hexahydrate [$Zn(NO_3)_2.6H_2O$] was purchased from Fluka (>99 % pure), hexamethylenetetramine [$(CH_2)_6.N_4$] (HMT) from Aldrich (>99% pure) and methyl amine [$CH_3.NH_2$] (MA, 40 % w/w aqueous solution) was purchased from Alfa Aesar.

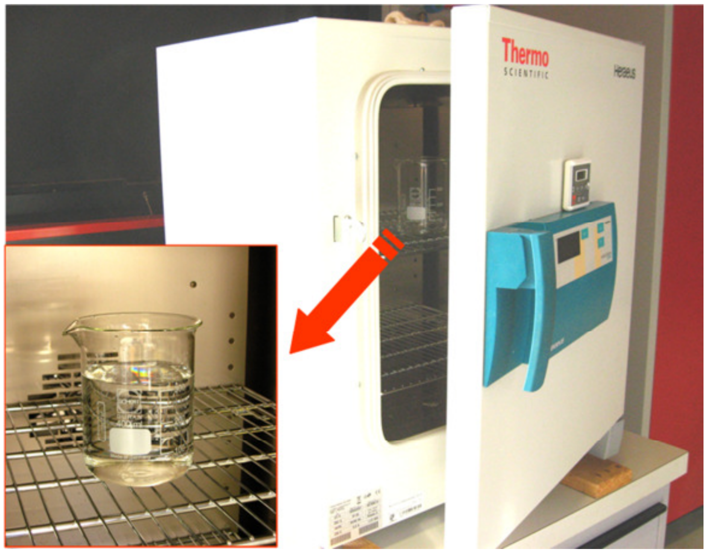

Figure 2.6: Experimental set-up used for the CBD growth of ZnO NWs. A convection oven for heating the solution and a beaker with the growth solution from inside the oven (inset picture)

Precursors and ratio	**Concentration**	**Substrate (Si/SiO_2)**	**Parameters**	**Hierarchical superstructures**
$Zn(NO_3)_2.6H_2O$ + $(CH_2)_6.N_4$ (1:1)	0.25 mM each	Seeded	85^0C for 44 Hrs. precursor preheated for 4-5 hrs	NWs (1D)
$Zn(NO_3)_2.6H_2O$ + $(CH_2)_6.N_4$ (1:1)	0.5 mM each	Not seeded	85^0C for 36 Hrs.	Flower-like (3D)
$Zn(NO_3)_2.6H_2O$ + $CH_3.NH_2$ (1:1)	0.5 mM each	Not seeded	85^0C for 36 Hrs.	Viscous-fingers-like (2D)
$Zn(NO_3)_2.6H_2O$ + $(CH_2)_6.N_4$ (1:1)	0.5 mM each	Not seeded	100^0C for 4 Hrs. + 85^0C for 36 Hrs.	Rolling-pin-like (1D)
$Zn(NO_3)_2.6H_2O$ + $(CH_2)_6.N_4$ (1:1)	0.25 mM each	Seeded	85^0C for 15 Hrs. + 85^0C for 15 Hrs. + 85^0C for 15 Hrs.	Yagi-Uda-antenna like (1D)

Table 1: Reaction conditions for obtaining ZnO NWs and various hierarchical superstructures

Table 1 lists the CBD growth methods for ZnO NWs and hierarchical constructions. ZnO and Gold NPs were used for several growth experiments for ZnO NWs synthesis, using them as seeds. A colloidal synthesis method developed by Bahenmann et al. was used for the preparation of ZnO colloids[77]. Gold NPs were synthesized in a citrate reduction method first developed by Turkevich et al[78]. In order to grow Yagi-Uda-antenna like structures, the samples were seeded with gold NPs before putting the samples in the growth solution. The methods were repeated couple of times to assure the reproducibility of grown superstructures. Samples taken out after the growth process were rinsed in de-ionized water and ethanol before conducting SEM measurements for the product morphology.

2.3 Growth of ZnO NWs

ZnO NW based transistors discussed in thesis were exclusively synthesized in aqueous CBD growth method. A heterogeneous nucleation method employing NPs as seeds was used for the growth of ZnO NWs. However the growth method posed challenges to obtain uniform NWs required for FETs fabrication. This section investigates the heterogeneous ZnO NW growth and suggests a modified CBD growth method that gives highly uniform low diameter ZnO NWs.

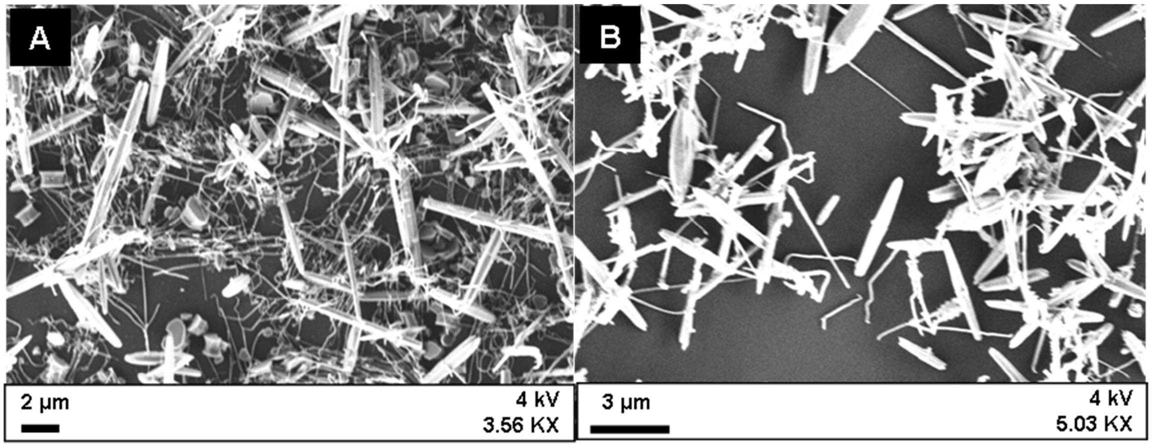

Figure 2.7: SEM images (A) and (B) show ZnO NWs grown in a standard Chemical bath deposition growth method on silicon substrates using gold and ZnO NPs as the seeds.

ZnO NWs/nanorods can be routinely synthesized in solution growth methods using catalyst NPs and employing Zinc salt and a suitable reducing agent as precursors. Usually Hexamethylenetetramine or similar reducing agent are used which ensure the slow release of OH^- ions in the growth solution. This situation is favorable for 1D growth i.e. NW/Nanorods

[79] due to aforesaid reasons. **Figure 2.7** shows the SEM images of the grown product on the wafers. It is apparent from the images that two types of nanostructures are formed in the growth process: (i) ZnO NWs of a small diameter (<100nm) and (ii) spindle like ZnO microscale structures having large diameters (>150nm). Several runs with differing precursor concentration and varying seed diameter did not result in ZnO NWs with a unimodal diameter distribution. For the applications envisioned with ZnO nanostructures here and otherwise, it is important to obtain homogeneous ZnO NWs over large areas.

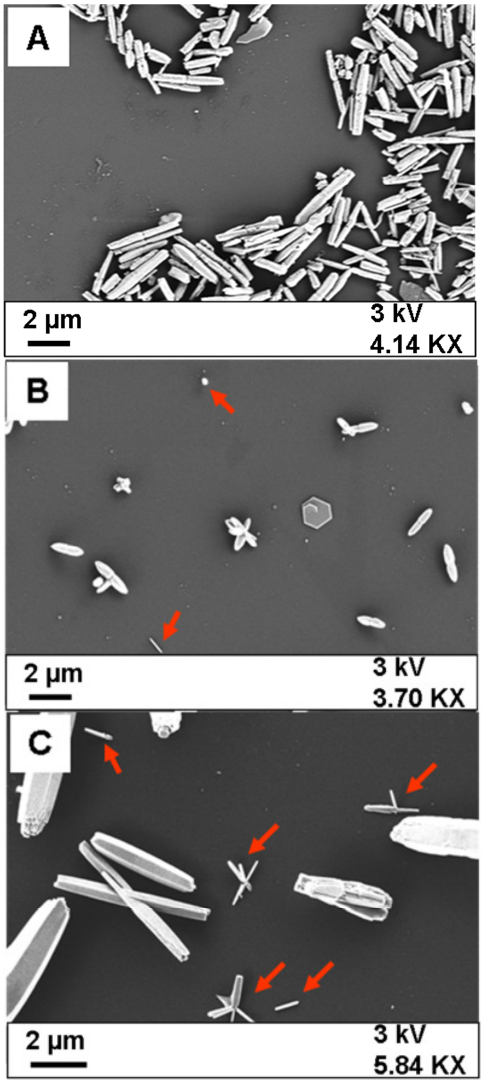

Figure 2.8: SEM images of the product grown on the seeded Si/SiO2 substrates after 1 hr (A), 4 hrs (B) and 6 hrs (C). The red colored arrows show the growth of thin diameter ZnO NWs from the seeds, while spindle like structures are already present on the substrate after only 1 hr from the start of the growth.

Towards this purpose, it is important to refine the diameter distribution while simultaneously preserving the simplicity and effectiveness[80] of the HMTA-based growth procedures. To understand the growth mechanism we conducted the experiment again and collected the growth products at various time intervals during growth. The SEM images of samples collected after different intervals during the growth are shown in the **figure 2.8**. SEM images shown in figure 2.8 were obtained at consecutive growth times at a fixed precursor concentration and temperature. From **image A**, it can be observed that predominantly bigger diameter spindle-like ZnO nanorods are formed during the initial hours.

Examination of several samples suggested that these wires grow by homogeneous nucleation (discussed in the previous section) of dehydrated zinc hydroxyl ions. These wires are formed in solution soon after the target temperature is reached and start to settle down on the substrate. NWs of smaller diameter can be seen in **figures B** and **C** obtainable only after at least 3 hours of growth. The smaller diameter of these wires is indicative of the fact that these wires are growing from the seeds deposited on the substrate following a heterogeneous nucleation. These observations lead us to conclude that spontaneous homogeneous growth leading to spindle-like structures happens within the first 4 hours after the start of the reaction and seeded growth follows subsequently. This implies that homogeneous nucleation is favored over heterogeneous nucleation during the initial hours which is unexpected. A possible reason could be the limited diffusion of active species towards the NPs which are lying on a substrate, thereby restricting the growth to a later period of time and becoming dominant eventually. Another possibility might be the presence of some foreign particles in water which favor the nucleation in the solution.

On the basis of this growth mechanism, we designed a modified solution growth method whereby Si/SiO_2 substrates coated with ZnO and gold NPs were introduced into the reaction mixture 4 to 5 hours after the start of the reaction. **Figure 2.9** shows representative SEM images taken on such substrates. They show clearly that homogeneous ZnO NWs with a high aspect ratio (at least 100) are obtainable using this growth technique. Moreover, it is apparent that spindle-like structures and bigger diameter NWs are almost completely absent. The length and the diameter of ZnO NWs were found to be between 4 and 6 micron and 40 and 70 nm respectively in case of ZnO and gold nanoparticle based growth as inferred from AFM and SEM measurements. Further support for the homogeneous distribution of the obtained wires was gathered by detailed analyses of the diameter of the ZnO NWs from SEM images and AFM images. The following **figure 2.10** shows an AFM scan image of such ZnO NWs grown in the modified growth method.

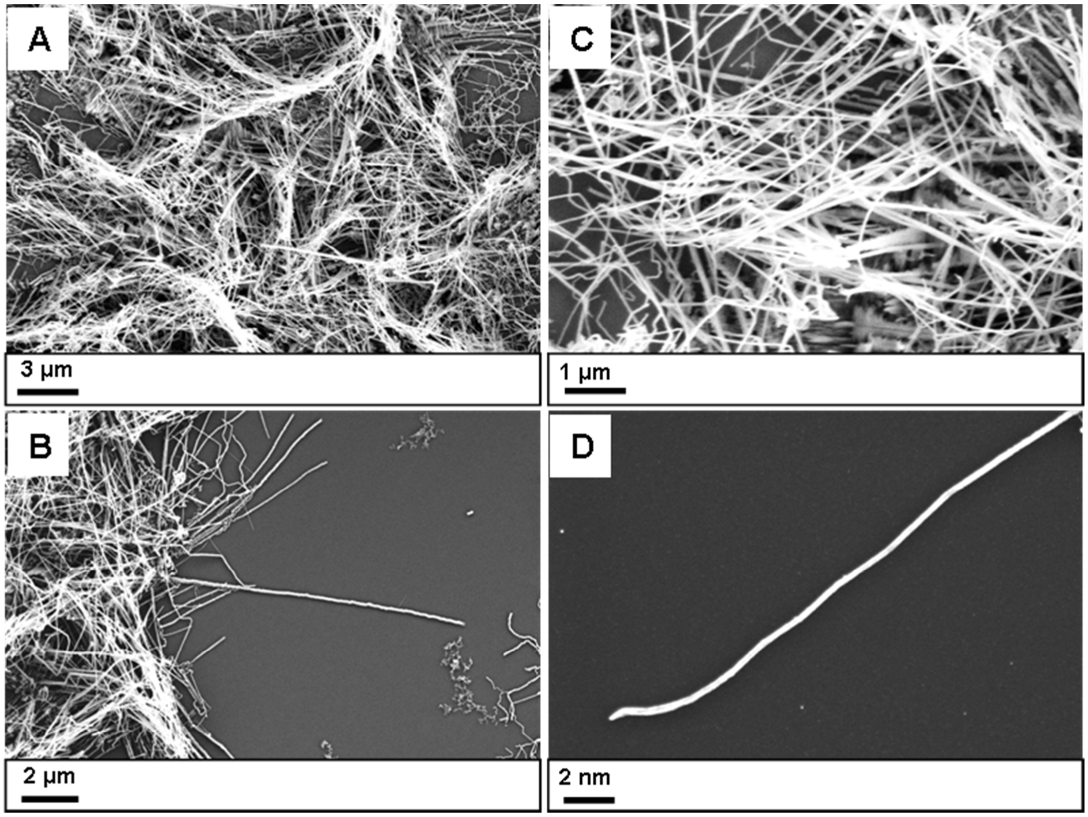

Figure 2.9: SEM images of the ZnO NWs grown in a modified solution growth method with ZnO and (A and B) gold NPs (C, D)

A comparative study of the size of ZnO NWs grown in standard solution growth method and the modified growth method was performed over several substrates and number of experiments. The histograms in **figure 2.11** summarize the distribution of NW diameters obtained using the standard and modified growth technique.

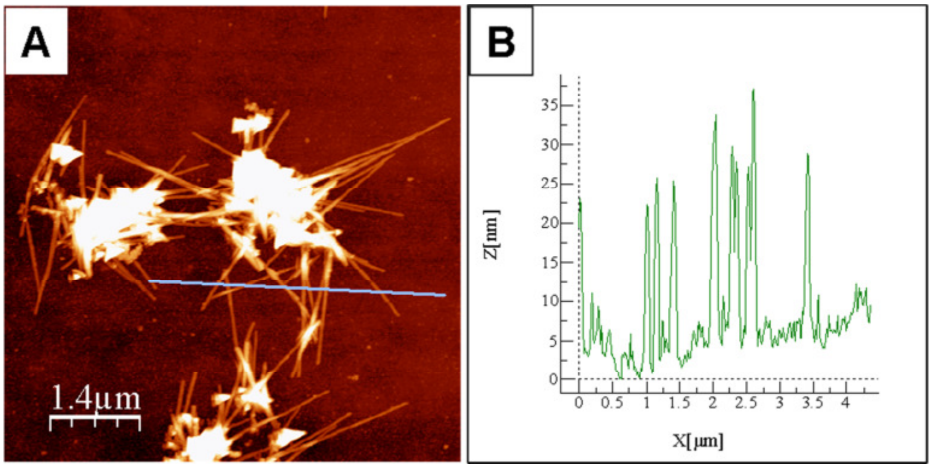

Figure 2.10: (A) AFM scan images of the ZnO NWs grown in the modified growth method on a silicon/silicon oxide substrate using gold NPs as seeds and (B) height profile showing the diameter of NWs.

The histogram in figure A shows two size distributions: One showing a diameter distribution with a mean of 54.9 nm (by fitting a gaussian) belonging to the ZnO NWs grown from seeds and another at 149.4 nm corresponding to the big spindle like structures deposited from the solution as a product of homogeneous nucleation. However the histogram in the figure B shows a very sharp Gaussian fit centered at 54.5 nm confirming very narrow diameter distribution of the ZnO NWs. It can be inferred that the former method provides for both small as well as larger diameter wires (**figure 2.11 A**), while the latter method is efficient in providing for a unimodal distribution with an average diameter of 54 nm. The lowest diameter was 25 nm as inferred from AFM (**figure 2.10** and **figure 2.11 B**).

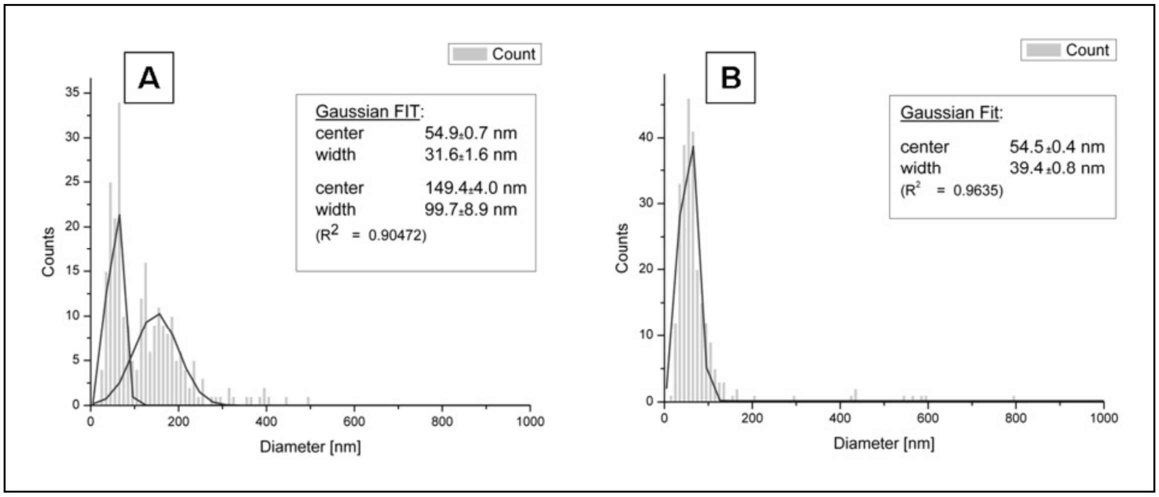

Figure 2.11: The distribution of diameter of the NWs synthesized on the wafer in a standard hexamethylenetetramine based growth (A) and diameter distribution of NWs grown in the modified method (B).

TEM Characterization

Transmission Electron Microscopy investigations of the synthesized NWs were carried out using a JEOL 2000 TEM. **Figure 2.12** shows TEM images obtained on the as grown ZnO NWs (A and B) and after annealing the NWs (C and D). NWs as grown showed a crystalline core towards the center and an amorphous sheath around the central core. The Central core appeared to be polycrystalline as seen from the TEM images and also from the diffraction pattern. The selected area electron diffraction pattern as shown in **figure 2.13** can be compared with the simulated diffraction pattern of a ZnO NW grown in solution based method preferring a c-axis growth and having a wurtzite crystalline structure[81, 82].

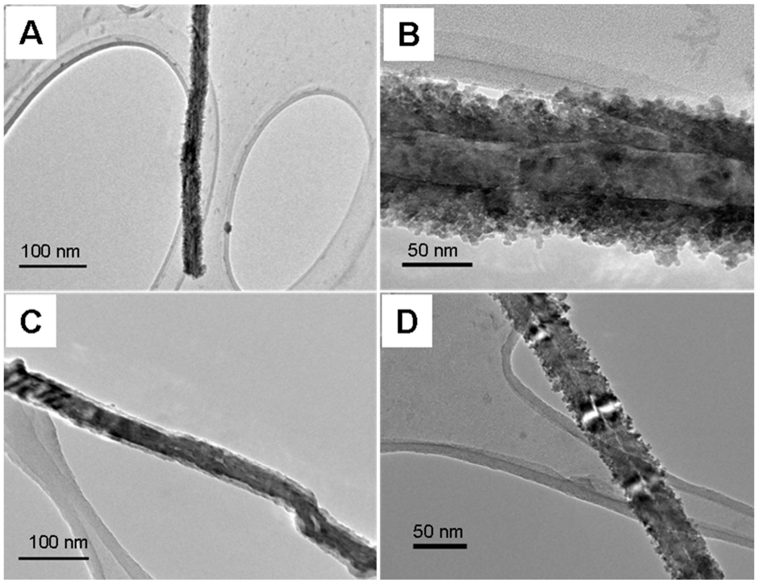

Figure 2.12: Transmission electron microscopy (TEM) images of individual ZnO NWs (grown from Au nanoparticle seeds) before (A,B) and after (C,D) the rapid thermal annealing procedure. While the as-grown structures in A and B display a very rough and inhomogeneous morphology, C and D show that annealing improves the morphology of the grown ZnO NWs.

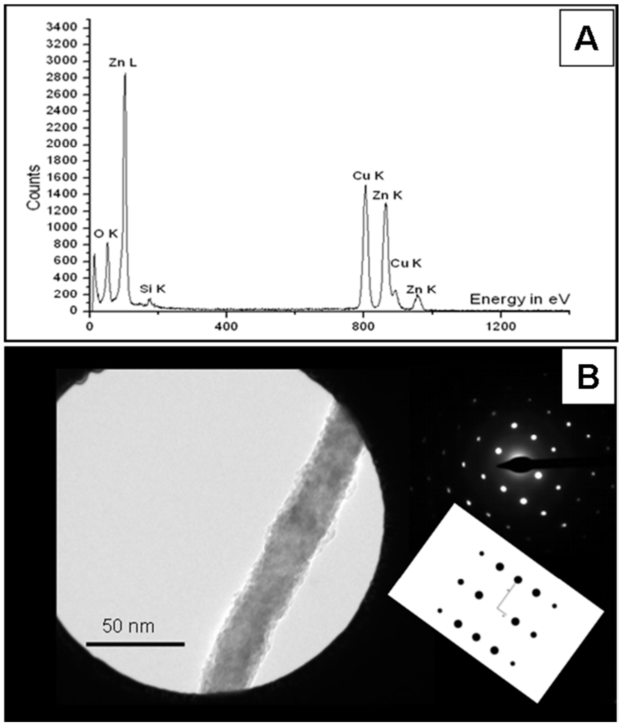

Figure 2.13: (A) Energy dispersive X-ray (EDX) spectrum of an individual ZnO NW showing the composition of the grown NWs. Zn and O peaks are clearly observed. In addition Si and C peaks are seen due to remains from the growth substrate and the holey carbon grid. (B) Selected area diffraction pattern of an individual NW shown on the left. The inset shows a simulated pattern assuming a *c*-axis growth, typical for solution-grown ZnO NWs.

These NWs, when subjected to rapid thermal annealing improve their crystallinity as also seen from the TEM images which show the disappearance of the amorphous sheath and a crystalline NW core. Energy Dispersive X-ray Spectrum analysis of these NWs shows the composition as can be seen in **figure 2.13**. The main peaks seen on the spectrum can be attributed to oxygen, zinc from NWs and to carbon and silicon coming from Grid and growth substrate respectively.

2.4. Hierarchical constructions of ZnO

In addition to synthesis of 1D nanostructures of ZnO in solution based methods, 2D and 3D nanostructures synthesis have been reported in literature by using-

1. morphology directing agents such as surfactants[83], weak acids and organic compounds [84, 85], different NPs as seeds [86] or
2. different precursor concentrations, reaction temperatures specifically or a combination of all [87].

There also exist indirect methods to synthesize ZnO nanostructures by calcination of Zn nanostructures formed in solution by self-assembly [88]. All of these methods build probably the biggest class of hierarchical structures available. Hierarchical nanostructures are attractive for their significance in self-assembly processes and other appealing applications like catalysis [89, 90]. Furthermore, the surface area of such structures increases rapidly as the complexity is increased making them promising candidates for a variety of sensing applications [91, 92]. Hierarchical superstructures are generally composed of a basic building block that repeats itself in a defined manner. In order to generate the hierarchy a growth directing agent is usually used which controls the direction in which the growth is repeated. Majority of the hierarchical ZnO structures that have been reported make use of-

1. capping agents, surfactant molecules or growth promoters/inhibitors [93]
2. solid material templates [94]
3. biological motifs [95, 96].

In all these cases, the hierarchical organization is defined by the underlying template or the growth-directing agent and cannot be altered arbitrarily without affecting the reaction equilibrium. Hierarchical superstructures have also been demonstrated using other methods such as vapor phase growth [97] or electrodeposition [98]. However, such procedures require either high temperatures or a suitable substrate and hence show very little versatility or flexibility for tuning the underlying architecture. The following text illustrates the formation of hierarchical structures without the use of templates or growth directing agents, which otherwise tend to increase the complexity of the system and in some cases affect the purity of the products. Furthermore, we use a simple low-temperature CBD growth that shows high potential for large-scale fabrication of hierarchical nanostructures in a very versatile manner[99]. Simple nanostructures such as nanoplatelets and NWs serve as building blocks and the hierarchical morphology is dictated by a judicious variation of the reaction conditions. At very low reactant concentrations, the pH of the growth medium, the temperature and other conditions have a decisive effect on the growth leading to 1D, 2D or 3D hierarchies with multiple levels. **Figure 2.14** show SEM images of the products obtained with HMT in a chemical bath at 85°C for 44 hours. These conditions deliver flower-like ZnO structures as can be seen in **images E** and **F**. These flowers comprise of individual hexagonal ZnO platelets that are assembled in a hierarchical manner. This is apparent in the figure **2.14** images from **A** to **E**, showing the evolution of the growth. The platelets are not always complete hexagons, 50-100 nm in thickness and typically 2-4 microns in diameter. The structures in **images C** and **D** exhibit a 2-level hierarchy, where a main hexagonal plate can be seen in the centre of the structure on which secondary platelets are attached. In **image E**, tertiary growth can be seen originating from the secondary platelets, while the final structures in **image F** show higher level of hierarchical self-assembly. Since the platelets from the secondary level onwards are oriented in all possible directions, the repeat direction can be considered to be an arbitrary vector in 3D and hence we refer to these structures as 3D multi-level structures[100]. In a second series of experiments, we replaced hexamethylenetetramine with methylamine keeping all the other reaction conditions the same as before. **Figure 2.15** shows SEM images of typical products observed at the end of the reaction. It is evident that dendritic structures are obtained with up to 3 levels of hierarchical self-organization. The repeat direction in this case is a 2D vector lying in the plane of the substrate. We refer to these viscous-fingers-like structures as 2D, 3-level hierarchical structures. The basic building block is again nanoplatelets similar to the previous case. However, as is apparent in the zoomed-in image in **2.15 B**, the basic block is not an individual platelet but is composed of stacks of a large number of platelets. Under the reaction conditions used here (mainly the concentration of the precursor and the absence of growth promoters) the ZnO nuclei which were formed [101-103] start coagulation in preferred orientations promoting the formation of nanoplatelets. These nanoplatlets act as a building-block for the grown nanostructures. After a certain growth period, the nanoplatelets may start assembling together in different configurations most likely to minimize the surface energy and give the final morphology of the product or may represent a primitive level of hierarchy which might serve as nucleation sites for further growth at subsequent levels of hierarchy (scheme)[104].

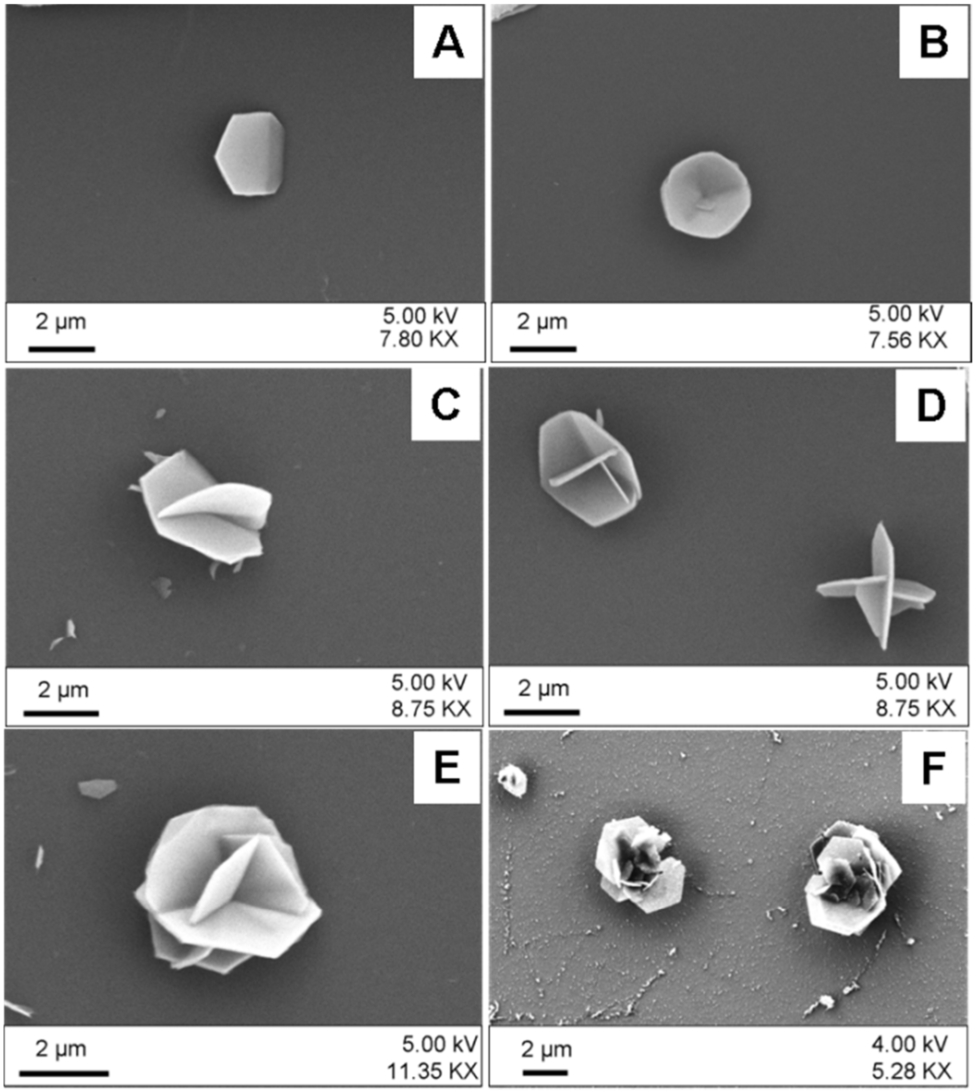

Figure 2.14: Temporal evolution of hierarchical 3D flower-like ZnO superstructures self assembled from nanoplatelets. The SEM Images show representative structures after (A and B) 6 h (C and D) 15 h (E) 24 h and (F) 36 h of growth. The basic building block here is a nanoplatlet that self-organizes in three dimensions to form multiple levels of hierarchy: (A and B) 1-level (C and D) 2-level (E) 3-level and (F) multi-level.

In order to shed light on the mechanism behind the growth of the different types of hierarchical structures (2D or 3D), we take a closer look at the chemistry of the formation of ZnO nuclei in solution. The reactions involved here for the case of HMT are-

$(CH_2)_6N_4 + 4H_2O <-> (CH_2)_6N_4\text{-}4H^+ + 4OH^-$

$Zn^{2+} + 4OH^- <-> Zn(OH)_4^{2-}$

$Zn(OH)_4^{2-} <-> ZnO + H_2O + 2OH^-$

Complete: $(CH_2)_6N_4 + 3H_2O + Zn^{2+} <-> (CH_2)_6N_4\text{-}4H^+ + ZnO + 2OH^-$ …….. (1)

The growth of ZnO nanoclusters with MA follows the following pathway:

$CH_3.NH_2 + H_2O <-> CH_3.NH_3^+ + OH^-$

$Zn^{2+} + 4OH^- <-> Zn(OH)_4^{2-}$

$Zn(OH)_4^{2-} <-> ZnO + H_2O + 2OH^-$

Complete: $4CH_3.NH_2 + 3H_2O + Zn^{2+} + 2OH^- <-> 4CH_3NH_3^+ + ZnO$ ....(2)

Both the chemical processes involved in the growth of nanostructures are similar yet yield different morphologies of the product.

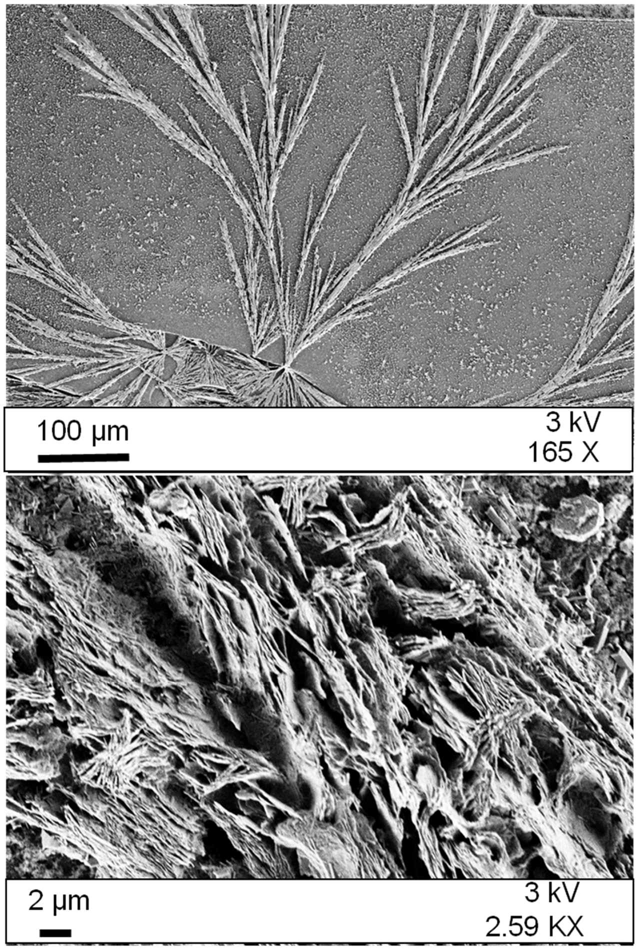

Figure 2.15: Dendritic viscous-fingers-like ZnO superstructures obtained at the end of growth in methyl amine and zinc nitrate at 85^0C. (A) SEM images showing an overview and (B) showing a zoomed-in region of the grown structures. The nanoplatelets tend to stack together and such stacks form the basic building block of the hierarchical structure. At least three levels of hierarchy can be identified in A.

This is attributed to different crystal growth behavior of ZnO nanostructures depending on the varied coagulation patterns of ZnO nuclei in preferred axes, affecting the shape, size and assembling pattern of the building blocks (hexagonal nanoplatelets in our case). The preferred axes of coagulation are due to the capping of cation-complexes and anions on to the differently charged crystal planes of ZnO nuclei. The resultant morphology is largely dependent on the amount of capping which in turn is a function of the stability of the cation-complexes and the anion's in the solution and also the amount of ZnO nuclei (concentration and temperature dependent) in the solution [105-107].

HMT is a weaker base than MA and dissolves at a slower rate. Furthermore, closed-chain hexamethylenetetrammonium cation complex is more stable than Methylammonium cationic complex which dissociates readily in water. This is consistent with the reactions shown in equations (1) and (2). The reaction equilibrium is shifted to the right when MA used for the growth accelerating the formation of ZnO nuclei. **Figure 2.16** shows the evolution of solution pH for both these reactions. Higher pH values in the start of reaction for MA than HMT is reflected as their difference in basicity and solubility in the solution. As the growth proceeds, solution pH reduces in the case of MA, while increases slowly for the HMT-based growth consistent with the fact that HMT-cation complex is more stable and dissolves rather slow than the MA-cation complexes.

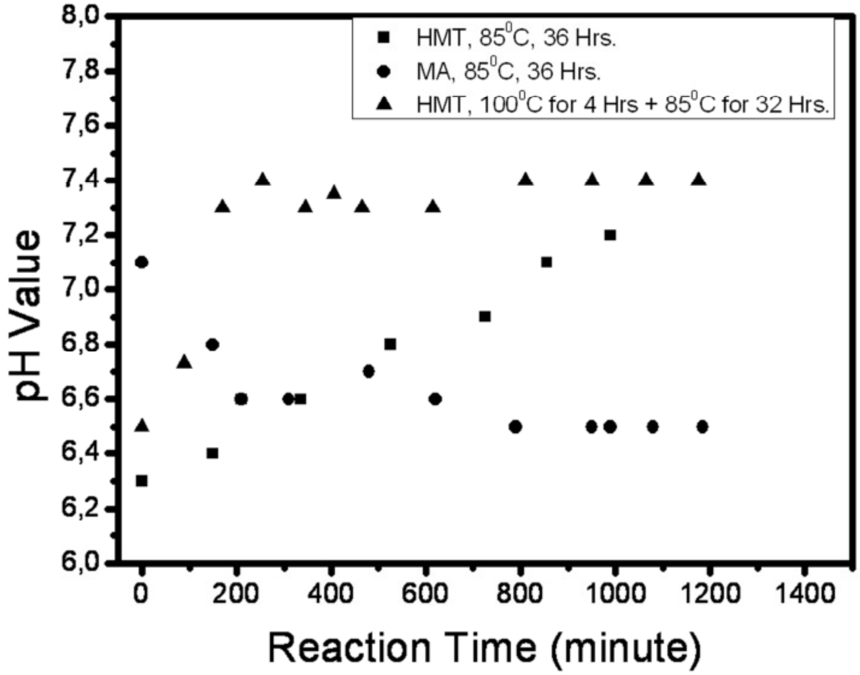

Figure 2.16: Evolution of solution pH during the growth of different hierarchical structures: (A) Rolling-pin-like structures, (B) Flower-like structures and (C) Viscous-fingers-like structures.

Imaginable that slow dissolution of HMT-cation complexes and anions is rather ineffective to prohibit ZnO hexagonal nanoplatelets stacking together unlike less stable MA-cation and anion. This aspect coupled with the pH decrease induces the stacking of sheets. In addition to this, in the case of HMT the slow formation of ZnO nuclei over time leads to the possibility of secondary and tertiary growth happening on the nanoplates formed already. In addition to these kinetic effects, electrostatic effects induced by the surface charge of the platelets (or nanostructures), crystal's polarization [108] might also play a role in self-assembling process in solution based growth processes.

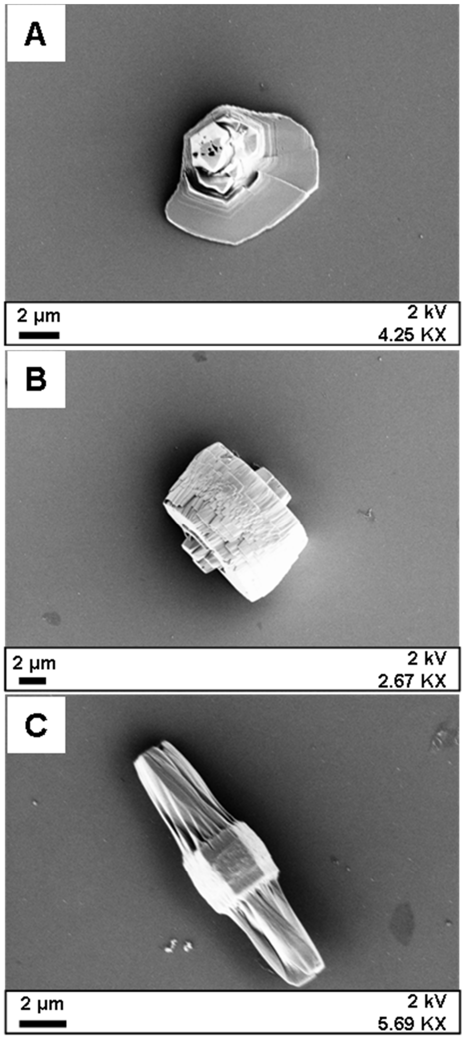

Figure 2.17: SEM images of rolling-pin-like structures at different growth stages: (A) after 7 hrs (B) after 15 hrs and (C) final structure after 36 hrs. The basic building block here is a thick platelet. In (A) the platelet in the first level is still growing. In (B) the first level is complete and the second level starts to grow. The diameter at the second level is lower due to the depleted amount of zinc ions in solution. In (C) the final structure with two levels of hierarchy can be clearly identified.

In order to gather support that the reaction kinetics has a strong effect on hierarchical organization, another series of experiments were conducted using HMT but at an increased temperature during the initial growth phase. As expected, the pH increases much more rapidly in this case as shown in **figure 2.16**. Typical examples of the resulting structures are shown in **figure 2.17**. The only difference in the reaction conditions between this case and that of **figure 2.14** (flower-like structures) is the higher temperature for the initial 4 hours.

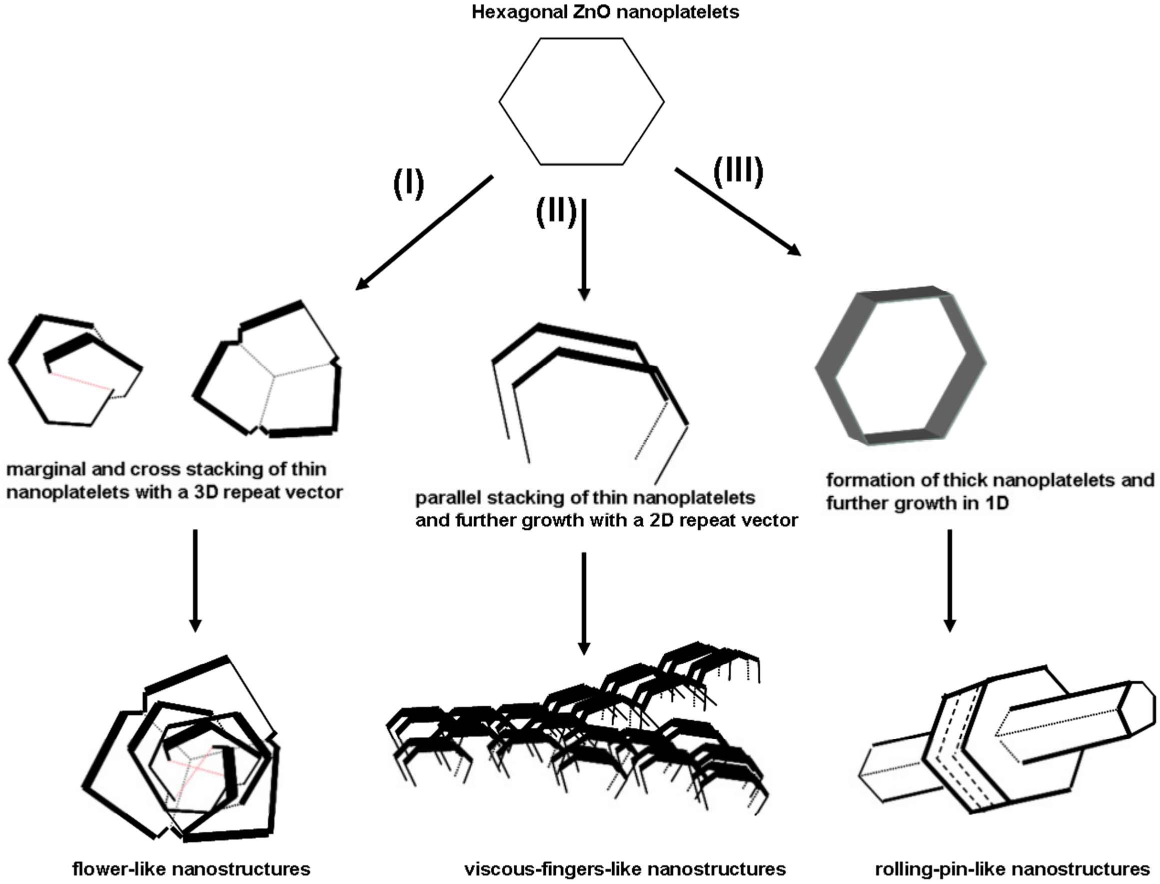

Scheme 1: The scheme shows the formation of different ZnO hierarchical superstructures from nanoplatelet building blocks. (I) Flower-like superstrucutures where the nanoplatelets self-assemble in arbitrary orientations. (II) The nanoplateletes stack together to form the basic unit that repeats itself in two dimensions resulting in dendritic viscous-fingers-like superstructures. (III) Thick nanoplatelets act as a building block to self-assemble in to rolling-pin like structures along one dimension.

It is apparent from **figure 2.17** that just this increased reaction rate is sufficient to change the morphology of self-assembly. At an increased temperature, hexamethylenetetramine will have more rapid dissolution and hence pushing the reaction towards producing larger amount of ZnO nanoclusters, cation-complexes and anions in the growth solution (reaction 1).The relatively higher OH^- concentrations can accelerate the dehydration rate of hydroxides ($Zn(OH)_2$) and promote the burst of the homogeneous nucleation. In this case, the coagulation rate would be much higher in the solution which ca lead to the formation of thicker hexagonal nanoplatelets [109-111]. Taking the thick platelets as the basic building block here, the repeat direction is a vector in 1D (along the axis of the structure). Hence, we refer to these structures as 1D, 2-level hierarchical superstructures. The smaller diameter at the second level is probably due to a reduction in Zn species and/or a different capping behavior. From the foregoing discussions, it is clear that by just varying the reaction conditions without the use of templates or growth directing agents, we have demonstrated 3D, 2D and 1D hierarchical structure with varying levels of complexity. The underlying structure can be understood by assuming that nanoplatelets or stacks of nanoplatelets are the basic building blocks and that the repeat direction can be a vector in 3D, 2D or 1D. A schematic of the three kinds of structures and the underlying organization is summarized in a **scheme 1**. These examples clearly demonstrate that the kinetics of the reaction and the choice of reducing agent can be varied to dictate the kind of hierarchical structures obtained in the investigated regime of low concentrations.

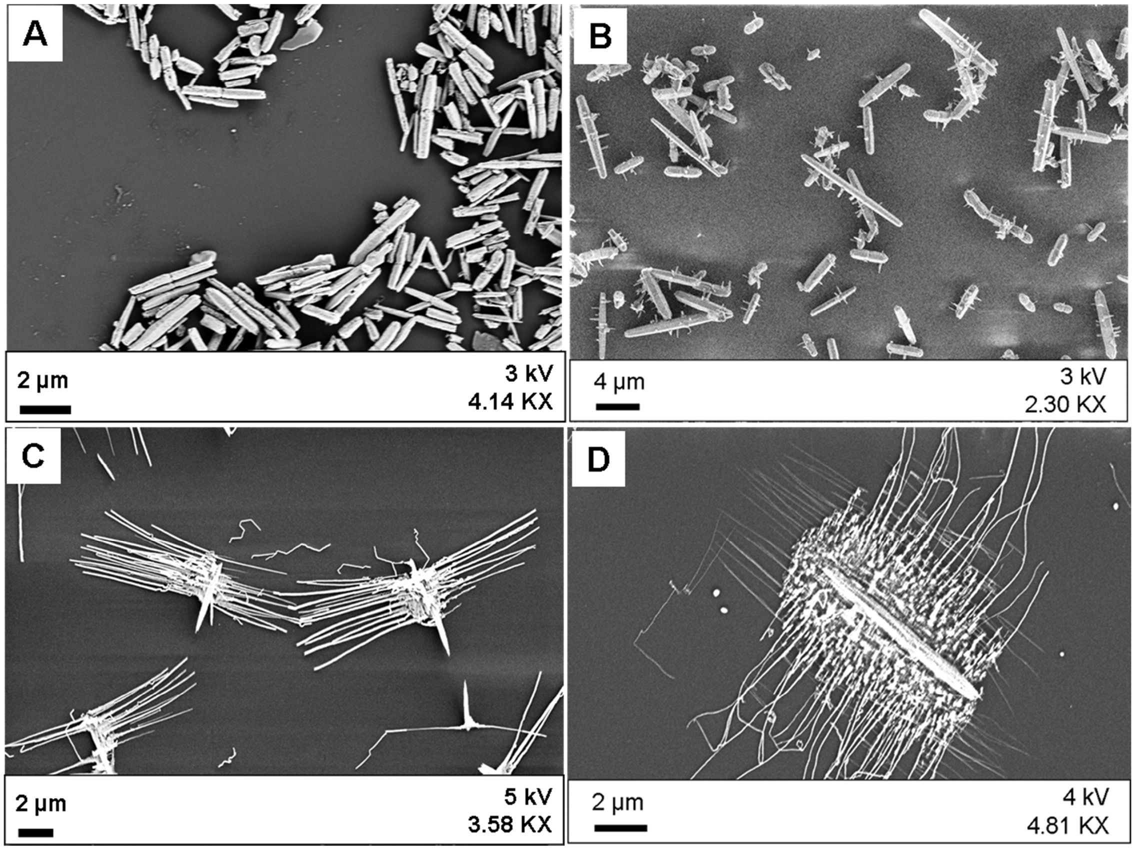

Figure 2.18: Yagi-Uda-antenna like ZnO superstructures obtained with NWs as building blocks. The SEM images show different stages of growth: (A) after 1 cycle of growth in 0.25 mM HMT at 85^0C for 2 hours; after a (B,C) second and (D) a third repeated cycle in a fresh growth solution with same composition. Au NPs were used as seeds only in the first cycle.

We explore the possibility of a hierarchical self-assembly further by deploying an alternative building block namely NWs. For this purpose, we have reduced the concentration of the precursor and HMT to 0.25 mM[99] In addition, Au NPs are used as seeds for the growth of

NWs in the first stage. A representative image of such a sample with NWs after the first growth stage is shown in **figure 2.18**.

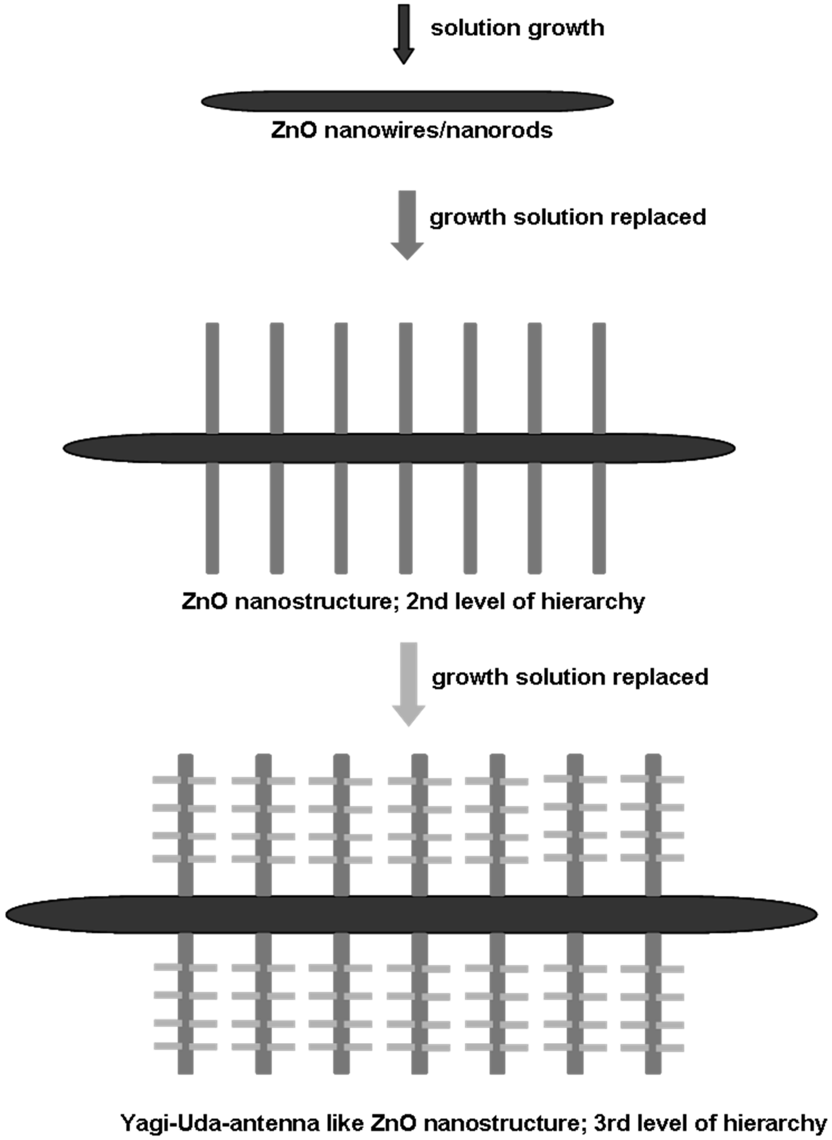

Scheme 2: The scheme shows the route of the formation of hierarchical ZnO superstructures with ZnO NWs as building blocks. Every new level of hierarchical self-assembly is achieved by refreshing the growth solution while maintaining the same composition of the reaction mixture.

In order to obtain hierarchical structures, we just replace the solution and start the growth afresh. **Image 2.18B** shows a typical image of samples a few hours (3 hrs.) into the second growth stage. It is apparent that new NWs start to grow from positions along the NW grown in the first stage. At the end of the second stage, secondary NWs of comparable lengths have grown from the first level NW as shown in **image 2.18C**. Upon repeating the same procedure by replacing the solution a second time, tertiary NWs are found to grow from the secondary

NWs, as shown in **image 2.18D**. Since the repeat direction is in 1D (the growth of NWs at any level happens predominantly perpendicular to the sub-level NW) and the structures show three levels of growth, we refer to these Yagi-Uda antenna-like structures as 1D, 3-level hierarchical superstructures. The formation of these superstructures is presented as in **scheme 2**. The choice of the reaction conditions (the lower concentration and the use of growth seeds) has determined the kind of building block that one can have in solution. The repeat direction for the hierarchical self-assembly is then a consequence of the solution pH, concentration ratio of precursors, their dissolution rate, and reaction kinetics etc. in low temperature solution growth processes, as also suggested in some recent reports [111]. It would be worth mentioning here, that the substrate on which the superstructures grow have an effect on the morphology. With NWs as building blocks we may obtain mainly 1D superstructure. However, structures with a 2D-repeat vector and 2-, 4- and 6-fold symmetry have also been reported[100]. The absence of these kinds of structures here supports the argument that the substrate has a considerable effect on the formation of these superstructures. Future experiments may be devoted to changes in morphology observable by tuning surface charge of the substrate with varying solution pH.

Chapter 3

Site-specific realization of ZnO NW transistors

This chapter will discuss the methods to fabricate ZnO NW field-effect transistors (FETs) on silicon chips and flexible kapton foils. The substrates were photolithographically written with microelectrodes which made the source and drain contacts. NWs were self-assembled in the source drain gap using (i) either dielectrophoretic (DEP) deposition of NWs from a solution or (ii) by using the solution based CBD growth method for NWs and growing them specifically in the electrode gaps. Here the advantages of using a CBD based self-assembled growth method over the DEP deposition of NWs for transistor fabrication will be discussed. The integration of microfluidics with ZnO NW transistors performed in different set-ups for transport characterization in liquids is discussed. Finally the chapter deals with the CBD based fabrication method of ZnO NW transistors and their integration with microfluidics for scalable fabrication.

3.1 Experimental

The experimental part of this chapter refers to all preparation steps involved in the fabrication of ZnO NW transistor deployable in liquid environment for sensing purposes. The following continues with the discussion of types of substrates used for the preparation of transistors and strategies to facilitate a liquid gate for transistor operation and handling of liquid samples for sensing.

3.1.1 Substrates

Si/SiO_2 chips were used in a first step for the fabrication of ZnO NW FETs. The strategies for fabrication of ZnO NW transistors using self-assembled growth of NWs and DEP deposition started with the use of prewritten silicon chips. Microelectrode pairs working as source and drain were written photolithographically on the substrate. ZnO NWs could be grown on top of silicon substrate between the source and drain electrodes forming a transistor channel or alternatively deposited from a solution using DEP technique. Generally the transistors fabricated in this configuration use Si/SiO_2 substrate as a gate and referred as back-gated transistors. The insulation between NW channel and Si/SiO_2 gate is provided by the several hundred nm thick SiO_2 layer formed on the Si surface by its oxidation. The thickness of the insulating layer can be varied by controlled oxidation process of Si chips. Normally the thickness of a few hundred nanometers (from 150-600 nm) serves well for back-gated FET applications. Because of the insulatiory material used between the gate and the channel, back-gated FETs can also be called as insulated-gate FETs.

Back gated FETs deployed widely in electronic appliances and many applications where devices are deployed in a non-liquid environment. However, back-gating is not required in FETs when needed deployment in liquids and this opens up opportunities to use insulating and flexible polymer materials as substrate for transistor fabrication. The use of such flexible substrates can be exploited widely for *in vivo* applications of transistor devices e.g. biosensing[112, 113]. Polymer substrates which are wear-resistant, temperature stable, flexible and robust for packaging can be promising candidates to be used as substrate material for such practices. For the fabrication of liquid gated field-effect transistors on such flexible substrates, a polyimide polymer material commercially known as Kapton was used in this work. **Figure 3.1** shows the schematic of a liquid gated transistor fabricated on a Kapton foil.

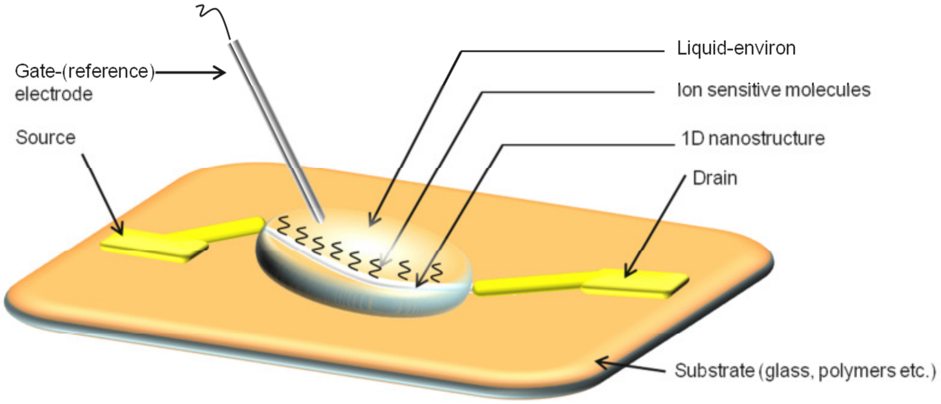

Figure 3.1: Schematics of a liquid-gated FET for sensing in liquids. A NW transistor can be fabricated on polymer substrate and deployed in an electrochemical gate. Source and drain microelectrodes can be written using photolithography.

Kapton is a polyimide film developed by DuPont which is stable for wide range of temperatures. Kapton is used in, among other things, flexible printed circuits (flexible electronics) and thermal micrometeoroid garments, the outside layer of space suits. The chemical name for Kapton K (as used in the experiments) and HN is poly(4,4'-oxydiphenylene-pyromellitimide). It is produced from the condensation of pyromellitic dianhydride and 4,4'-oxydiphenylamine in step polymerization. The ring closure is carried out at high temperatures (200–300 °C, 473-573 K). Kapton provides very smooth surface for electrode writing and possess Young's modulus up to 430,000 lb/inch^{2}at 25^0 C.

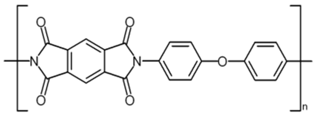

Polyoxydiphenylene-pyromellitimide

3.1.2 Photolithography

FET fabrication on polymer materials often poses engineering hurdles as the polymer substrates are often not compatible with photolithography or e-beam lithography electrode writing owing to their soft surfaces and chemical properties. Kapton surfaces are stable at high temperatures and can be used for electrode writing photolithographically. However, Kapton foils need surface modification to convert the intrinsically hydrophobic surfaces to hydrophilic surfaces for better adhesion of microelectrodes. The Kapton foils for this work were written with Ti/Pt or Cr/Pt microelectrodes at the Technology Group at Max Planck Institute for Solid State Research Stuttgart. Before this, the Kapton foils were modified by chemical treatment in order to achieve the desired hydrophilic properties. Following is the description of photolithography procedure on Kapton foils.

500 micron thick Kapton roll was obtained from DuPont which was cut into smaller 80×80 mm pieces for the fabrication of microelectrodes. However, owing to the chemical composition of the polymer, it has hydrophobic surface and makes a very poor adhesive to other materials. The foil surface was modified as follows before beginning with the photolithography. The foils cut in to smaller pieces were cleaned in methyl alcohol and acetone for 5 minutes each to remove any greasy contents from the surface. The pieces were then put in 1M NaOH/KOH for 10 minutes which changes the polymer surface into polyamate of Na or K respectively. The pieces are removed from basic solutions and kept in 0.2M HCl for 5 minutes to protonate the polymer surface. The protonation of the surface molecules results in polyamic acid [114]. The opening of the molecular rings of the surface molecules and introduction of carboxylic groups make the polymer surface hydrophilic and better adhesive for other materials such as Cr/Ti/Pt which were to be written in form of microelectrodes over the surface. The schematics to clean a Kapton foil, surface treatment and the lithography process are presented in **figure 3.2**. **Figure 3.3** shows the mask used for the development of the Kapton wafers.

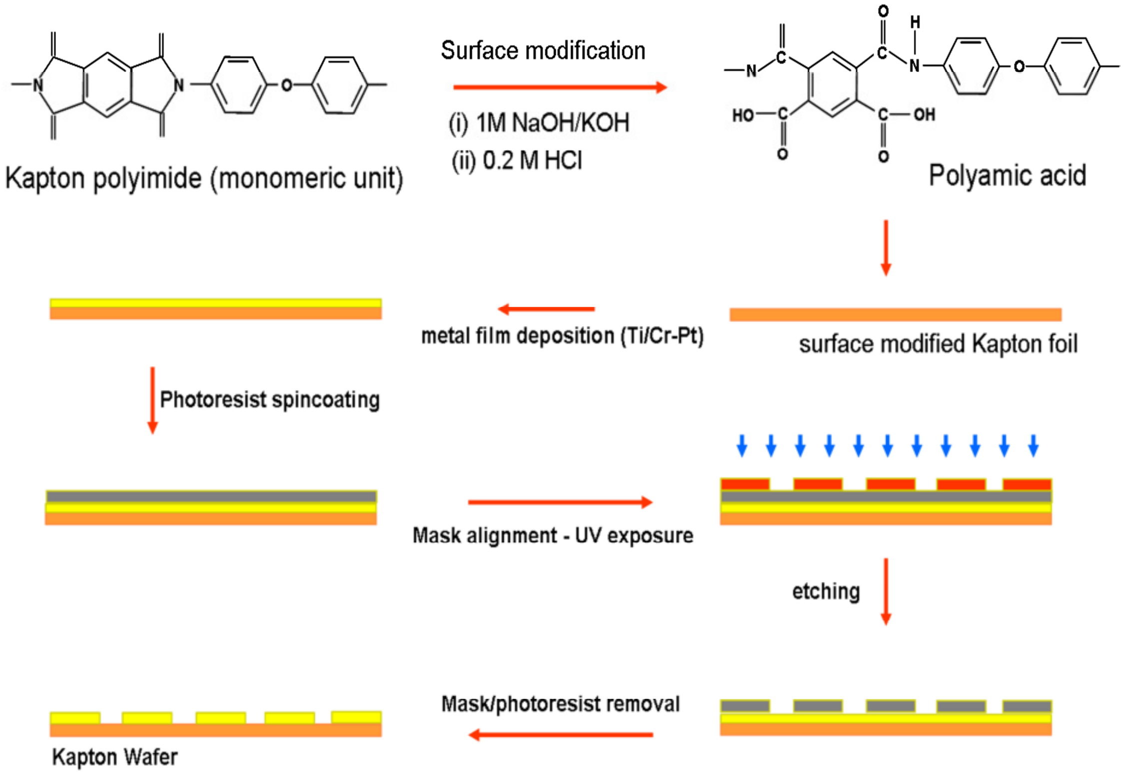

Figure 3.2: Schematics of the surface modification of Kapton in a chemical process.

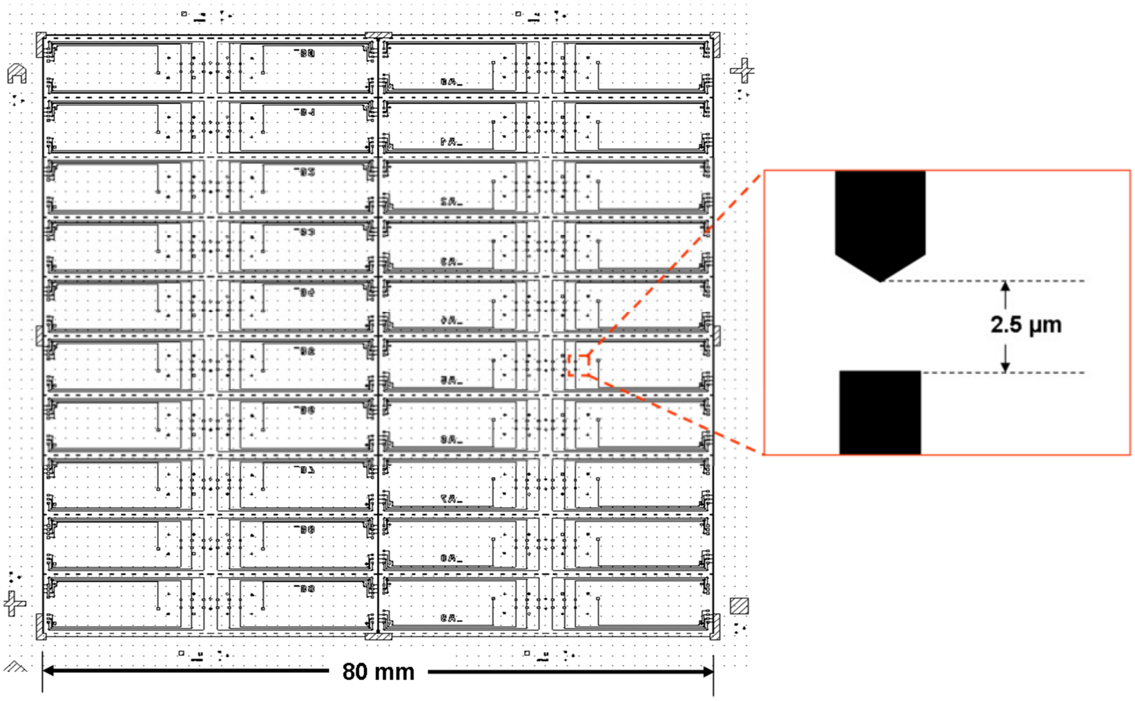

Figure 3.3: 80×80 mm Kapton foil photolithography mask defining 20 units each one having 6 microelectrode pairs and 2 reference electrodes (Pt). A microelectrode pair is shown in inset with a 2.5 micron gap between the source and drain electrodes.

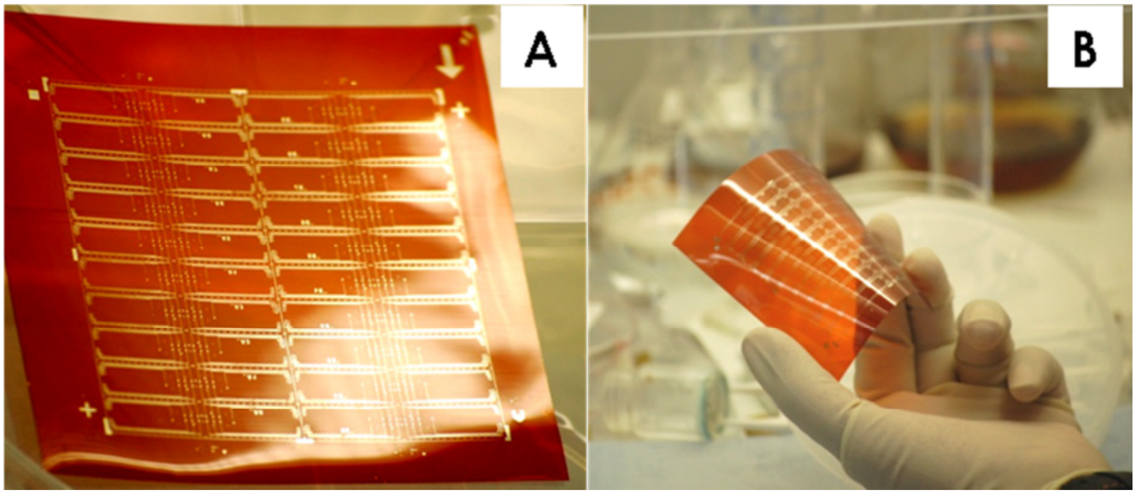

Figure 3.3: (A and B) 80×80 mm Kapton foil written with 120 position microelectrode positions to be deployed for the transistor fabrication.

A Kapton foil at the end of the fabrication procedure is shown in **figure 3.3 A** and **B**. Cr/Pt microelectrodes are written on the foil using the mask as shown in **figure 3.2 B**. The foil shows 20 units each having 6 microelectrode gaps, thus yielding a sum of 120 electrode gaps on 80×80 mm surface. As apparent from the image in **3.3 B** the foil is bendable and exhibit microelectrodes robustness.

3.1.3 Microfluidics

Integration of fluidics with electrical and optical devices in recent years has provided thrust for sensing applications in liquids and has generated huge scientific interests. Low sample volume dependence of the label-free and direct electrical detection methods with the evolution of nanoscale electrical sensors needs to be complimented with new strategies for handling these ultra-small liquid samples. Thus fluidic integration with electrical sensors also holds promise in developing lab-on-a-chip systems (L-o-Cs) for future applications in medical diagnostics, chemical sensing and other analytical purposes [12, 115, 116]. For example, the latest diagnostic plate assay techniques used in healthcare consuming hundred of microliters (μl) of reagents would largely benefit from the micro-fabricated nanoliter volume arrays. This could already reduce the consumption of reagents by a factor of $10^3 - 10^4$ and save the costs on the repetitive assays often performed in a diagnostics lab.

NW/NT FETs used for label-free electrical sensing provide large surface area for the functionalization of receptors in significant numbers. High density of receptors on transistor channel significantly increases the probability of analyte-receptor interaction from smallest fraction of a liquid sample and adds to a maximum sensor response. Using microfluidic channels helps confine smallest sample volumes in the vicinity of receptors (functionalized on the transistor channel) and ensuring a continuous flow of analytes thus achieving sensor response from small sample volumes of low analyte concentrations. Hence handling of small sample volumes is critical to the development of future electrical sensors with high-sensitivities and fluidics is an integral part of the strategies to achieve that. Main advantages of integrating fluidics in electrical sensors are as follows-

1. Low volume consumption, faster analysis and short response time of the devices -due to short diffusion distances inside micro-fluidic channels, fast heating, small heat capacities and high distribution of analyte molecules on the device surface.
2. Possibility of high level integration and parallelization on chip -provides scope for multifunctional devices and compact µTAS allowing high throughput analysis.
3. Integration of a closed fluidic system -provides safe platform for chemically and biologically active materials and lowers fabrication costs, allowing cost-effective disposable chips fabricated in mass production.
4. Prevents evaporation of liquid maintaining a homogeneous concentration of analytes.
5. The flow of liquid sample in a closed channel helps preventing the accumulation of analytes on the surface of devices.

Fluidic systems started to appear when semiconductor technology was extended to liquids for some applications in life sciences in 1970s [117]. The first devices to explore microfluidics were fabricated on silicon and glass chips using photolithography and etching techniques borrowed from microelectronics [118, 119]. Expensive and inflexible, but these techniques provided a platform to study the fluidics in micron and submicron channels. With over two decades of scientific practice in micro-fluidics and integrated systems have developed techniques to fabricate advanced microfluidic components. Microfluidic valves, pressure systems, and reaction chambers etc. can be constructed using soft fabrication techniques (injection molding, hot embossing, laminar flow patterning etc.) using printable and moldable organic materials [120-124]. Flexible and transparent organic polymer materials like polydimethylsiloxane (PDMS), SU-8 (developed by IBM), TOPAS COC-A resins, PMMA/plexigels, polycarbonates are available for building microfluidic components in desirable shape and size. Several metals can be integrated with these polymer materials to be used as various components of L-o-C systems.

This section of the chapter mainly presents the methods of handling liquids while performing electrochemical gating with ZnO NW transistors. Integration of open microfluidic channels made of silicon nitride onto silicon chips and closed PDMS microfluidic channels on to silicon chips and Kapton foils will be discussed in detail as a measure to facilitate the flow of liquid analytes.

(i) Spotting/Microfluidic Well

A droplet spotting was used to immerse the ZnO NW transistors in small liquid volumes for electrochemical gating. Microliter volumes of liquid can be placed in this manner covering the transistor channel with the help of a micropipette. The Ag/AgCl reference electrode could be placed touching the droplets in order to apply gate voltage through the liquid. The evaporation of liquid droplet during the transport measurements was prohibited by squalene covering. Alternatively, microfluidic wells made of PDMS were also used to facilitate set up for liquid gating. **Figure 3.4 A** and **B** show optical images of liquid gating set-up using PDMS microfluidic wells assembled on top of silicon chip and Kapton chip respectively.

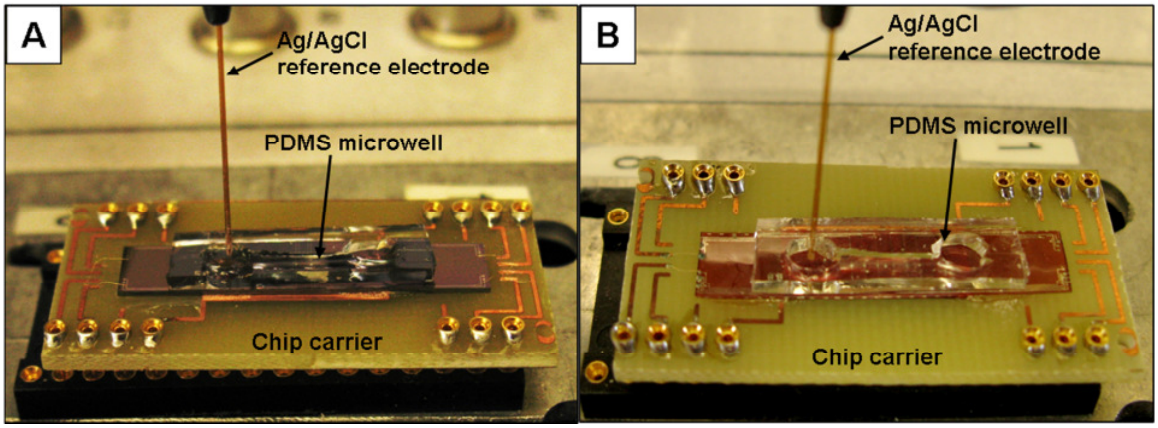

Figure 3.4: (A) PDMS based microwell assembled on top of silicon chip and (B) on top of Kapton chip.

PDMS blocks were prepared using two components SYLGARD(R) 184 Silicone Elastomer Kit. 184 polydimethylsiloxane elastomer and a curing agent from the kit are mixed in 10:1 ratio and cured at 70^0C for 2 hours to form transparent and flexible blocks of the polymer. The polymer formed is compatible to ceramic, plastics, glass and polyester materials which are advantageous when working with different materials. The microwells were carved out in the PDMS manually and assembled on top of silicon and Kapton chip just exposing the transistor channel. Small volumes of liquid samples could be filled inside the microfluidic channel. Reference electrodes were also placed in the microwells in order to apply gate voltages through the liquid.

(ii) Integrated open channels

Silicon nitride made microfluidic units were assembled on top of silicon chips during the fabrication steps. The silicon nitride layer was deposited by plasma enhanced chemical vapor deposition on the silicon substrates while Pt microelectrodes were photolithographically written before. Microfluidic channels ending into two reservoirs on both sides were carved out in Si_3N_4 layer using reactive ion beam etching technique. **Figure 3.5** shows the design of silicon chips with open microfluidics. Image A in the figure shows an optical image of 4×4 mm silicon chip with four microfluidic units on each corner.

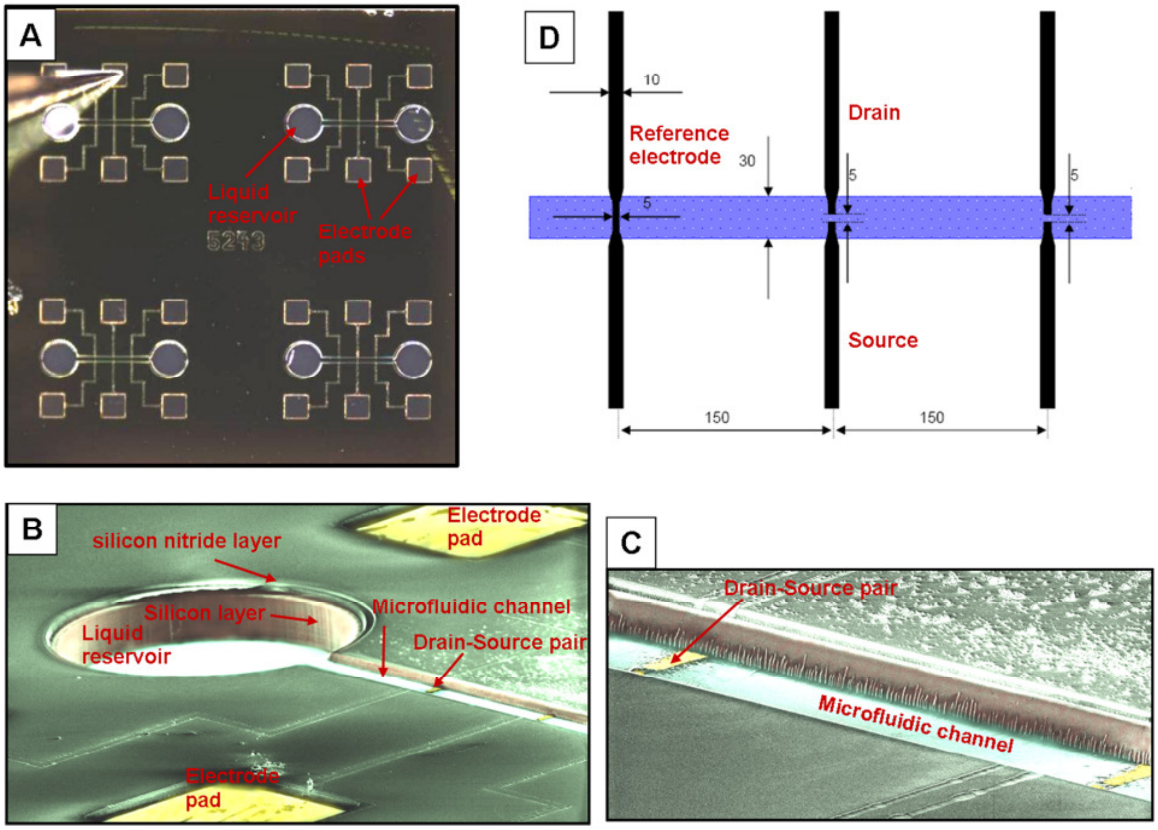

Figure 3.5: (A) An optical image of 4×4 mm silicon chip integrated with 4 open microfluidic units. (B) SEM image of a part of microfluidic unit showing silicon nitride made liquid reservoir and microfluidic channel. (C) SEM image of a part of microfluidic channel showing two drain-source microelectrodes lying in the microfluidic channel. The ZnO NWs are assembled on these positions to fabricate a transistor. (D) Schematics of dimensions of electrodes and MF Channel (all numbers in microns).

Over this lies a 600 nm thick layer of Silicon nitride. Each microfluidic unit consists of a microfluidic channels with 30 micron width and 10 micron depth. The reservoirs can be filled with the liquid sample and the liquid travels through the microfluidic channel running over microelectrodes which also lie in the channel. Image B shows SEM image of a part of one microfluidic unit showing the liquid reservoir and a microfluidic channel running on the surface. Image C shows SEM image of middle part of the microfluidic channel showing Pt microelectrode lying inside forming drain-source pairs. The electrodes run towards each other and make a gap of 5 microns in the channel. Image D shows the lay-out of microelectrodes in a microfluidic unit. Two microelectrode pairs forming a 5 micron gap in the channel lye together with a continuous Pt microelectrode separated by a distance of 150 micron. The continuous microelectrode running across the microfluidic channel serves as a reference (gate) electrode. All four microfluidic units together provide 8 microelectrode gaps to for device fabrication. The microfluidics integration to silicon chips served dual purpose of electrical characterization of ZnO NW devices in back-gated and also in an electrochemical gate.

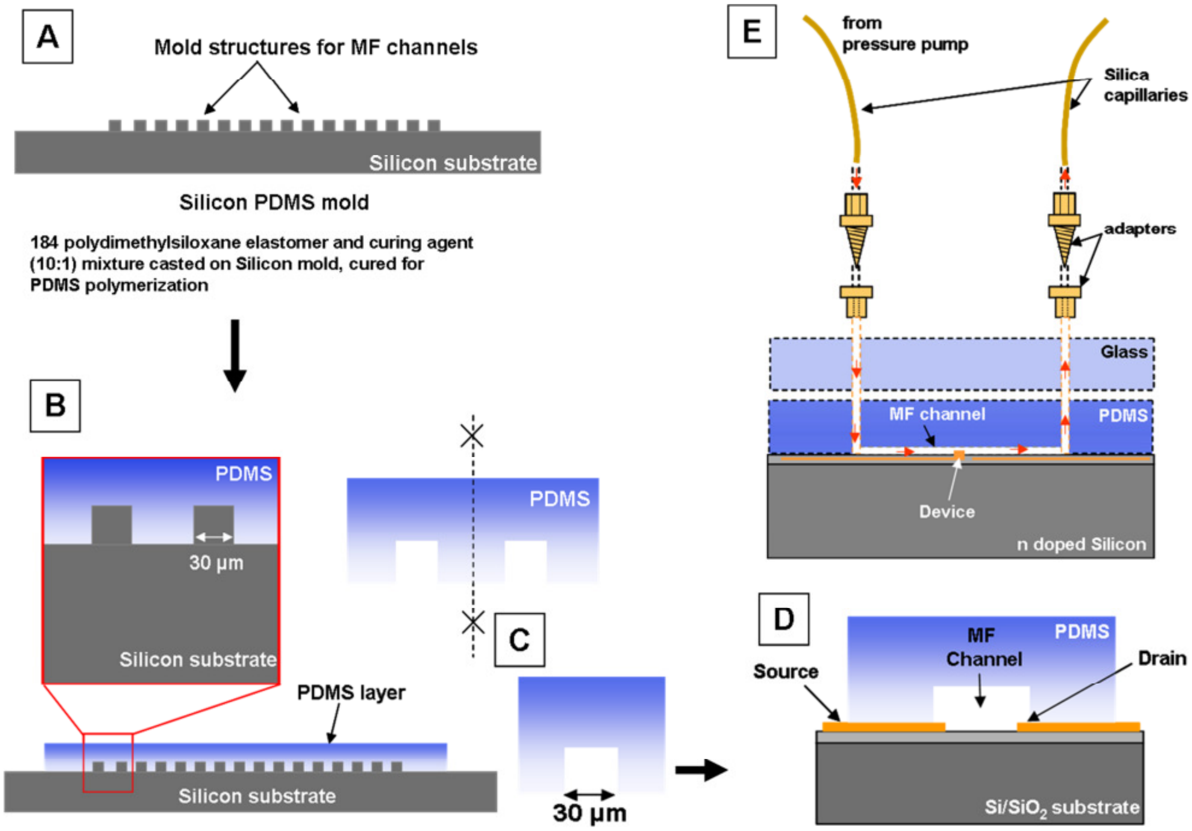

Figure 3.6: (A) gives a schematic view of the mold used for PDMS based microfluidic system. The mold is prepared using photolithography on a Si/SiO$_2$ substrate. (B) A mixture of elastomer and curing agent is coated on the mold and put to curing conditions. (C) A solid PDMS polymer layer is formed on the mold with micron sized channels, which were carved into the layer by the structures on the mold surface. The polymer is transferred from the mold and cut into suitable pieces to assemble on top of the Chips. (D) PDMS pieces with carved in MF channels are assembled on the devices creating a closed microfluidic channel as shown in the schematics. (E) This Chip integrated with closed microfluidics on top is connected to an external system to provide the liquid flow. PDMS layer is covered with a perforated glass chip which connects the MF channels to the capillaries with the help of adapters.

(iii) Continuous flow microchannels

Closed microfluidic systems are important for liquid sample handling for electrical sensing purposes for the reasons discussed before. The methods to carry out integration of a closed microfluidic systems on to silicon and Kapton chips will be discussed here. PDMS was used as a material for the construction of channels. **Figure 3.6** illustrates the processes involved in assembling the channel on top of chip. A layer (2mm thick) of the mixture of PDMS elastomer with curing agent was poured over a mold and kept for curing. The mold was prepared by standard photolithography technique on a Si/SiO_2 substrate which has 30 micron wide structures defined on its smooth surface. These structures carve into the polymer matrix coated on the mold and leave a groove behind in the solid PDMS layer post polymerization. The solid polymer layer is then cut into substrate size pieces. The PDMS pieces with the channels can now be assembled on to the Silicon chips or Kapton foils with a chip aligner or manually to expose the transistors on chip inside the MF channel. The silicon and kapton chips now integrated with closed microfluidic channels can be connected to a flow system with the help of capillaries and connectors.

3.2 Fabrication of field-effect transistors (FETs)

Fabrication of NW transistors conventionally involves deposition of NWs on a substrate followed by identification and mapping of their location on the substrate and subsequent e-beam lithography process.

There exist other methods to fabricate a transistor where contacts of NWs are not written with methods like e-beam lithographic deposition of contacts, but by the alignment of NWs from solution onto prefabricated microelectrodes. Dielectrophoretic deposition of NWs is such a method for the fabrication of NW transistors. Another possibility is to grow NWs on the microelectrodes which can bridge the gap between source and drain electrodes to form a transistor channel. Such a method would require a self-assembly growth of a desired 1D nanostructure in the microelectrode gap. The following presents the work done on the dielectrophoretic fabrication of ZnO NW transistors followed by self-assembled fabrication of ZnO NW transistors.

3.2.1. Dielectrophoretic fabrication

Movement of particles when subjected to a non-uniform electrical field is called Dielectrophoresis (DEP). The term was first coined by Herbert Pohl [125]. Pohl defined in his book [126] dielectrophoresis as the translational motion of neutral matter caused by polarization effects in a nonuniform electric field. Particles are attracted to the stronger electric field regions given the permittivity of the particles exceeds the medium. When the permittivity of the medium exceeds that of the particles, the particle motion reverses. DEP (dielectrophoresis) is readily observed for the particle sizes from 1 micron to 1000 microns.

In theory, the dielectric force F_{dep} for a homogeneous isotropic dielectric sphere is given by:

$$F_{dep} = 2\pi r^3 \varepsilon_m \mathit{Re}\, [K(\omega)](dE/dx)^2$$

where, r is particle radius, ε_m is permittivity of the suspending medium, *d* is gradient, *E* is the RMS electric field and *Re* [K(ω)] is real part of the Clausius-Mossotti factor determined by the complex permittivities (which is ratio of the conductivities and angular frequency of applied field) of the medium and particles. The frequency and particle polarizability dependence of Clausius-Mossotti factor indicates that the force on the particle varies with the frequency of the electric current and the relative polarizability of particle in the suspension medium. From the Clausius-Mossotti factor we can say that if the value of the factor is positive, then the particle moves to regions of highest field strength (***positive dielectrophoresis***) or away (***negative dielectrophoresis***) from the highest field region if the value is negative.

Manipulation of nanometer sized objects was first demonstrated by NG Green and H Morgan 1997 where they separated different populations of NPs applying a non-uniform AC electric field between castellated microelectrodes[127]. Dielectrophoresis until then was considered as a practical technique for separation of mammalian cells and microorganisms [128], e.g. separating cancer cells from blood [129], enriching CD34+ Cells in bone marrow samples [130] and for detecting the viability of pathogenic organisms in water [131]. Dielectrophoretic methods to assemble NWs/nanotubes began to emerge soon after and were reported from several groups who demonstrated orientation, purification or alignment of nanostructures to make devices [132, 133].

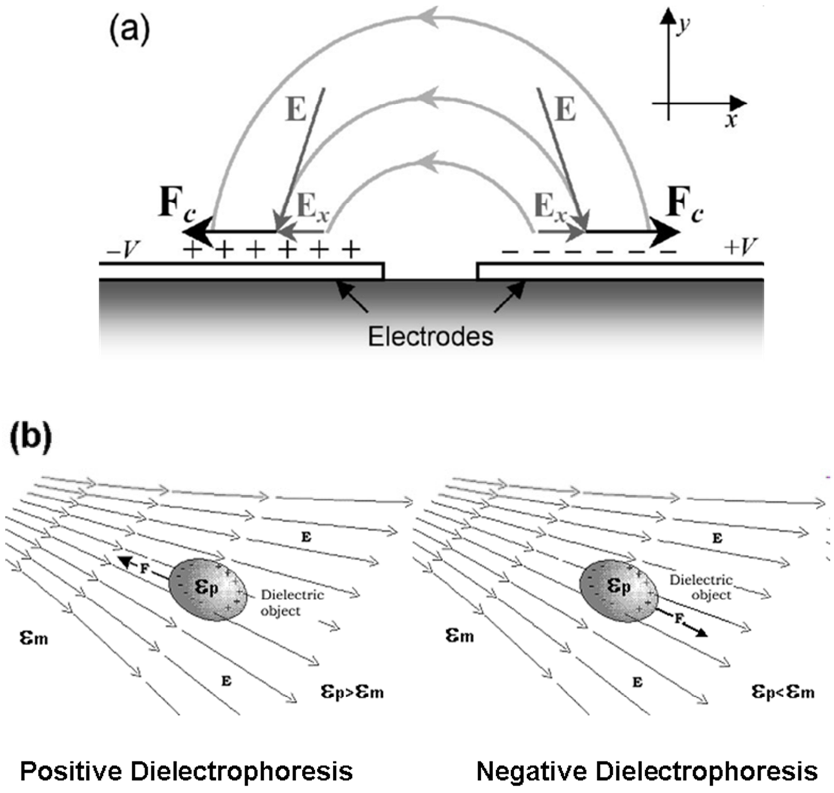

Figure 3.7: The schematics showing the field lines in cross configuration of a dielectrophoretic set-up (a) and representing the movement of a particle in electric field; (positive and negative dielectrophoresis. (-reproduced from www.blazelabs.com)

These methods were further developed by some other groups in making devices with NWs and carbon nanotubes [134, 135] and self-assembly of NPs [136] etc. Most of the works relate to the fabrication of nanoscale devices with different nanostructures for various applications[32, 137-140]. The dielectrophoretic methods represent a promising method to fabricate nanoscale device at small and large scales on different substrates [141-144]. For the fabrication of transistors, we deployed AC dielectrophoresis on CVD grown ZnO NWs. CVD grown wires on Si/SiO$_2$ substrates were obtained from Max Planck Institute Halle. NWs were peeled off from the substrate with the help of a sharp razor and brought into ethanol solution. The ethanol solution with the scrapped off NWs were subjected to sonication to disperse the NWs in the solution. Dielectrophoresis is performed as depicted in the **figure 3.8**. Si/SiO$_2$ chips having microelectrode pairs of Ti-Pt with a 2 micron gap were used for the trapping of ZnO NWs from the ethanol solution. The microelectrodes were connected to a function generator as showed in **figure 3.8**. A drop of ZnO NWs in ethanol is dropped on the gap between microelectrode pairs as shown in the figure.

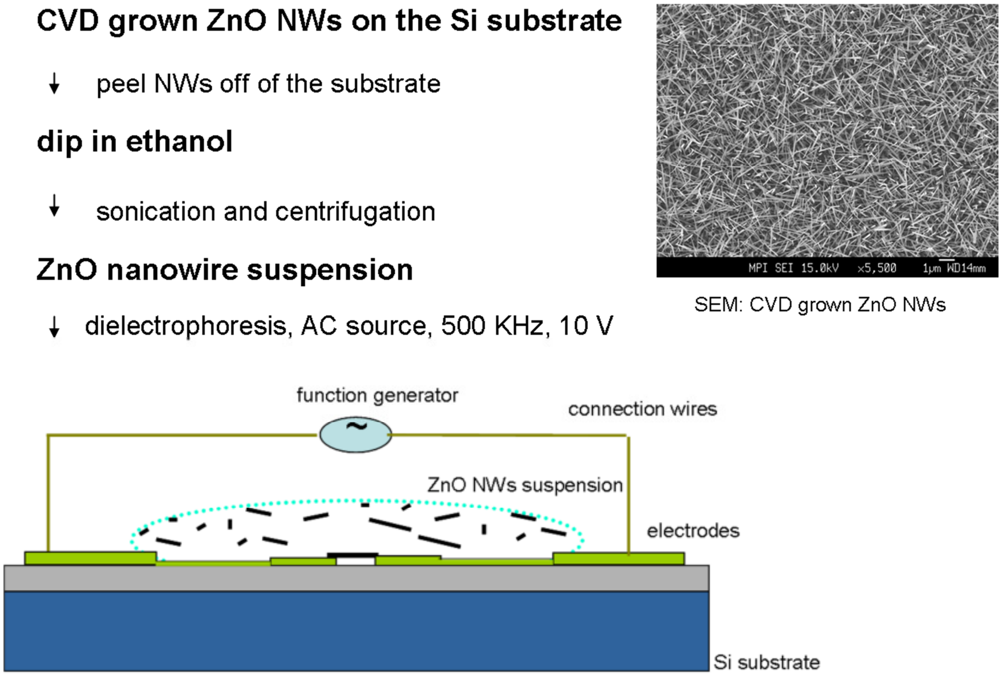

Figure 3.8: Schematic of the dielectrophoretic deposition of ZnO NWs on prefabricated microelectrodes.

The dielectrophoretic field between the electrodes aligns the NWs across the gap resulting in a connection between the two electrodes. The number of ZnO NWs deposited depends on the time of dielectrophoresis and the strength of the field applied.

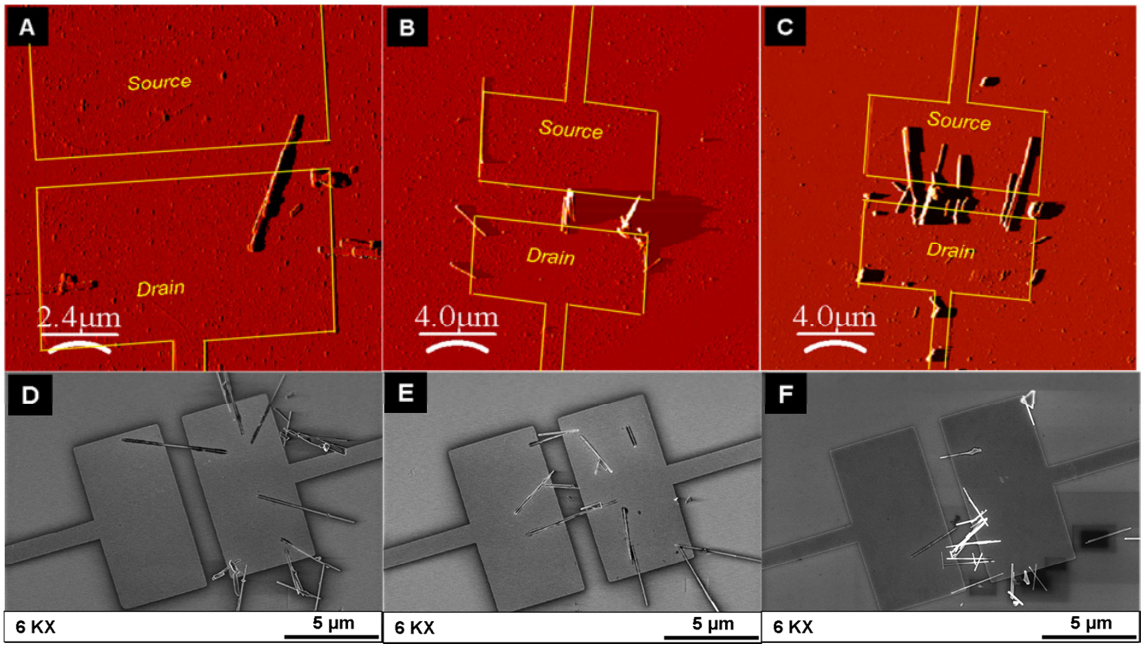

Figure 3.9: ZnO NW transistor fabricated using dielectrophoresis. A, B and C show AFM images of devices where DEP was applied for 30 s, 45 s and 60 s respectively at a constant field. D, E and F show SEM images of the devices respectively where 500 kHz, 1 MHz and 10 MHz AC at 10 Vpp was applied for the DEP deposition of ZnO NWs.

The fabricated devices were characterized using a confocal laser scanning microscope, scanning electron microscope and an atomic force microscope. **Figure 3.9** illustrates confocal images of some devices where ZnO NWs are deposited using differing parameters of the electrical field (figure 3.7 A to F)

Electrical Characterization:

The experimental set-up used for the electrical transport measurements comprised of a voltage source (Keithley 2400) that supplies the drain-source bias. A home built current-to-voltage converter was used to amplify the drain current signal, which was then recorded by a multimeter (Keithley 2000).

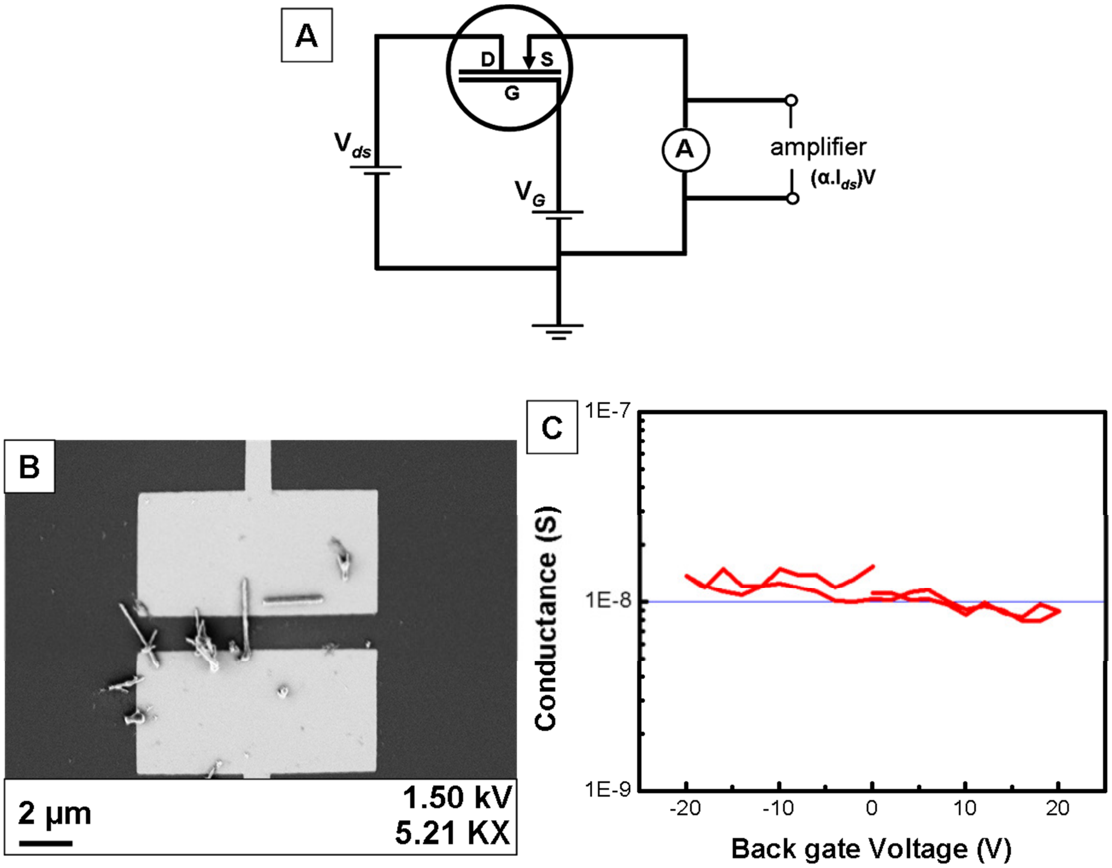

Figure 3.10: (A) Schematic of the back-gated electrical measurement set-up (B) SEM image of a ZnO NW transistor fabricated using dielectrophoresis and (C) Field-effect characteristics of the device in a back-gated configuration after annealing in air at 800^0C for 25 seconds.

In addition to this, another voltage source (Keithley 2400) was used to supply the gate-source voltage and to measure the leakage current flowing through the substrate. A manual wafer probe system (Süss Microtec PM5) with probe heads and probe needles was used to contact the pads leading to the electrodes. The current-voltage (*I-V*) characteristics of the samples were measured by recording drain current as a function of applied drain-source bias. Conductance vs gate voltage (G vs Vg) plots were obtained repeating this procedure at different gate voltages. It is noteworthy mentioning that only two-probe configuration was used for the electrical measurements on all the devices. The measured resistance of the device comprises of the intrinsic resistance of the NW and the contacts. Typical devices fabricated using dielectrophoresis showed high resistivities measuring several hundred megaohms or gigaohms. The devices did not show any significant conductance variation on gate voltages applied. One of the reasons could be very low level of ‘oxygen vacancies’ in CVD grown wires. Oxygen vacancies are further lowered by the annealing treatment of the devices to achieve optimal contacts. Thus despite the good quality of CVD grown wires it was not possible to fabricate high performance devices in a scalable method using dielectrophoresis. The effect of annealing ZnO NW transistors in air will be discussed later in this chapter.

3.2.2 Site-specific self-assembly of ZnO NW transistor

In any conventional method to fabricate ZnO NW transistors, NWs are usually produced ex-situ in various synthesis methods [37] which requires the use of a different substrate. As a result, the NWs need to be transferred from the growth substrate in to dispersion via scratching or sonication methods. While these methods however lack the possibility to provide a scalable method for device fabrication, strategies to the grow ZnO NWs from predefined positions advocated for a global fabrication method.

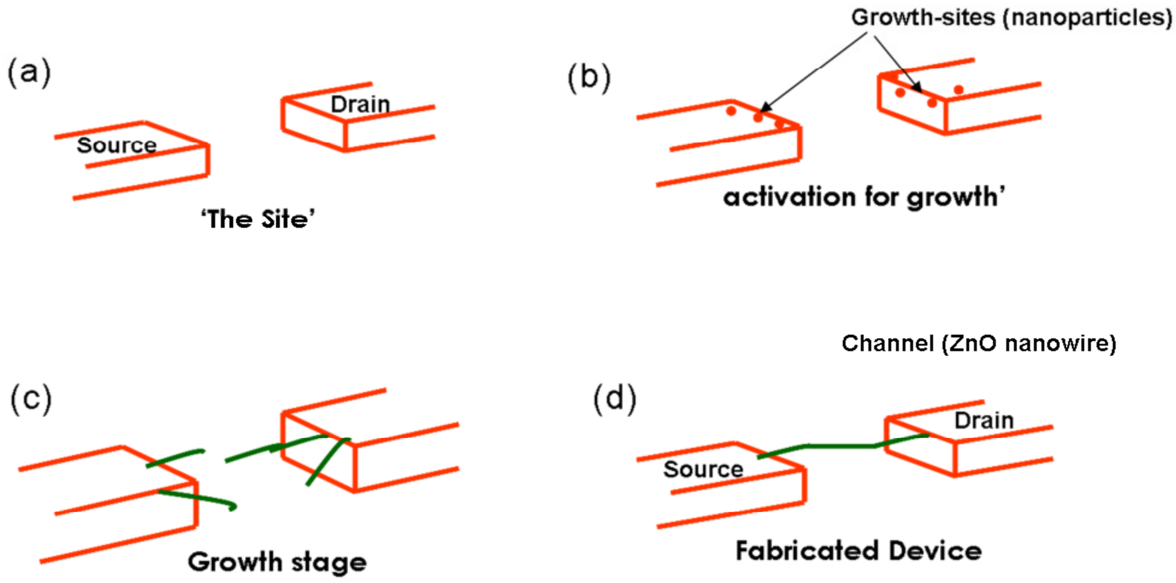

Figure 3.11 Schematic of the site-specific fabrication of ZnO NW transistors.

A method to grow ZnO NW transistors site-specifically on a chip is here developed by making use of solution based CBD growth technique for ZnO NWs as discussed in the last chapter. The proposal for doing this is shown in **figure 3.11**. The procedure starts with the selective deposition of nanoparticle seeds to create 'growth-sites' on prefabricated electrode pairs. ZnO NWs could be grown from these growth sites to bridge a microelectrode gap and form a device. The figure shows a schematic of a microelectrode pair constituting source and drain electrodes on a desired substrate and the mechanism to grow ZnO NWs on the growth sites. The chips prepared in **3.11b** with the NW growth sites could be immersed in a ZnO NW precursor solution and put for the growth at a desired temperature. The NWs are expected to grow from the seeds and bridge the microelectrode gap forming a channel between the source and drain.

Gold or ZnO NPs were deposited on the microelectrode pairs from their solutions by using AC dielectrophoresis. The set-up for the deposition of gold/zinc oxide NPs in this case was same as that showed in **figure 3.8**. An electric field was applied between the two electrodes by connecting them to a function generator on a manual wafer probe system. The deposition of NPs for most of the devices was carried out at 10 V_{PP} @ 10 MHz. A drop of colloidal solution of gold or ZnO NPs is placed covering the gap of microelectrode pairs while applying the field for desired time. NPs are attracted towards the electrodes due to positive dielectrophoretic force, (high electrical field intensity) and get deposited. AFM images in **figure 3.12** show microelectrode pairs with different gold and ZnO NPs densities depending on the time of field applied.

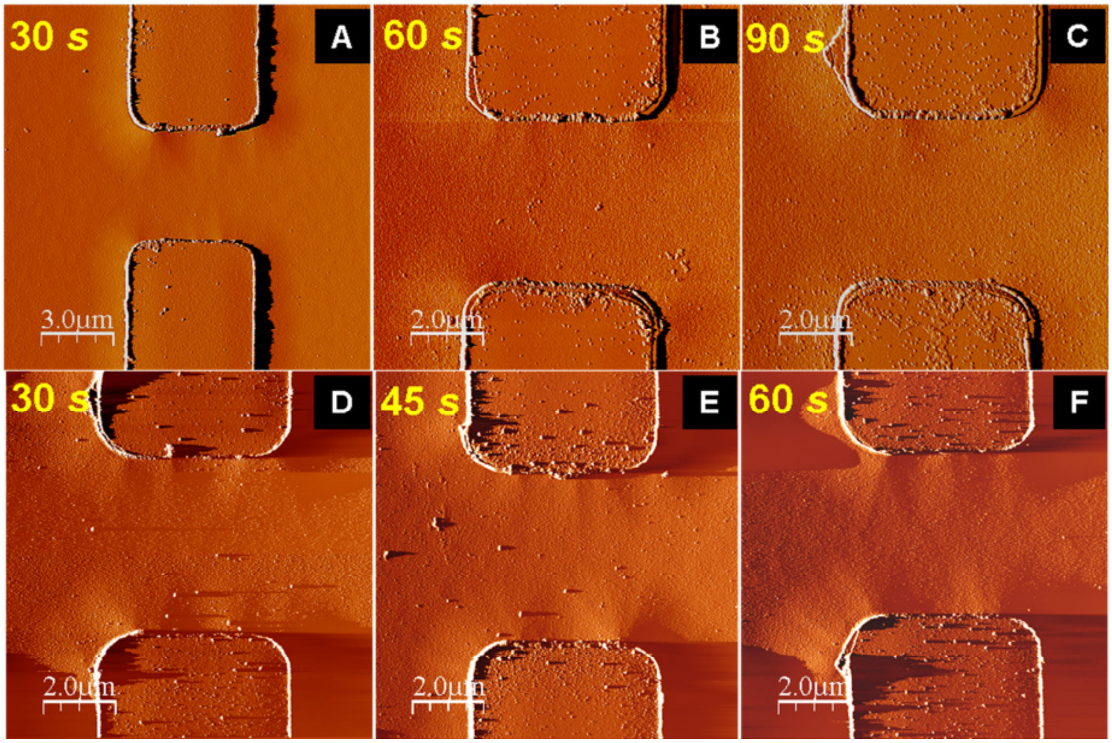

Figure 3.12: AFM images of the microelectrode pairs dielectrophoretically deposited with gold (A, B and C) and ZnO NPs (D, E and F).

Following the creation of growth sites selectively on the microelectrodes, the chips were subjected to the modified solution growth procedure as discussed before for ZnO NWs in chapter 2. The precursor solution contained 0.25 mM Zinc nitrate and 0.25 mM hexamethylenetetramine in an aqueous solution (100 ml each). This mixture in a 400 ml glass beaker was placed in a convection oven (Thermo Scientific Heareus). A schematic of this self-assembled growth is shown in **figure 3.13** and starts with the heating of precursor at 85^0 C. After 4*1/2* hours, the chips are immersed into the precursor mixture. The chips prepared using this method were used for FET and sensing measurements. After the NW growth on chips, they were characterized by SEM. **Figure 3.13C** represent SEM images of 5 micron microelectrode gap where ZnO NWs are grown and bridge the gap to form a device.

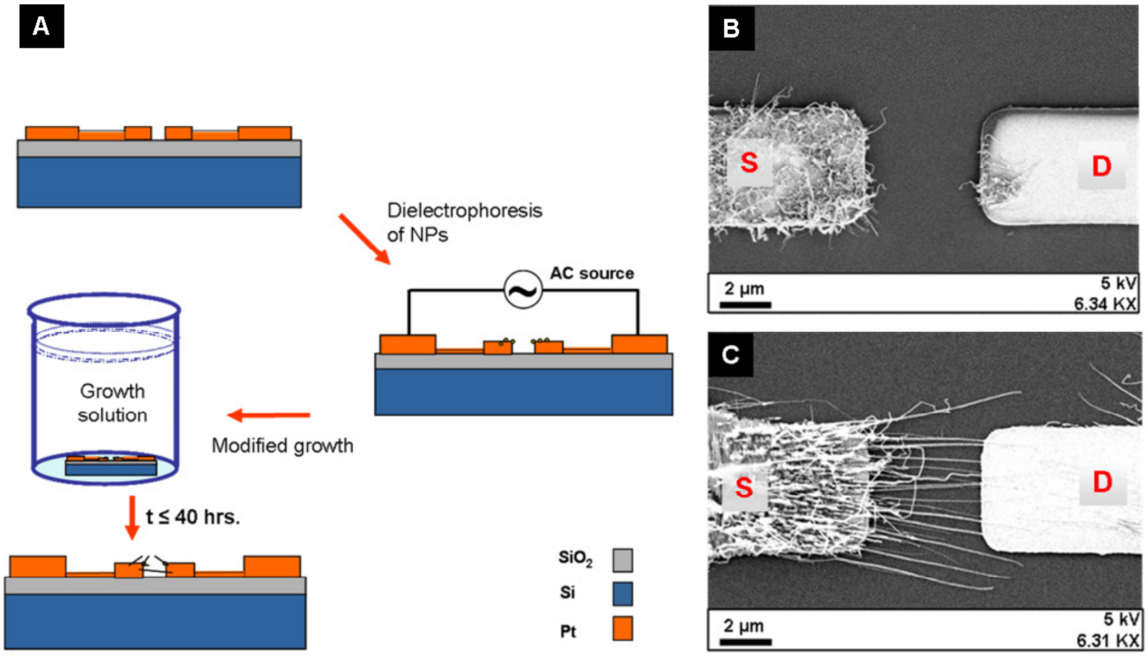

Figure 3.13: (A) Schematic of the modified growth method for the site-specific realization of ZnO NW transistors (B) The SEM image shows ZnO NWs growing selectively from the microelectrodes (after 8 hours) (C) SEM image showing fully grown NWs spanning between source and drain.

Electrical Characterization-

The field-effect characteristics of self-assembled ZnO NW transistors were carried out in a way similar to that of dielectrophoretically fabricated ZnO NW transistors. The chips were annealed in air at 800^{0}C for 30 seconds in a tube furnace before their electrical transport characterization. Figure **3.14** shows the transport characteristics of a typical device. The drain current vs drain-source bias plot showed in **figure 3.14A** illustrates the formation of ohmic contacts between the NWs and microelectrodes after annealing. **Figure 3.14B** shows field-effect characteristics of the NW devices in a back-gated configuration applying a gate voltage range of ± 20 Volts. The devices showed a typical *n*-type behavior. Here it’s important to mention that as-grown wires always displayed very high resistances (in the GΩ range) and negligible field-effect indicative of nonoptimal contacts and deep-level impurity states introduced during the growth in the form of oxygen vacancies[145, 146].

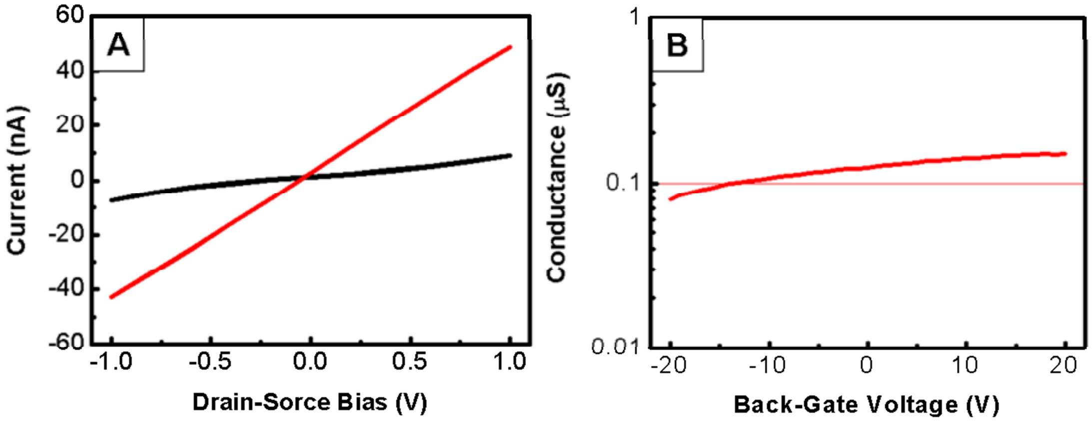

Figure 3.14: (A) Back-gated transport configuration for a transistor device (B) Current vs drain-source bias the ZnO NW transistor, before (black-curve) and after (red-curve) annealing and (C) gate dependence of conductance.

Both of these problems could be mitigated by subjecting the fabricated devices to rapid thermal annealing (RTA) as mentioned before. After annealing the resistance of the devices typically decreases by around 3 orders of magnitude with improvement in gate dependence.

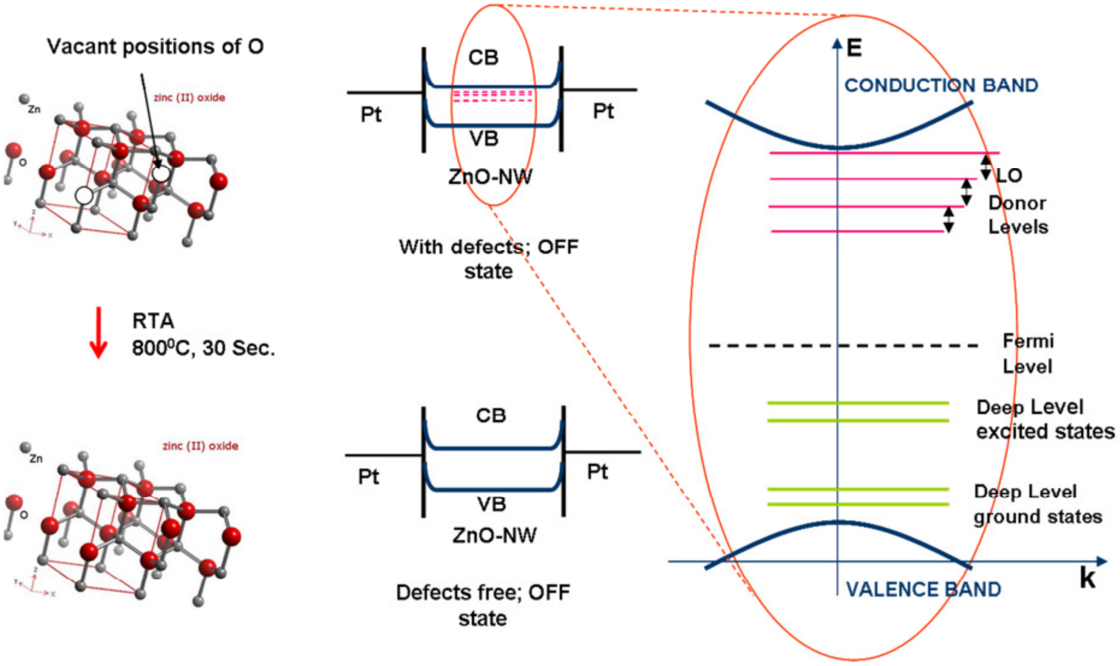

Figure 3.15: Schematic of the changes in lattice structure of ZnO NW upon rapid thermal annealing. O atom fill the Oxygen vacancies and remove low occupied donor levels below conduction band as represented in the band diagrams.

The RTA in air incorporates O atoms in ZnO lattice vacancies. The O vacancies in the ZnO lattice give rise to some unbound electrons (from Zn atoms) freely floating in the lattice network. This gives rise to some lower occupied donor levels just below the conduction band.

The origin of these extra states below the conduction band would give rise to an ineffective field-effect. However after annealing the device air, some vacancies are filled by O atoms and cause the extra donor states below the conduction band disappear. The disappearance of low occupied donor levels upon annealing is represented in the band diagram (figure 3.15).

3.2.3. Scalable fabrication

The method outlined in the previous section was subsequently extended large area silicon chips and Kapton foils. Silicon chips integrated with open Si_3N_4 based microfluidics consisting of 8 microelectrode gaps (discussed before) were used as substrates for ZnO NW growth. **Figure 3.15** shows ZnO NWs grown site-specifically on the microelectrode gaps on a single chip.

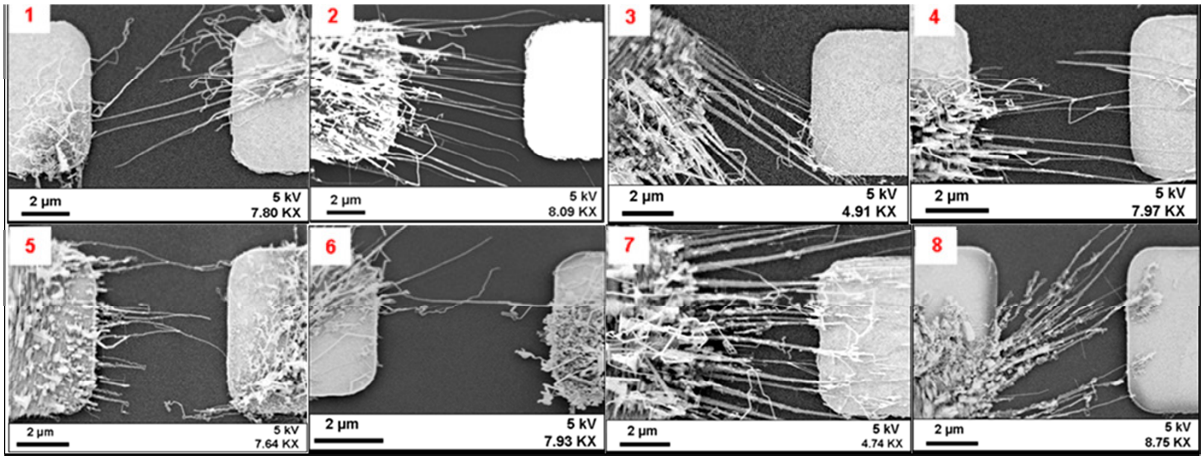

Figure 3.15: SEM images show 8 Source-Drain positions from the same chip, (2 positions from each microfluidic unit) where the growth of ZnO NWs spanning the gap between Source-Darin electrodes is apparent.

The ZnO NWs growing selectively from the microelectrodes are spanning the 5 micron gap forming transistor channel. This scalable method yielded 8 transistors per 4×4 mm area on chip and holds promise for fabrication of electrical L-o-Cs. The ZnO NW FETs fabricated in this method were deployed for sensing experiments and will be discussed in the next chapters. The method was repeated using flexible substrates. Kapton foils with 120 microelectrode gaps were chosen for this purpose. **Figure 3.16** illustrates the characterization of ZnO NW transistor fabricated on Kapton foil. **Figure 3.16A** represents the schematics of microelectrode written on the Kapton foil. **Figure 3.16B** illustrates laser scanning microscopic images of the transistors formed on the microelectrode gaps from one quadrant of the foil. **Figure 3.16C** gives a zoomed in view of a single ZnO NW transistor. A maximum yield of about 80 percent was achieved on Kapton foils following the growth procedure.

Figure 3.16D presents the transport characteristics of ZnO NW transistor showing the drain current vs drain-source bias after annealing in air for 10 minutes at 300^0 C. The resistances were in the range of hundreds of kilo-ohms to several mega-ohms.

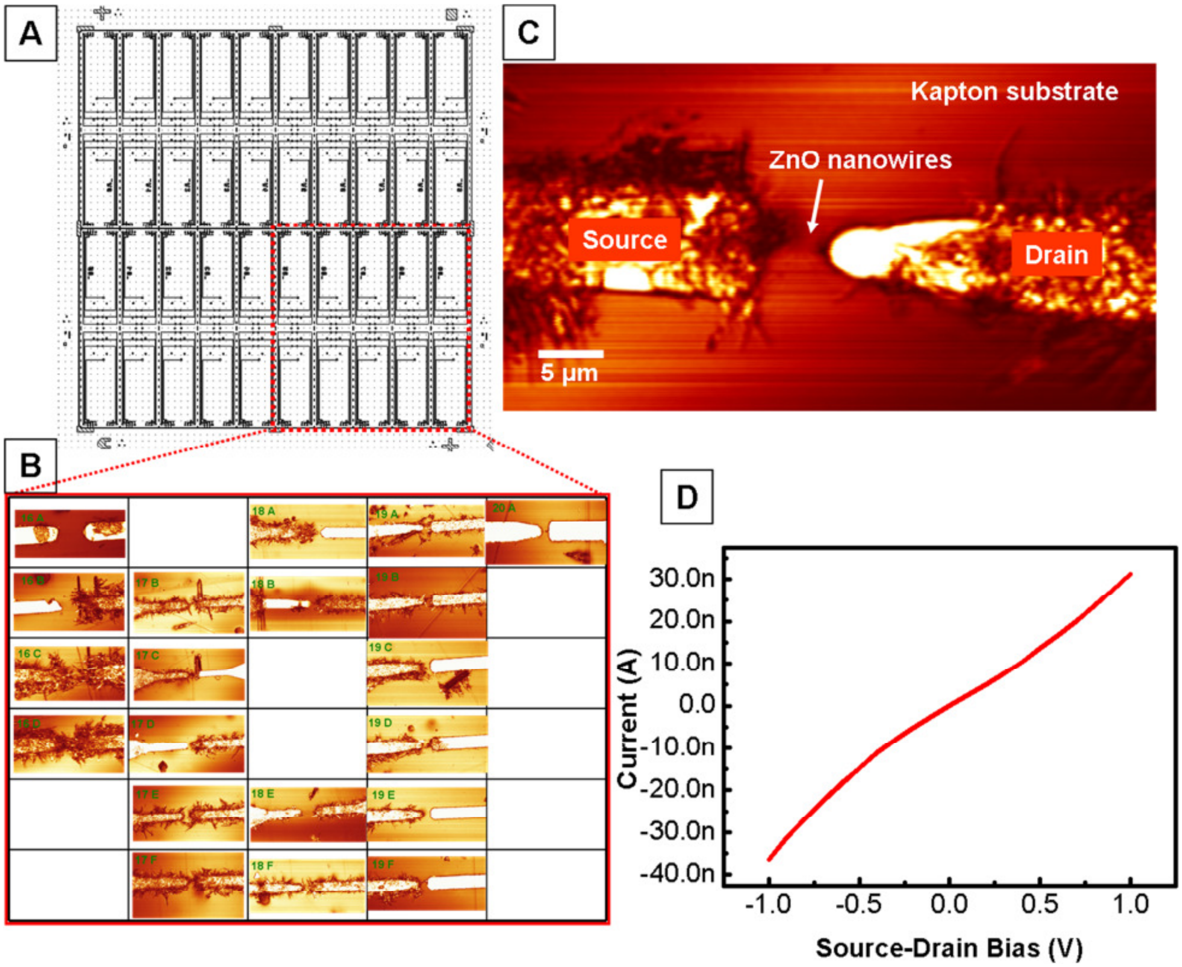

Figure 3.16: Site-specific growth of ZnO NWs on Kapton substrate and transistor fabrication. (A) Schematic representing a complete Kapton foil used for the fabrication procedure, (B) set of laser scanning microscopic images showing 25% of the 120 gap positions, (C) a ZnO NW device as seen in laser scanning microscopic image and (D) transport characteristic of the device shows current vs drain-source bias.

3.2.4. Direct self-assembly in microfluidic channel

Microfluidics equipped electrical sensors are pivotal for biological sensing purposes including chemical sensing. Thus, the experiments to characterize ZnO NW based FETs in fluidic environments are dealt with the integration of microfluidic channels on to silicon chips and Kapton foils in the work conducted during this thesis. Besides, this section discusses a novel technique to grow electrical devices such as ZnO NW FETs within the microfluidic channels site-specifically. The ZnO precursor solution was guided towards the microelectrode gaps with the help of PDMS based closed microfluidics assembled on top of silicon chips and Kapton foils.

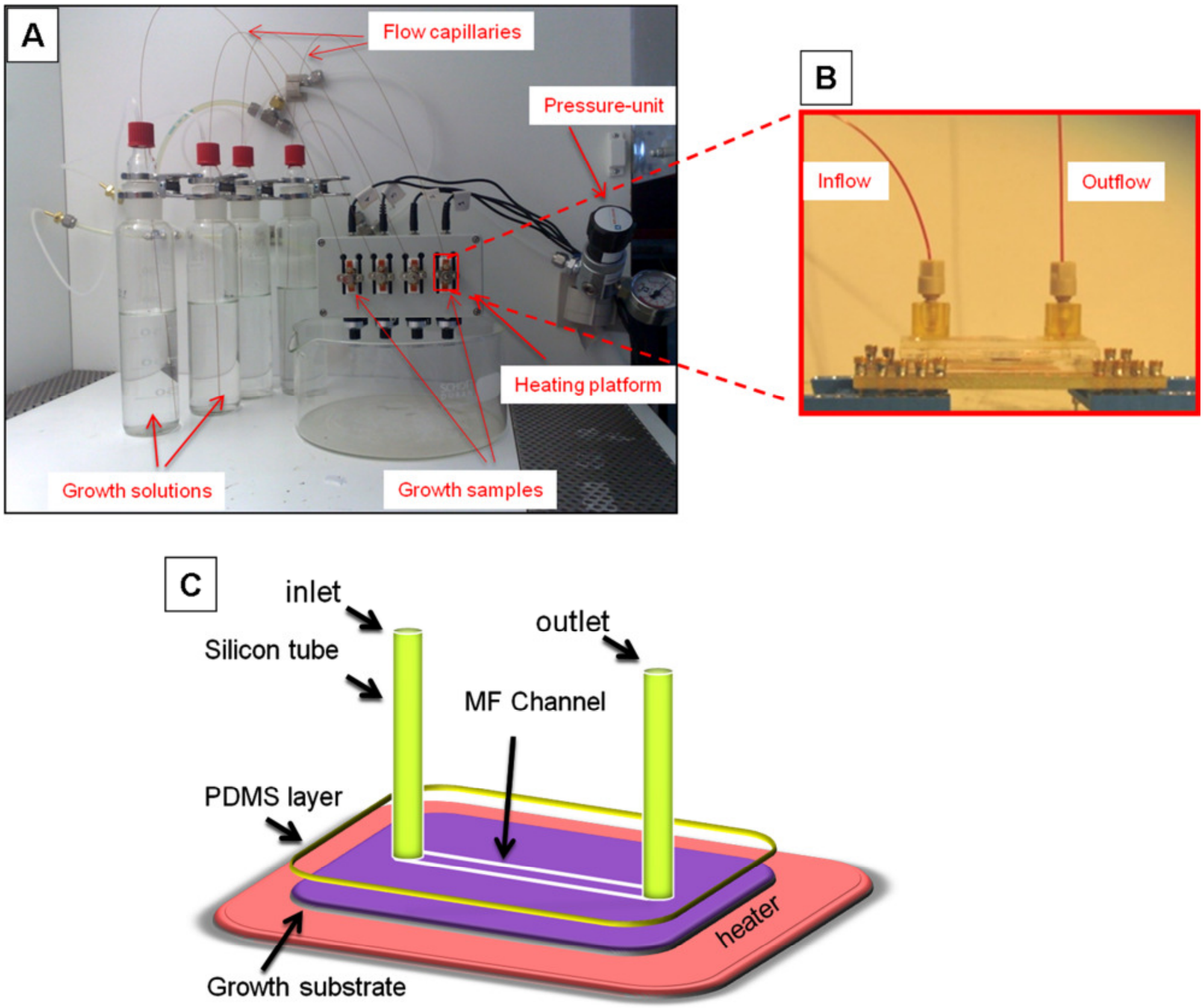

Figure 3.17: (A) Photographs of the set-up for microfluidic based direct self assembled growth of ZnO FETs and nanomaterials. (B) Microfluidic channel assembled on top of substrate and (C) schematic of the growth set-up around substrate.

The idea to perform a localized growth inside a microfluidic channel may offer many advantages such as low consumption of precursor material and prohibition of any unwanted reactions happening to the chip surface as immersed in the precursors solution. The microfluidic arrangement also provides for dynamic control of the reactant volumes during the growth. The morphology of the products can be engineered by varying reactants and their concentrations. **Figure 3.17** illustrates the setup to perform localized self-assembled growth inside microfluidic channels. Image A shows the assembly line of the set-up where the pressure unit is connected to the air-tight precursor containers. The pressure based microfluidic flow system was assembled on top of silicon chips and Kapton foils. Home built tiny resistive heaters (schematic view in image C) were placed under the chips and provided necessary heating for the growth.

The precursor solutions flow into MF channel through capillaries and can be controlled by the applied air-pressure. Several experiments of solution growth were performed with different growth times, concentrations of the precursor solution, ratio of the zinc salt to the reducing agent and the type of the reducing agent. Substrates were characterized by SEM after performing the growth processes.

Figure 3.18 presents SEM images of the nanostructures grown in several experiments with varying different growth parameters (except temperature = 85^0C and precursors concentration = 0.25 mM). Image A shows rhomboidal microcrystals of ZnO grown using a precursor solution of Zinc nitrate and Hexamethylenetetramine in 10 to 1 ratio in a 24 hrs growth time and gold NPs used as seeds. Image B shows granular microstructures of ZnO from a precursor solution of Zinc nitrate (1 part) and Hexamethylenetetramine (3 parts) while using selenium NPs as seeds. Images C and D also show flower like and spindle like nanostructures of ZnO using a precursor solution of Zinc nitrate and Hexamethylenetetramine in 1:3 and 1:1 ratio respectively for a growth time of 22 and 21 hours respectively. Images E and F show ZnO nanotubes bridging microelectrode gap positions which were grown for 30 hrs and 18 hrs respectively from a precursor solution with Zinc nitrate and Hexamethylenetetramine in 1:1 ratio. Experiments thus performed in the microfluidic channels required very small amount of precursor and conducted the growth of different morphology nanostructures at desired set of growth parameters. The microelectrodes could be used as Source and Drain pair while ZnO nanotube working as channel of a functional device.

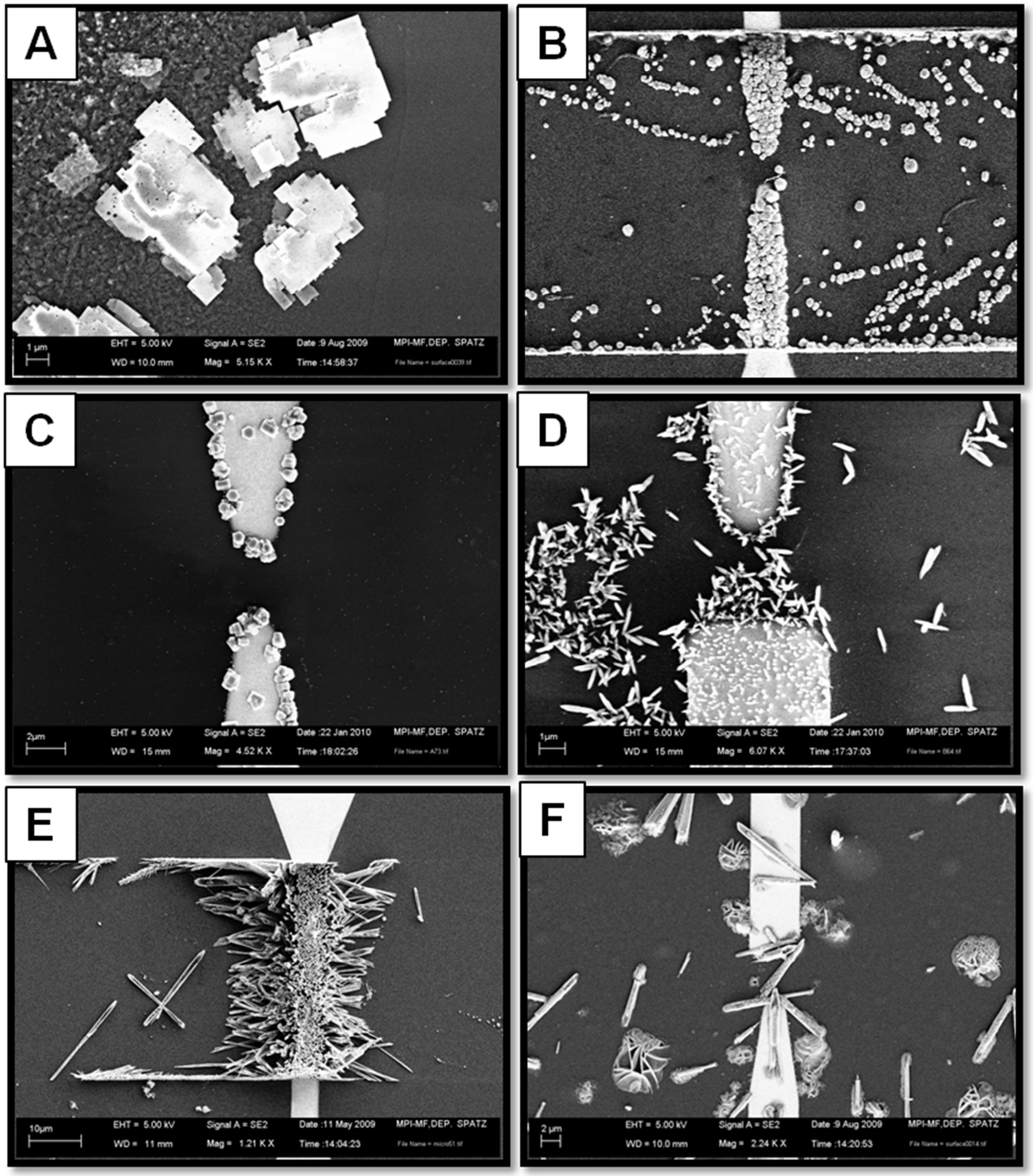

Figure 3.18: The figure shows SEM images from six different growth experiments for Zinc oxide conducted in microfluidic channels over silicon chips with prewritten electrodes. Images A to D show ZnO nanostructures grown using a precursor solution of Zinc nitrate and hexamine in different ratio and growth times but using same growth temperature (85^0C). Images E and F show the grown nanostructures (ZnO nanotubes) bridging the gap between two microelectrodes.

The self assembled microfluidic growth of ZnO nanostructures was further adapted to construct devices on Kapton. **Figure 3.19** represents optical and laser scanning microscopic image of a typical device fabricated in a microfluidic growth set-up. Image A shows a Kapton foil assembled with PDMS based microfluidics in a top view where a 30 micron wide microchannel runs through six Source-Drain electrode gap positions (only four in the view). The foil integrated with microfluidics was connected to the pressure based flow system as discussed earlier. The microelectrodes were deposited with gold NPs before the integration of microfluidics with the foil. It is apparent that ZnO NWs have grown on the microelectrode positions and spanned the gap. The devices formed in this method were characterized for transport properties after annealing in air for 10 minutes at 350^0C. Image C presents transport characteristics of a typical device showing drain current vs drain-source bias plot.

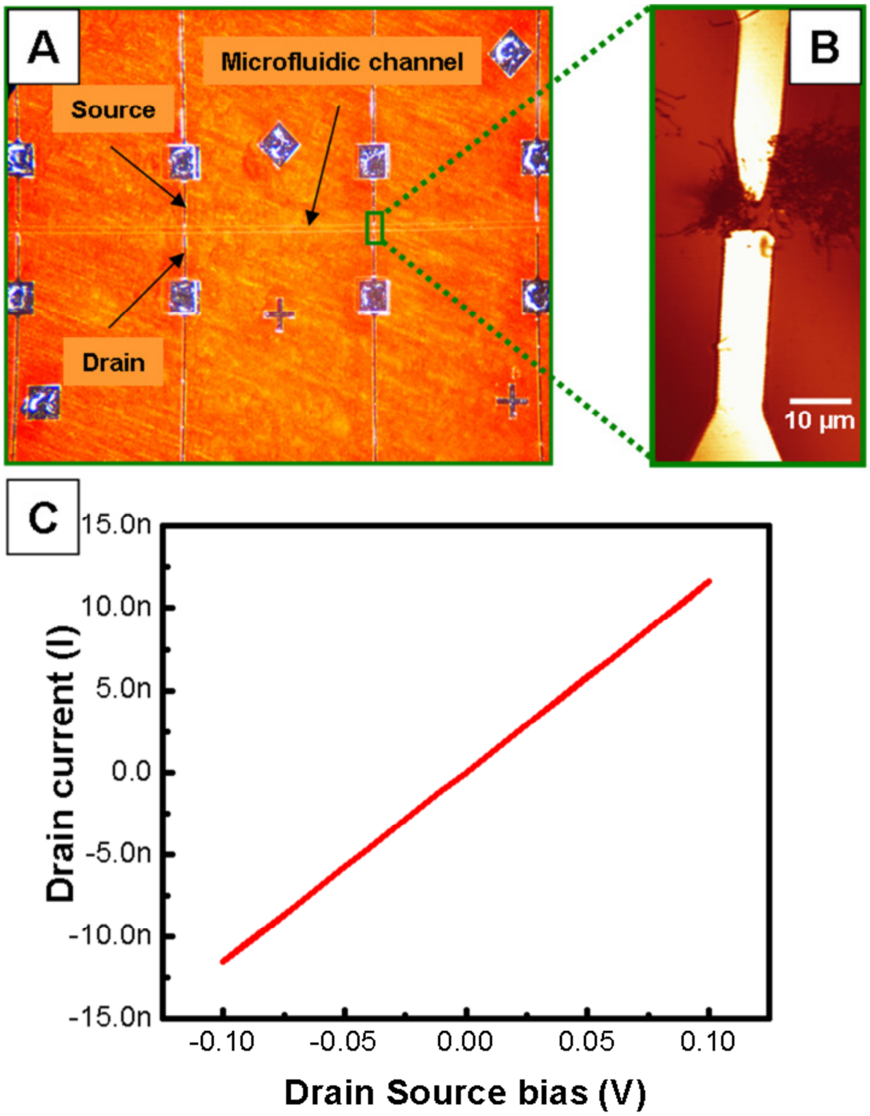

Figure 3.19: ZnO NW transistor fabricated directly in a microfluidic channel. (A) An optical image of the Kapton chip (from top view) integrated with PDMS microfluidic channel. (B) Laser scanning microscopic image of a device (C) transport characteristics of a typical device in current vs drain source bias plot.

The procedure to grow ZnO NW/nanotube based devices directly inside the microfluidic channel was tried to employ for the routine fabrication of transistors. However the method needs further corrections and optimizations in order to yield reproducible results on a routine basis. Besides, the direct fabrication of electrical devices inside microfluidic channels shows promise in future L-o-Cs based on electrical detection techniques. Especially, when the technology for electrical L-o-Cs till now has mainly been conceived with the idea to use the diagnostic chip and dispose after use. L-o-C assembling processes are complex and require considerable efforts and make it desirable to find ways for the reuse of a L-o-C once assembled. L-o-Cs with electrical detection platforms where devices can be fabricated inside the microfluidic channel may provide a critical solution.

Chapter 4

ZnO NW FETs: Liquid gating and sensing operation

The previous chapters discussed in detail the methods for site-specific self-assembled fabrication of ZnO NW transistors on silicon chips and Kapton foils. Devising biosensors based on FET require transistors in liquid medium. The field-effect is produced by using a liquid gate. The electrochemical gating effect in FETs originates by the formation of an electrochemical double layer capacitance (EDL) at the interface between transistor channel and surrounding liquid. Since the gate capacitance of electrochemical gate is dependent on the ionic properties liquid, the ionic/molecular composition of a liquid medium is reflected in the transport characteristics if the FET. The idea of ion-sensing FET operation was first proposed by P. Bergveld in 1970 and coined the term ISFETs [51, 147]. The development of FETs for liquid sensing has been carried out since then and reported in many articles related to the fabrication and working mechanisms[148]. Strategies of specific analyte detection for biological and chemical sensing purposes have been carried out and established as basic technology for electrical detection of single molecules [149]. The concept of so called ion-sensitive FET (ISFET) has been applied recently to nanoscale devices such as carbon nanotube (CNT) [150-153] and NW (NW) FETs [154-156].

This chapter will discusses transport characteristics of ZnO NW transistors in liquid medium. Transistors deployed in liquids were used as chemical and biosensor in an ISFET configuration. Methods employed to fabricate ZnO NW ISFETs for pH sensing and enzyme-FETs for urea sensing in liquids will be discussed. However before doing that, the mechanism and configurations of gate in different FET will be discussed as a basis to explain the experiments and measurements.

4.1. Gate capacitance

FET are three terminal devices where electron/hole transport in a channel connected to source and drain terminals is controlled by another terminal called gate by applying an electric field. Depending on the methods of applying the electrical field using gate, the FETs can be categorized into many types like junction field-effect transistor (JFET), metal oxide field-effect transistor (MOSFET), ion-sensing field-effect transistor (ISFET) and metal-semiconductor field-effect transistor (MESFET) etc [157]. While basic principles of applying electric fields are similar in all FETs, mechanisms do differ depending on the gate type.

JFET make the simplest form of a transistors available where a semiconducting material (n-type or p-type) makes the channel between drain and source contacts while a p-type (for n-type channel) or n-type (for p-type channel) material is diffused into the channel (**figure 4.1.A**) and connected with a gate source. The current flow between the source and drain is related to the bias applied between Source and Drain and the resistivity of the conducting material. The depletion region formed around the p-n junction of channel and gate can be controlled when a reverse bias applied. The resistance of the channel depends on the growth of the depletion layer and thus controllable by bias applied on the gate terminal [13, 158].

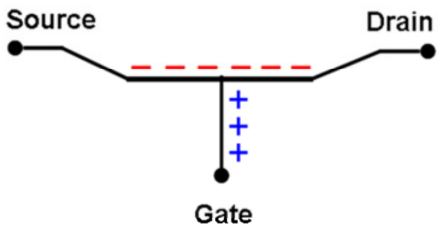

(A) JFET

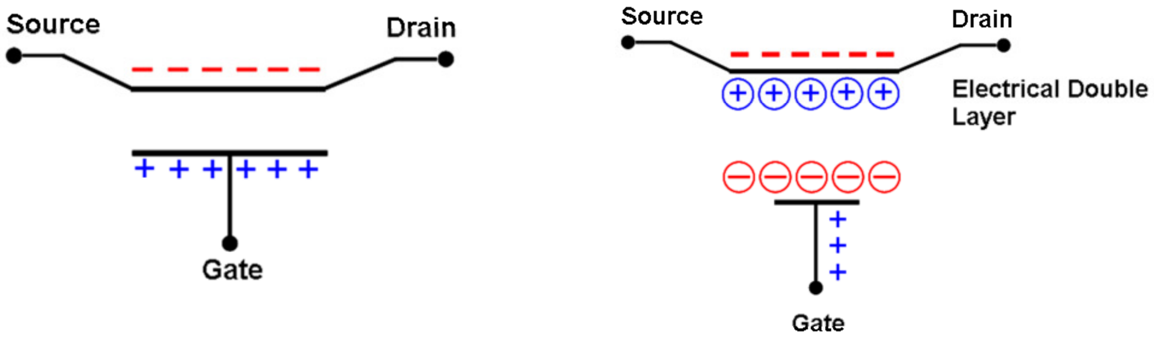

(B) MOSFET: insulated gate transistor

(C) ISFET: electrochemical gate

Figure 4.1: Gate capacitance in (A) Junction field-effect transistor (B) metal oxide semiconductor (back-gated) field-effect transistor and (C) electrical double layer capacitance in a liquid-gated field-effect transistor.

The back-gated ZnO NW transistors as discussed in the chapter 3 operate like a MOSFET. A low resistivity p-type material forms the substrate (highly doped Silicon in this case) and works as gate terminal. ZnO NWs lying on this substrate form n-type semiconductor channel connected to source and drain. A thin insulating oxide layer (600 nm SiO_2) grown on the silicon chip separates the channel from the gate. Prefabricated metallic electrodes formed source and drain contacts as mentioned. With the insulation layer between silicon substrate and ZnO NW there is no physical penetration between gate and channel. The silicon gate forms a capacitor with the insulating layer and the semiconductor channel (schematic in **figure 4.1.B**). Applying a positive voltage at gate induces correspondingly negative charges in the semiconductor. As the positive gate is increased, the negative charges "induced" in the semiconductor increases and current can flow between drain and source through the "induced" channel. In other words, the drain current is "enhanced" by the gate potential and the channel resistance is directly related to the applied gate voltage. The ZnO NW transistor just described is called a depletion-mode transistor with the device in the ON state at zero gate voltage, which is a common characteristic in almost all of the reported ZnO NW based transistors.

ISFET works on the same principle as insulated gate (or back-gated) FET except that it employs a liquid to apply gate voltage to modulate the charge transport between source and drain. The capacitive layer formed by the oxide between the gate and the channel in MOSFET is replaced by a capacitive layer formed by an electrical double layer (**figure 4.1.C**) in an ISFET. Formation of an electrical double layer on the solid-liquid interfaces (an electrostatic phenomenon, first described by Helmholtz in 1850s to explain electron transfer at solid-liquid interfaces) exerts an electric field across the interface[159, 160]. The thickness of the double layer (d_{el}) is variable by the accumulation on electrolyte ions present in the solution on the interface[160]. Hence the electrical field across the interface can be controlled by applying a voltage connecting an electrode to the solution. This electrical field exerted on the interface controls the flow of electrons in the channel.

ZnO NWs hold a negative charge density on its surface because of the unsatisfied oxygen valancies or OH^- groups. When contacted with a solution, this negative charge density (q_m) would attract positively charged ion from the solution in order to neutralize the interface as shown in **figure 4.2A** in a Gouy-Chapman model (1913) for EDL[161, 162].

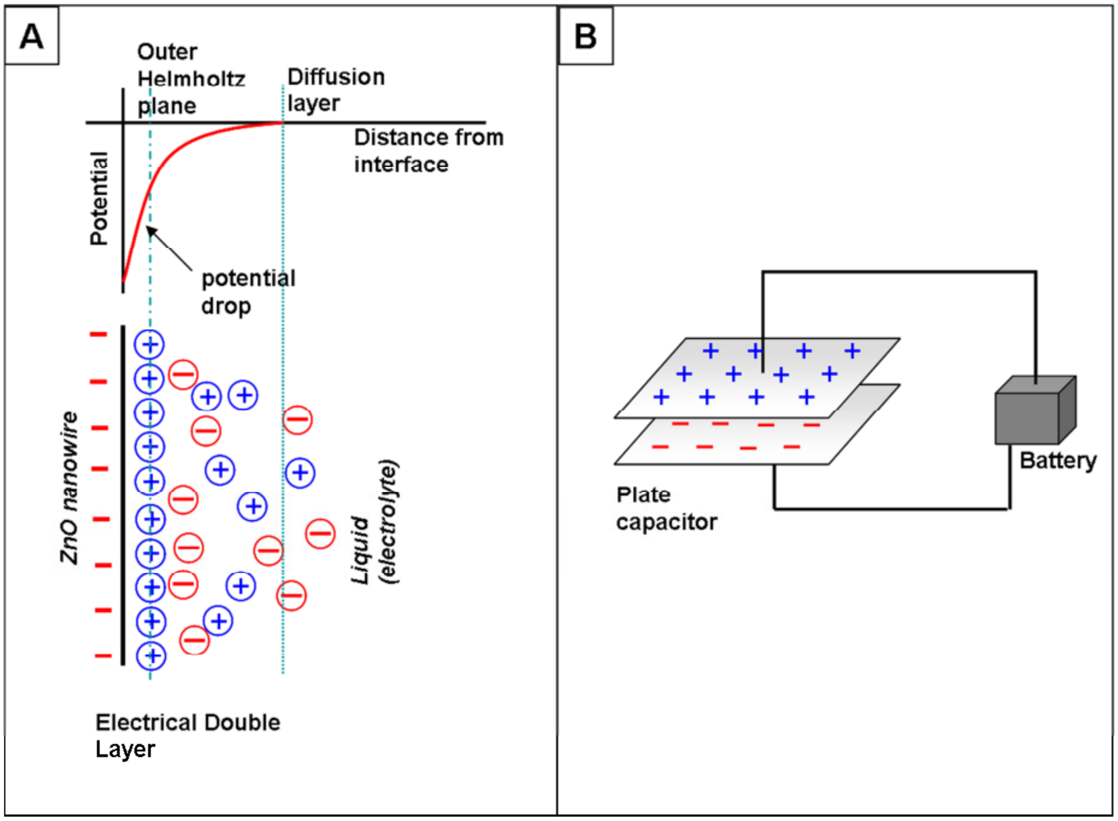

Figure 4.2: Schematic representation of formation of an electrical double layer on a NW/solution interface which is analogous to a plate capacitor at small separations between the charged layers.

The attracted ions approach the charged surface with a finite distance which is the sum of the radius of ion and its solvation sphere. This makes two oppositely charged ionic layers confined locally on a stable interface and a potential drop (Φp) on the interface. The potential drop exhibited by this system is now completely analogous to two oppositely charged plate capacitors.

The capacitance of a plate capacitor is the ratio of accumulated charge to the potential applied and is given by,

$C = Q/V$ (in farads)

The capacitance can be calculated for a capacitor considering its geometrical shape and dielectric property of the insulation in between. For example the capacitance for a plate capacitor as shown in **figure 4.2B** with area of overlap *A*, distance between the plates *d* is given as:

$C = k\,\varepsilon_o \cdot A/d$ ……………………………………………………………………5.1

Where *k* is the relative static permittivity (or Dielectric constant) of the material between the plates, and ε_o is the electrical constant or permittivity of the space (~ 8.854×10^{-12} F m^{-1}).

The geometrical dependence of capacitance can be considered here for a sphere model and a cylindrical model, as plate capacitor already been discussed. For a spherical capacitor with two concentric spheres of conductors (shown in **figure 4.3A**) the capacitance is obtained by evaluation of electric potential between the spheres:

$$V(r) = -\int_a^r E(r)\, dr \quad \text{or, } V(r) = -Q/4\pi\varepsilon_0 \int_a^r dr/r^2$$

Since the electrical field between the spheres $E(r) = Q/4\pi\varepsilon_0 r^2$ (using Gauss' law)

Now $V(r) = Q/4\pi\varepsilon_0[1/r - 1/a$

The Voltage between the spheres can be given by $V = V(a) - V(b) = Q/4\pi\varepsilon_0 \cdot (b-a)/ab$

Capacitance $C = Q/V = 4\pi\varepsilon_0 \cdot (b-a)/ab$……………………………………………………..5.2

To calculate the capacitance between two concentric cylinder plates (as shown in **figure 4.3B**) with radius a and b, we know that $C = Q/V$

In a cylinder of uniform charge distribution, given by $\lambda = dQ/dL$, Gauss' law gives the electric field between the plates, $E = \lambda/2\pi\varepsilon_0 r$. Now integrating the electrical field along a radial line to get the voltage between the cylinders, we get:

$$\Delta V = \lambda/2\pi\varepsilon_0 \int_a^b 1/r \cdot dr = \lambda/2\pi\varepsilon_0 \ln [b/a]$$

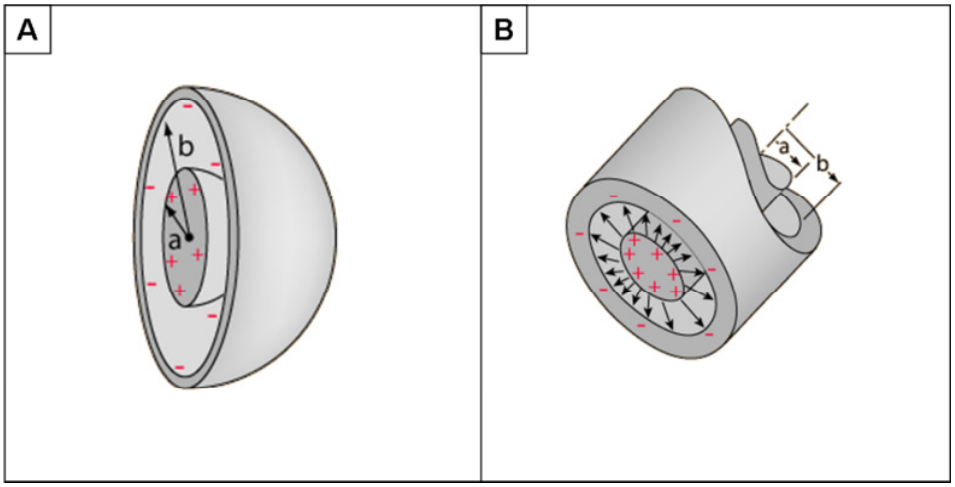

Figure 4.3: Schematics of (A) spherical capacitor and (B) cylinder capacitor.

Now, the capacitance per unit length for a cylindrical capacitor filled with a dielectric material with constant k is defined as:

$C = \lambda L/\Delta V = L \cdot 2\pi\, k\, \varepsilon_0/\ln[b/a]$……………………………………………………………………………5.3

The FET performance is specified by many characteristics such as transconductance (g_m), field-effect-mobility (μ) and the ability of current modulation (ON-OFF ratio). Apart from the intrinsic electrical properties of the channel and the gate material, these parameters also depend on the geometrical features of a device. The field-effect-mobility (μ) of a FET as given by $(dI_d / dV_{lg})\, L / (c_{edl}\, V_{ds})$ consist geometrical variables such as L (the length of the device channel) and C_{edl} (electrical double layer capacitance) dependent on the physical features of the device architecture. From the discussion of capacitance basics in the previous section it is understood that the magnitude of capacitance is directly proportional to the dielectric constant and inversely proportional to the thickness of the insulation layer. To improve performance, it is required to use high dielectric constant material in a minimum possible thickness as a spacer material[163, 164]. For example in the case of a NW FET as shown in **figure 4.4A**, the gate is positioned below the source and drain contacts. The gating effect here will be determined by the dielectric capacitance of the insulating layer between the NW and the gate electrode. This capacitance is best modeled by assuming a cylindrical capacitor geometry (equation iii), where capacitance per unit NW length is given by $Cox = 2\pi k\, \varepsilon_0 / \ln(1 + \lambda_D/r)$. Here k is dielectric constant of the oxide layer (~4 for SiO_2), λ_D is the thickness of the oxide layer and r is the diameter of the NW. More effective gate coupling can be achieved by using high *k* dielectrics or by decreasing the thickness of the insulating layer. Both the strategies have been optimized for planar FETs deployed in many commercial electronic devices[18, 165-169]. Planar FETs were configured already in 70s for sensing applications, by replacing the gate oxide with receptors for specific analyte. The specific binding of analytes to receptors affect depletion or accumulation of charge carriers in the transistor channel [170]. However the sensitivity and integration possibilities with such devices were limited.

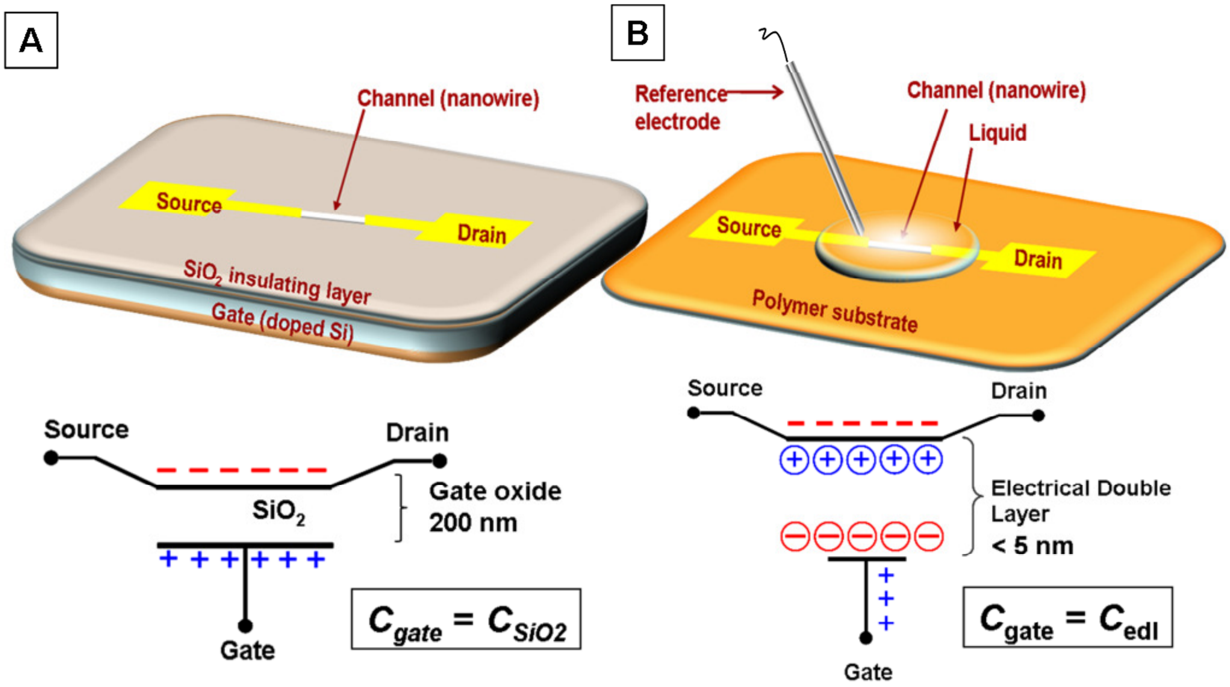

Figure 4.4: Schematic of back-gated FET, electrochemically gated FET and the comparison of geometrical gate capacitances. (A) The dielectric layer of SiO_2 determines the geometrical capacitance of back gated FET. (B) An electrical double layer (EDL) formed at the interface between the NW and the liquid determines the geometrical capacitance in an electrochemically gated FET.

The introduction of nanoscale FETs has overtaken many physical barriers that limited the planar devices with low sensitivities. Accumulation or depletion of charges on NW/nanotube surface by analyte-receptor interactions affects the number of charge carriers. 1D FETs provide large surface to volume for the functionalization of receptors for high sensitivities as compared to that of the planar FETs. In addition use of high *k* dielectrics and thin insulating layers have been experimented in back-gated and top-gated geometries in order to improve the sensitivities of nanoscale FETs [171, 172]. Having a FET immersed in liquid is discussed in **figure 4.4B** where geometrical capacitance of the gate is determined by the Debye length (λ_D) of EDL. A simple estimate of the EDL capacitance for Debye length of 5 nm and 50 nm diameter and *k* equal to 80 for water gives a value in the order of 2000 pF/m[173]. This capacitance also occurs in series with the quantum capacitance which gives a net capacitance in the order of 300 plus pF/m. The value is close to theoretical limit of 400 pF/m[164].

4.2. Electrochemical/Liquid Gating

The role of the gate capacitance in determining the field-effect characteristics of a transistor has been known for long, however the electrochemical capacitance for producing a field-effect was investigated no sooner than in 2001. Schönenberger and Forro first demonstrated an electrochemical gate based on a carbon nanotube (CNT) transistor. They employed a multi-walled CNT transistor to compare the gating-effect produced by a back-gate (400 nm thick SiO_2 spacer layer) and an electrochemical gate (~ 1nm Debye length of EDL) [174]. The gate dependence of conductance in electrolyte compared to that in air using back-gate showed an improvement by a factor of more than 200 times. Since then the FET performance in liquids has been investigated by numerous research groups employing CNTs and various 1D conducting materials [175].

Liquid gating experiments with ZnO NW FETs were conducted by spotting a drop of deionized water in the reservoir, which led to the filling of the MF channel. The liquid gating set-up is shown in the **figure 4.5** with one microfluidic unit on the chip. The gate is applied with a Pt electrode which is in contact with the ZnO NWs though the liquid. The liquids forms an electrical double layer (EDL) on NW surface and applying voltage on the gate electrode forms an effective capacitance between the ZnO NW surface and liquid. The thickness of the electrical double layer (4 -5 nm) around the NW surface being comparable to NW diameters (~50 nm) provided much better capacitance per unit channel length in the liquid gated transistors than their counterpart back gated field effect transistors.

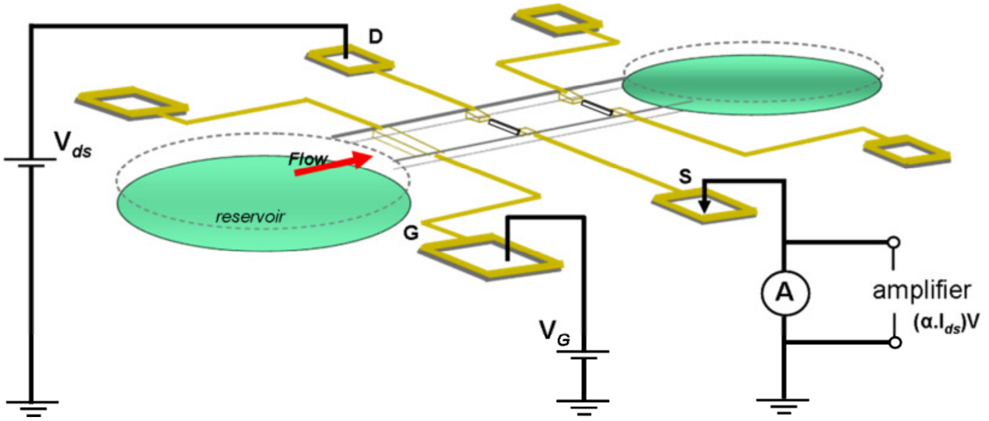

The

Figure 4.5: Schematic of the electrochemical gate set-up used to characterize ZnO NW FETs in liquids.

Figure 4.6 compares the field-effect characteristics of a self-assembled ZnO NW transistor in a back-gated and electrochemically gated configuration. **Figure 4.6A** shows SEM image of a typical device used for measurements and the field-effect characteristics of the device in a back-gated configuration. The gate dependence of conductance showed in the plot illustrates negligible current modulation while applying gate voltages in the range of ± 20 Volts. The field-effect characteristics of same device in an electrochemical gate is shown **figure 4.6B**.

The FETs show characteristic *n*-type behavior where conductance can be modulated by 4 to 6 orders of magnitude applying gate voltages in the range of ± 2 volts. The transistors showed sub-threshold slope values in the range of 105 to 200 mV/decade. Best sub-threshold slope values reported for ZnO transistors until now are around 130 mV/decade [176, 177]. The switching behavior in most of our devices is like a depletion mode transistor with the device in the ON state at zero gate voltage, which is a common characteristic in almost all of the reported ZnO NW based transistors. The gate leakage through the liquid medium was far below 100 pA in a gate voltage range of ±2 V. The transconductance of the device was found to be more than 1 μS at a drain bias of -100 mV. For a network of 20 wires with a diameter of around 50 nm, we obtain a normalized transconductance 0.02 S/cm, which is comparable to high performance nanorod transistors reported with a transconductance around 0.015 S/cm [176, 178].

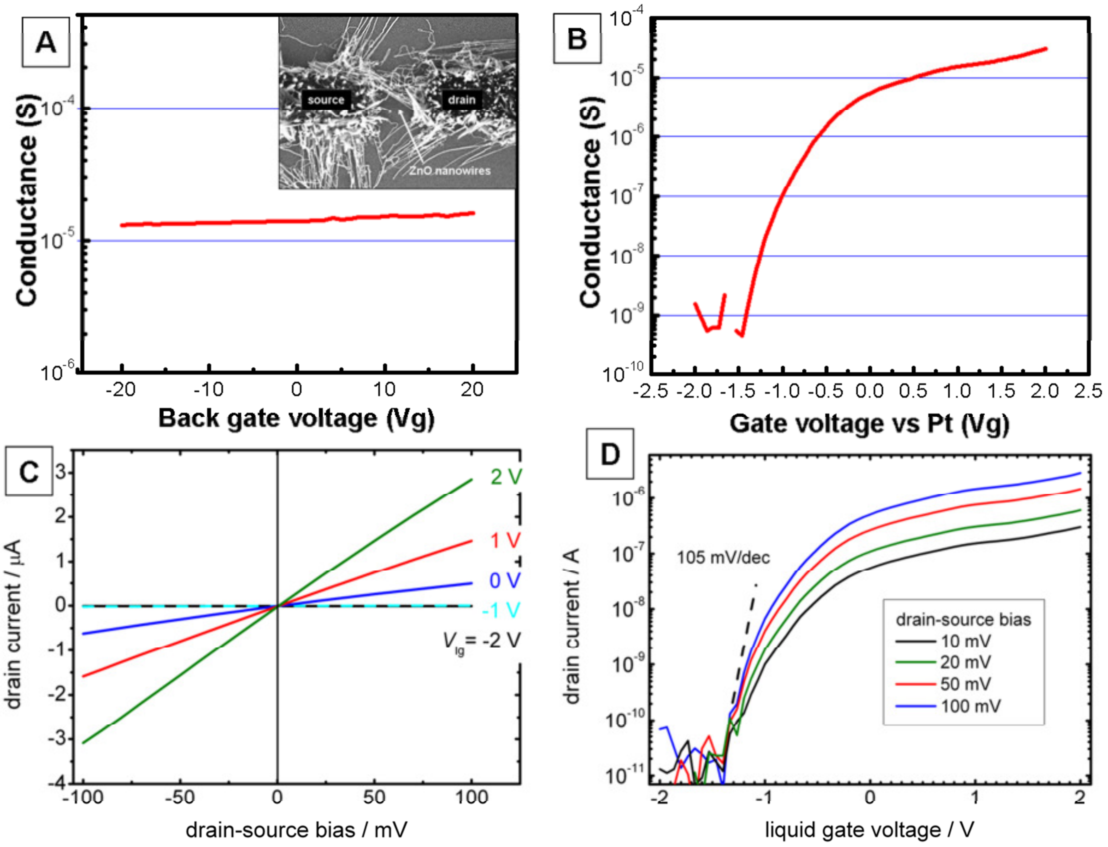

Figure 4.6: field effect characteristics of self-assembled ZnO NW transistor in electrochemical gate. (A) SEM image of the device used for measurements shown. (B) gate dependence of conductance in back-gated configuration and (B) gatedependence of conductance in an electrochemical gate.

The field-effect mobility (μ) of electrochemically gated FETs can be calculated in a way similar to that of their back-gated counterparts. It is given by $\mu = (\mathrm{d}I_\mathrm{d} / \mathrm{d}V_\mathrm{lg})\, L / (c_\mathrm{edl}\, V_\mathrm{ds})$, where I_d is the drain current, V_{ds} the drain bias and V_{lg} the liquid gate voltage, L is the channel length (5 μm in our samples), and c_{edl} is the capacitance per unit length due to the electrical double layer given by $c_{edl} = 2 \pi k_r k_0 / ln(1+\lambda_D/r)$ [179]. k_r is the dielectric constant of the liquid (80 for water), λ_D is the Debye length which is a function of ionic strength (around 4 to 5 nm for deionized water [180] and r the radius of the ZnO NW. In this manner, the field-effect mobility of the device in figure 4.6 has been calculated to be 1.85 cm^2/Vs. While higher values have been reported with back-gated individual wires that were either covered or functionalized [176, 181] or used a nanoscale air gap [177] this is the first report of a mobility value for a self-assembled ZnO NW network transistor operating based on the electrochemical field effect in liquid.

4.3. pH sensing

The first step towards practicing sensing in liquids is the determination of pH since it represents the chemical nature of the solution. Hence ZnO NW based FETs primarily deployed in an electrochemical gate were subsequently evaluated as chemical sensors in a liquid medium. For this purpose, self-assembled ZnO NWs were functionalized with pH sensitive receptors namely 3-aminopropyltriethoxysilane (3-APTS). NW transistors were immersed in a 1% toluene solution of 3-APTS for 18 hrs. **Figure 4.7A** shows schematic of functionalization of 3-APTS on ZnO NW. 3-APTS are molecules having an amino group at one end of the carbon atom chain while three ethoxy groups on the other end of the chain. The molecules functionalize on the NW surface in a manner that only amino groups are exposed. The amino groups on the surface of NWs get protonated when put into a solution of pH less than that of iso-electric point of amino groups (~9.8) and affect the charge density in the NW. Moreover, the solution pH determines the charge exhibited by functionalized groups which is reflected in the transport characteristics of the NWs. Figure 4.7B shows the device conductance vs gate voltage as a function of different pH solutions which constitutes the sensor response. **Figure 4.7C and 4.7D** show the threshold voltages of the devices at different pH values in repeated cycles. It is apparent that the threshold voltage of the devic continuously shifts as a function of pH. The results are consistent with a ion-selective field-effect transistor (ISFET) mechanism,[147] whereby the charge of the amino groups on the surface of the functionalized NWs introduces a voltage offset that is reflected as a pH-dependent threshold voltage shift.

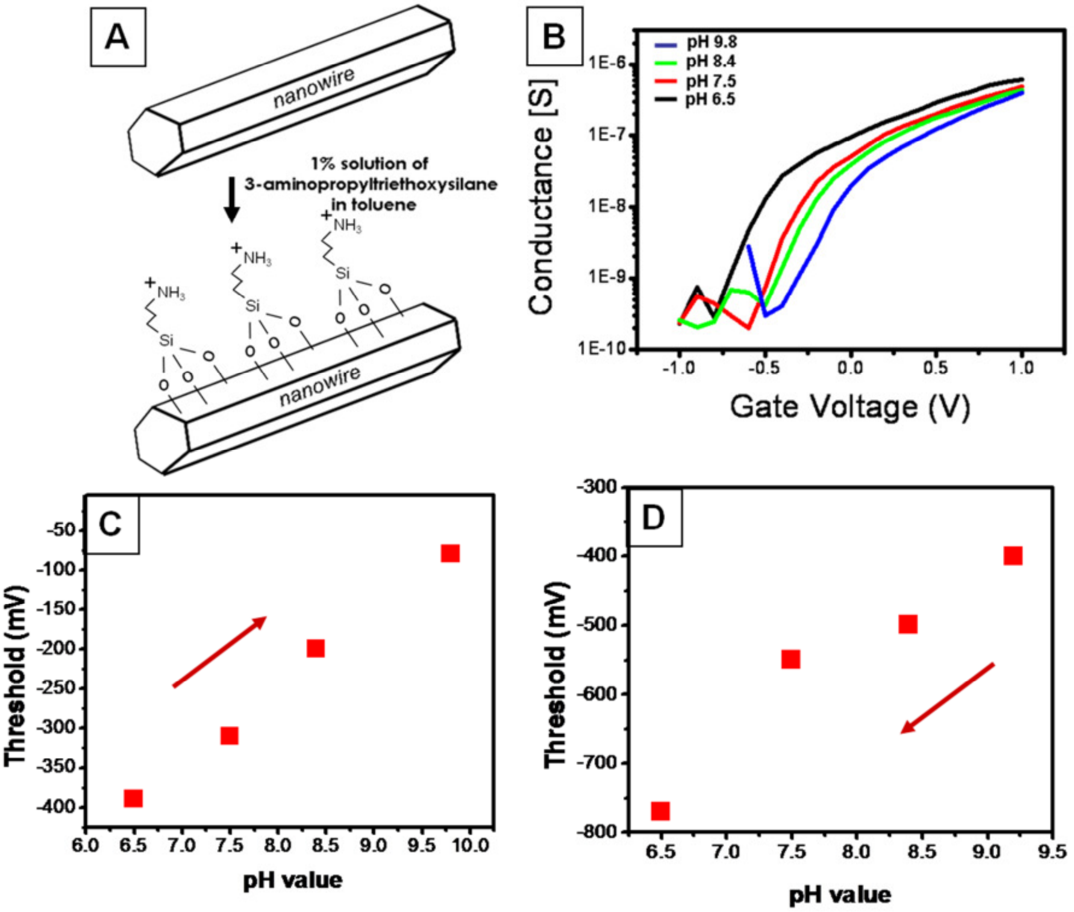

Figure 4.7: pH sensors using site-specific ZnO NW FET: (A) Schematic of the chemical functionalization of the ZnO NWs with 3-aminopropyltriethoxysilane to obtain pH sensitive functional groups on the surface. (B) Gate dependence of conductance of the functionalized device in various pH buffer solutions of varying pH. (C) Calibration plot showing the threshold voltage of the device as a function of solution pH in first cycle and (D) in second cycle.

4.3. Sensing of Urea

This section gives an overview of the experiments conducted with ZnO NW transistors towards performing label-free sensing of biomolecules. As an example, the transistors well established to perform chemical sensing in liquid environments as discussed in previous section were employed to detect urea in a buffer solution.

Blood urea nitrogen (BUN, Urea: $H_2N\text{-}CO\text{-}NH_2$) gives a measure of the protein breakdown during metabolism. BUN tests are regularly exercised by medical diagnostic labs as a measure of many biological functions in the body especially the excretory system. Discrepancies in

BUN are associated with liver damage, protein deficiencies, drug poisoning, impaired intestinal absorption, nephritis, shock, irregular protein catabolism, myocardial infraction, pregnancy [182] etc. The latest procedures to perform a BUN test involve the extraction of non-hemolyzed serum from a blood sample and an enzyme based chemical analysis. The urea is hydrolyzed by enzyme urease (extracted from jack beans) to ammonia and carbonate. The ammonia produced reacts with alphaketoglutaric acid in the presence of Gutamic-acid dehydrogenase enzyme and oxidizes NADH (Nicotinamide adinine dinucleotide hydrate) to NAD [183]. The amount of BUN present is then proportional to the conversion rate of NADH to NAD which is monitored in an absorption spectrometer at a fixed wavelength.

Though the enzyme based chemical analysis of the blood urea provides an accurate procedure for diagnostic purposes, the limited sensitivities of the test require it to use large amount of blood samples to conduct a test. These tests are carried out by following invasive procedures which are always traumatic for patients and shall be avoided. Besides it takes at least tens of hours to analyze samples in these methods and the results may not reflect the latest physiological conditions *in vivo*. In addition, chemical analyses need bulky apparatus and are not particularly suitable for use outside a diagnostic lab. Therefore, techniques are required to make devices with improved sensitivities[184] where it is possible to analyze as small a sample volume as possible. This will help minimize the ordeal for patients, use of bulky instruments for analyses and fasten the time taken for analysis.

Electrical sensing methods are ideally suited to avoid bulky analytical instruments and provide for a fast analysis. The devices used for electrical detection are based on either the field-effect or on electrochemical phenomena. In order to achieve the highest sensitivities for field-effect based electrical detection, many nanostructured materials have been proposed to act as active element of these devices[185-187]. One dimensional nanostructure like semiconducting NWs are among the most promising candidates which can be used for such applications[187-189].

(i) Experimental

This section discusses the fabrication and operation of ZnO NW based enzyme FETs for electrical detection of urea. The NWs were functionalized with enzyme urease (E.C. No. 3.5.1.5) embedded in polypyrrole polymer matrix serving as receptors for urea molecules. A mixed solution containing 110 IU/ml urease solution with 10 mM pyrrole molecules in phosphate buffer saline (final concentration with salts = 150 mM) was used for selective functionalization of ZnO NWs in a standard electropolymerization[190] method with polypyrrole using cyclic voltametry (from -0.1V to +0.9 V). Figure 4.8 illustrates the fabrication of enzyme based FET using an electrochemical cell for electropolymerization of pyrrole on NW surface (**figure 4.8A**). Enzymes are embedded in the polymer matrix during the electropolymerization process as depicted in **figure 4.8B**.

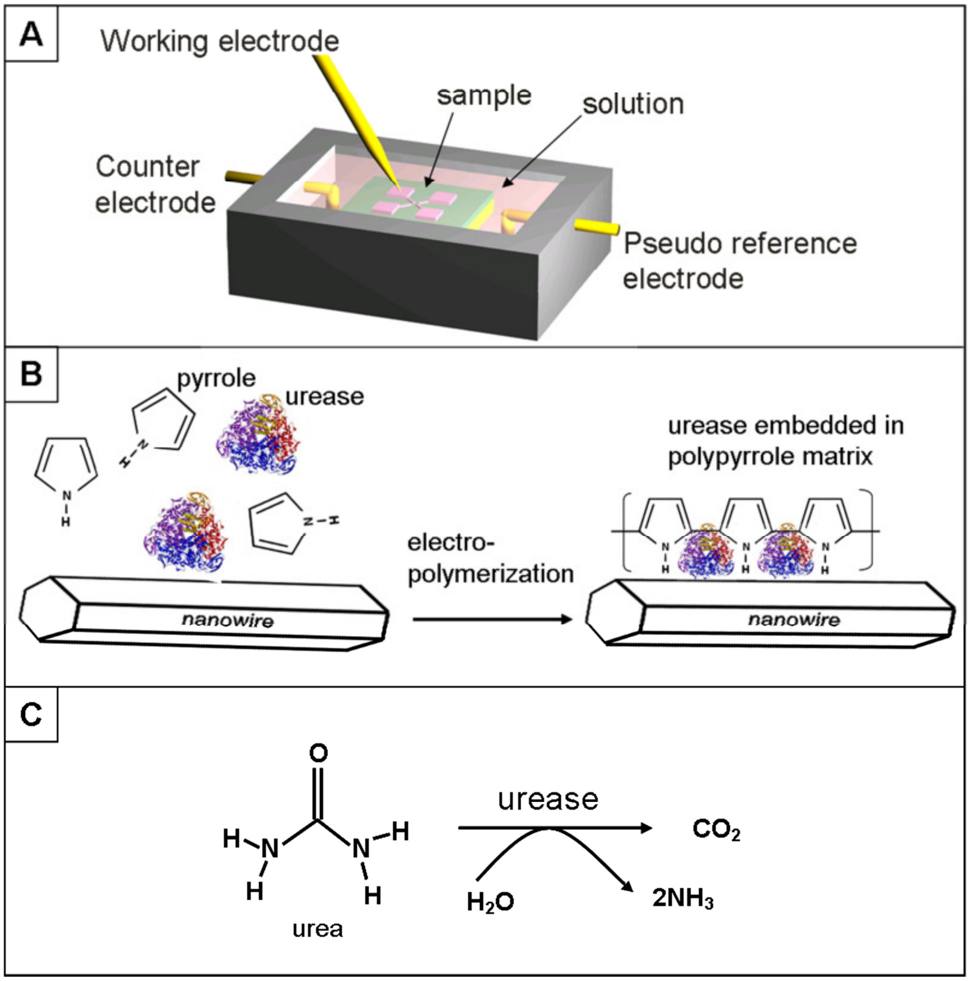

Figure 4.8: Preparation of ZnO NW based enzyme FETs. (A) Schematic of an electrochemical cell used for functionalization of enzyme urease on ZnO NWs. (B) Schematic of the functionalization of urease embedding it in polypyrrole matrix (C) enzymatic conversion of urea in to ammonia and carbon dioxide.

The sensing trials were performed using 100 µM urea solutions in phosphate buffer with 0.1M NaCl (pH 7.4). The enzyme urease functionalized on the ZnO NW surface initiates the degradation of urea molecule into carbon dioxide (CO_2) and ammonia (NH_3). The production of ammonia changes the pH of the solution in contact with NW surface which is reflected in the transport characteristics of transistor. The measurement set-up is shown in figure 4.9.

Enzyme functionalized self-assembled ZnO NWs transistors fabricated on silicon chips were mounted on a chip carrier and wire-bonded to the leads. A microwell was prepared by manually carving out reservoirs and a microchannel in a polydimethylsiloxane (PDMS, Sylgard 184, 10:1) layer (discussed earlier in chapter). The microwell was stuck to the chip surface after wire bonding. An Ag/AgCl reference electrode placed in contact with the liquid in the microfluidic circuit allowed us to set the potential precisely on the surface of the NWs. The field-effect was measured as dependence of impedance (Z, a complex quantity with magnitude and phase) vs applied gate voltage (Vg) in liquid.

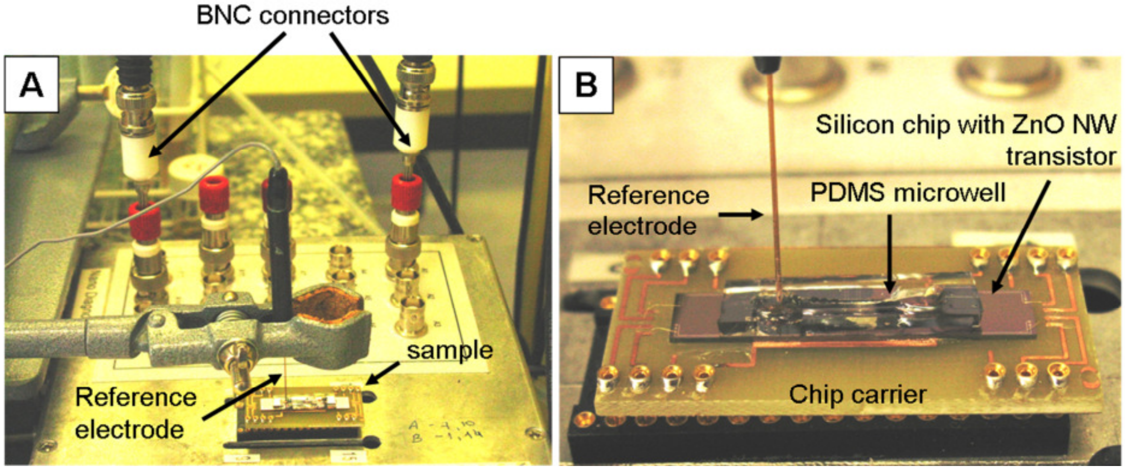

Figure 4.9: The electrical probe system for ZnO NW transistors for urea sensing. (A) BNC probe system with a sample mounted on probe stage. (B) Zoomed in image of the silicon chip with ZnO NW transistors mounted on a chip carrier and an Ag/AgCl reference electrode immersed into the PDMS microwell assembled on top of chip.

The impedance signal constituted the sensor response, which was measured using an impedance analyzer (Agilent 33250A LCR Meter) in a frequency range of 20 Hz to 2 MHz. AC measurements improved the signal-to-noise ratio and thereby stability and reproducibility in comparison to DC measurements [191]. The semiconducting nature of ZnO NWs which exhibit a high gate modulation, the AC measurement strategy coupled with the use of a reference electrode shall enhance the sensor response as compared to others.

The resulting dataset can be visualized in the form of a 2D magnitude Z-map. The Y-axis corresponds to frequency and the X-axis corresponds to the liquid gate voltage. Every point in the map corresponds to the impedance (phase or magnitude) at a certain frequency and gate voltage.

(ii) Sensing Characteristics

This frequency response is measured at varying gate voltages to characterize the field-effect behavior. The gate voltages are maintained in the range of -0.4 to +0.4 V (at the Ag/AgCl reference) to ensure that no parasitic electrochemical processes can take place. The resulting data set can be visualized in the form of a magnitude map as shown in **figure 4.10**.

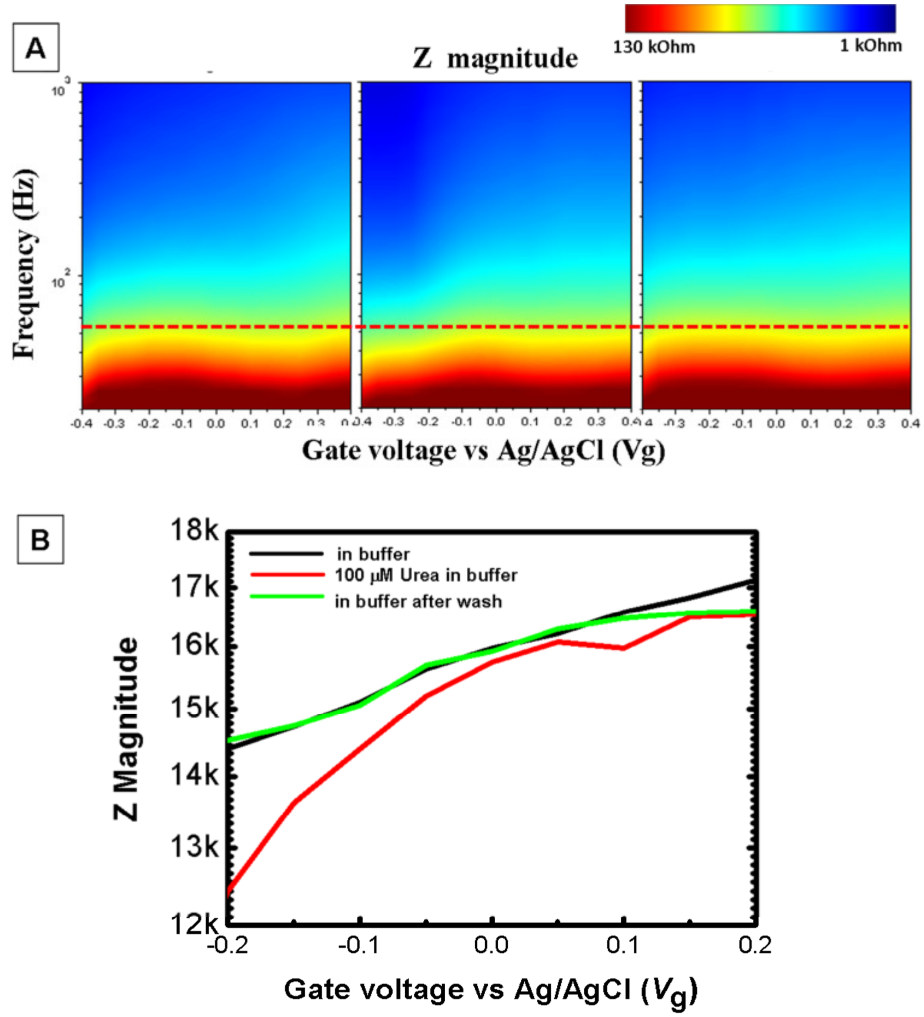

Figure 4.10: Urea sensing. (A) Plots showing the magnitude z-maps in different solutions. The data acquired presents from left to right- the response in buffer, with 100 µM urea solution in buffer and the response after wash in buffer. The sensor response shifting to the right in magnitude is clearly perceptible indicating the urease action in the presence of urea. (B) The plots show the sensor response at a fixed frequency. Gate dependence of impedance is extracted along the section profile shown in figure A for magnitude. The reversible gate response is apparent from the graphs presented in the figure.

To understand the sensor response of the urease functionalized ZnO NW device impedance magnitude and impedance phase maps are first recorded in the buffer without introducing any urea. The resistance of the NW devices is dominant at low frequencies where the device impedance exhibits a low gate modulation.

At high frequencies, the capacitive components originating from electrical double layer capacitance and parasitic capacitances dominate as seen in the **figure 4.10B**. When the sensor is exposed to urea, it is apparent that the Z-magnitude response shifts to right on the gate voltage scale (x-axis). After performing the sensing trial, device was washed with buffer solution. After the wash, the sensor response recovers coming back to the initial response. The sensor response can be understood after analyzing the section profiles at a certain frequency. **Figure 4.10A** shows a plot for gate dependence of impedance (Z-magnitude). The threshold shift towards positive gate voltages can be associated with the production of ammonia and increase in the pH around the NWs. Upon washing with the buffer, the ammonia concentration is reduced and the sensor response comes back to the initial.

Demonstration of ZnO NW based enzyme-FETs for urea sensing shows promise for the future applications in electrical sensing of biomolecules. Many enzyme based electrical sensors can be developed on this basis for the direct sensing of molecules like creatinine, glucose, triglycerides, cholesterol etc. from blood and plasma samples.

Chapter 5

ZnO NW based MESFET

Metal-semiconductor field-effect transistor (MESFET) is a 3 terminal devices where a metal gate electrode is directly in contact with the semiconductor channel forming a Schottky barrier. The semiconductor channel makes ohmic contacts with source and drain electrodes. Flow of charge carriers in the channel is controlled by the metal-semiconductor Schottky contact established between the gate and the channel. The Schottky contact induces a depletion layer underneath the metal gate in the channel and the thickness of this depletion layer can be controlled by applying a voltage on the metal gate. This chapter discusses the fabrication of a novel ZnO NW based MESFET and its application in liquid sensing. ZnO NW MESFETs are fabricated depositing metal NPs on the NWs and employing these metal NPs as metal gate in liquids. The advantages of employing metal gate architecture in transistors for liquid sensing will be discussed. Experiments will demonstrate improvement in field-effect mobilities of such transistors by employing a metal nanoparticle gate and possibility of very low voltage operation.

5.1 Background

MESFET were first invented in 1966 by Carver Mead as GaAs FET using a Schottky barrier metal gate [192]. Carver had pointed out the high performance achievable in MESFET configuration where filed-effect mobilities, and limiting frequencies of the devices would be larger than their counterpart devices made in silicon technology. This dream was realized in 1969, when GaAs MESFETs made with short gates (typical gate length of 1µm) showed cut-off frequencies of about 30GHz-around four times higher than that of silicon devices with same layout[193, 194]. Since then MESFETs have been the workhorse of radio and microwave applications. After the development of new fabrication techniques to build heterojunction structures, high electron mobility transistors (HEMT) have been made (as proposed by Ray Dingle[195] and the devices find applications in cellular phone technology, fibre-optics communications, electronic test equipments and military. Devices built in a MESFET architecture can have advantages over MOSFET and JFET design for certain applications[13]. The unique Schottky gate architecture brings high-electron mobilities and requires very low gate voltage for transistor operation.

In the following, the basic mechanism of MESFET operation of planar devices and its application to nanoscale MESFET is discussed.

5.2 Metal-Semiconductor contact

Metals with high work functions such as gold, silver, platinum, palladium etc. form highly rectifying junctions when brought in contact with semiconducting materials. The contact formed is called a Scottky contact and simply works as a diode. For high quality Schottky contacts in a unipolar transistor, the reversed biased leakage current must be sufficiently low. The low leakage current on the contact produces sufficient gate-channel isolation and thus enables the fabrication of a MESFET without using an insulator layer between the channel and gate. The Scottky contact between a metal and n-type semiconductor is shown in **figure 5.1**.

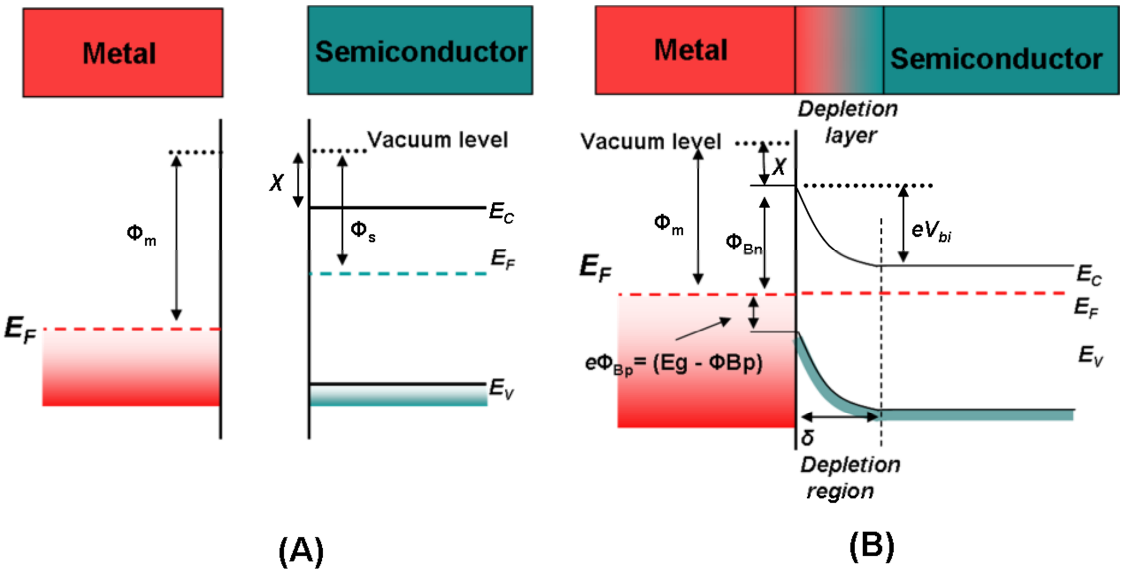

Figure 5.1: A schematic representation of metal-semiconductor bands in a Schottky contact. (A) The band alignment in metal and semiconductor before formation of contact and (B) band rearrangements after formation of the contact.

If the metals work function is larger than the semiconductor electron affinity$X$, bringing a metal to the semiconductor leads to electron flow from the semiconductor to the metal in order to align the Fermi levels. The remaining positively charged atoms in the semiconductor create a space charge region which forms a barrier of height Φ_{Bn} for electron flow from semiconductor to metal.

$\Phi_{Bn} = (\Phi_m - \chi)$

where Φ_m is the work function of the metal and χ is the electron affinity.

$eV_{bi} = \Phi_{Bn} - (E_C - E_F)$

5.3 Shockley model

The JFET model of Shockley[196] can be applied to model MESFET with small channel length and gate sizes with the inclusion of smaller size effects. In order to explain the results obtained for ZnO NW MESFETs, the following text will assume a simple model of MESFET considering a planar device with n-type channel covered with gate [13]. Applying a negative bias (V_G) on the gate forms a depletion channel in the semiconductor of width 'w' as shown in **figure 5.2.** Applying a positive bias shrinks the depletion layer width and will forward bias the junction. The width of the depletion layer formed is given by-

$W = \sqrt{}2\varepsilon_s (V_{bi}-V_G) / q N$ ……………………………………………………….5.1

Here, ε_s is the permittivity of the semiconductor, q is electron charge, V_{bi} is the voltage at Schottky junction and N is the density of electrons in the material.

When applying a positive bias on the gate, the thickness of the depletion layer decreases till the channel thickness reaches a maximum at w = d, the thickness of the semiconductor layer. Conversely, applying a negative bias increases the depletion layer width till a maximum of semiconductor layer thickness where the current stops flowing from source to drain. This voltage is called the threshold voltage (V_{th}) of the device:

$V_{th} = V_{bi} - qNd^2 / 2\varepsilon_s$…………………………………………………………..5.2

The threshold voltage depends on the Schottky contact voltage (built-in potential) and the channel thickness d. The threshold voltage can also be seen as function of the pinch-off voltage Vp-

$V_{th} = V_{bi} - V_p$………………………………………………………………… 5.3

The current density 'J' of a MESFET can be calculated by considering a small section of the device in a Shockley model and is given by-

$J = qnv = qN_d\mu_n \varepsilon = - q N_d \mu_n \cdot dV_c (y)/dy$.. 5.4

Where V_c is the channel voltage at position y.

The current density is related to the drain current by following equation-

I_D = -JW (d- $x_n(y)$) where x_n is the depletion layer width at position y related to the channel voltage- $x_n(y) = \sqrt{2\varepsilon s}\ (V_{bi} - V_G + V_c(y)/qN_d$

The drain current can now be obtained based on the assumption that the steady current in the device is independent of position.

$I_D = qN_d\mu_n\, d\cdot W/L\ [V_D\text{-}2/3(V_{bi}\text{-}V_G + V_D)^{3/2}/\sqrt{Vp} - (V_{bi}\text{-}V_G)^{3/2}/\sqrt{Vp}\ ]$..............5.5

Equation 5.5 is valid as long as the width of the undepleted channel (d- $x_n(y)$) is positive, namely for:

$V_D \leq V_G - V_T$.. 5.6

This equation would also define that for larger drain voltage, the current saturates and,

$V_D = V_G - V_T = V_{D.\,sat}$

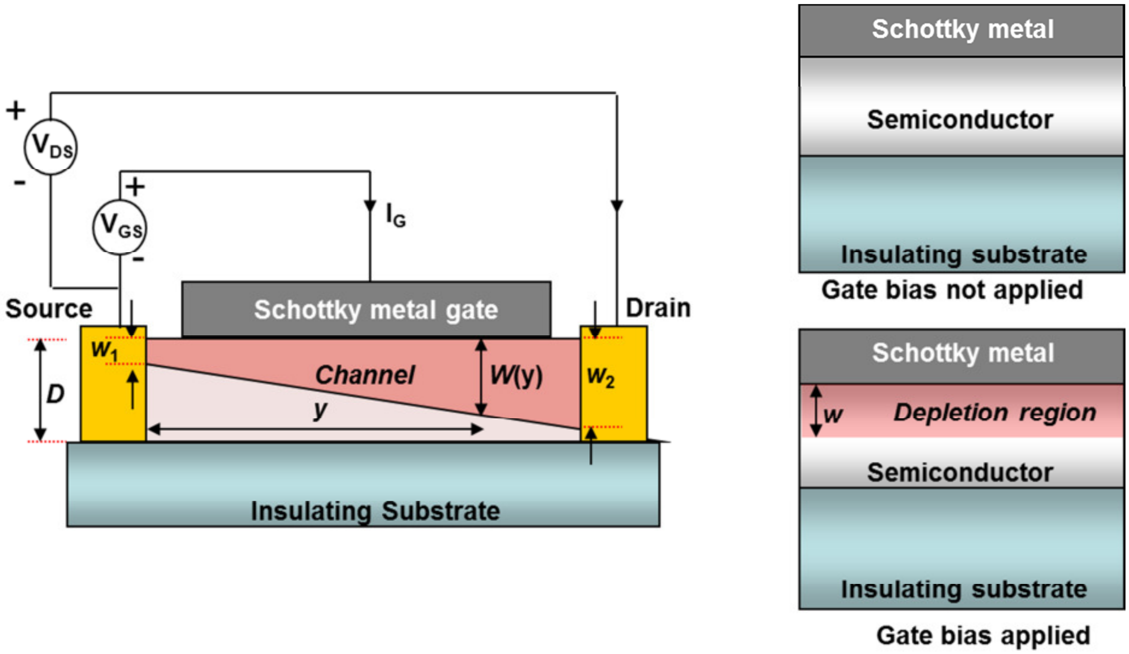

Figure 5.2: Shockley model for linearly graded depletion region in a MESFET with finite drain-source bias and the formation of depletion layer on an applied gate bias.

5.4 Nanoscale MESFET

The MESFET model for planar devices is advantageous over MOSFET since it induces higher mobility of the charge carriers in the channel as compared to the MOSFET. The carriers located in the inversion layer of a MOSFET have a wave-function extending to the oxide insulation layer. As a consequence the mobility of charge carriers is less than a half of that of the bulk material channel. However in MESFET, the depletion layer is formed with in the channel material and it separates the charge carriers from the surface and hence their mobilities are close to that of the bulk material. This higher mobility leads to a higher current and transconductance of the device while operating at low voltages.

In addition to obvious advantages of using a depletion layer potential for charge modulation across the channel in a MESFET configuration, the performance can be improved by further optimizations. Increasing the gating-effect by Schottky contacts and using a high surface to volume channel such as NWs and nanotubes can provide opportunities to fabricate high-performance MESFET devices. The effects of different metal gate architectures on a 1D channel must be look into as a basis for fabricating highly effective Schottky contacts in 1D MESFETs. The dependence of gating-effect on the gate geometries in a 1D MESFET will be discussed here as a basis to understand the gating mechanism in ZnO NW MESFETs in liquid gate.

(i) Effect of gate architecture

The effect of the gate geometry dictates the formation of the depletion layer in the MESFET channel and hence the transistors characteristics. The operating voltage of a device is determined by the pinch-off voltage i.e. the voltage when the depletion layer width is at maximum and the channel is turned off completely. **Figure 5.3** illustrates three limiting cases in a MESFET where (A) the gate length l_G is comparable to channel length l_{Ch} (B) gate length is shorter than the channel length and (C) employing small length Schottky contacts in parallel (gate).

In the case of device A, the channel is pinched off by a planar portion of depletion layer. In the Shockley model analysis for pinch-off in a planar depletion layer is given by-

$V_{PO} = qN_Da^2/2\varepsilon_r \varepsilon_0$……………………………………………………………… (5.7)

Where q is electron charge, N_D is electron density, a is channel depth, ε_r permittivity of the medium and ε_0 is permittivity of free space. So the pinch-off current is directly proportional to the area of depletion layer.

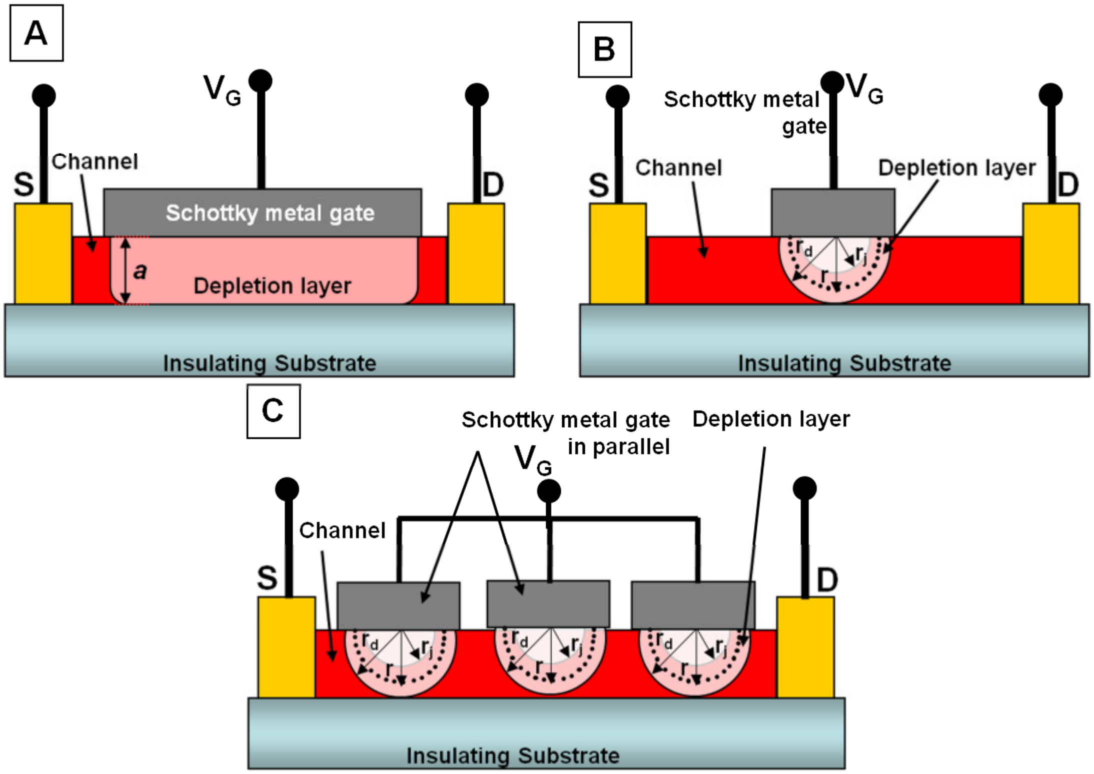

Figure 5.3: Effect of gate geometries in a MESFET. (A) when the metal gate length is equal to channel length, (B) when gate length << channel length and (C) parallel addition of short gate lengths in a MESFET

Device B has a gate length much less than the channel length which generates a cylindrical/spherical depletion layer in the channel. The pinch of voltage for this configuration is calculated assuming a cylindrical model and applying Gauss's Law. The distances from the metal contact in the channel r_d, r and r_j denote the depth of the spherical depletion layer, mean radius of the depletion layer and the junction depth of the metal-semiconductor contact in the depletion layer respectively.

Now applying Gauss's Law for the total electron flux-

$$\int_0^x \varepsilon_r \varepsilon_0\, \varepsilon(r)\, r_d\, \theta = -q N_D \int_0^x \int_r^{rd} r_d\, \theta\, dr$$

where $r_d\, \theta\, dr$ is elemental voltage.

$$\varepsilon_r \varepsilon_0\, \varepsilon(r) = -q N_D \cdot (r_d^2 - r^2)/2$$

Since the field is dependent only on 'r'-

$$\varepsilon(r) = -q N_D / 2 \varepsilon_r \varepsilon_0 \cdot (r_d^2 - r^2)/r$$

When integrating the above equation in the field from the point of junction:

$$V_{PO(spherical)} = - q N_D/ 2 \varepsilon_r \varepsilon_0 \int_{rj}^{rd} dr \cdot (r_d^2 - r^2)/r$$

or, $V_{PO(spherical)} = - q N_D/ 2 \varepsilon_r \varepsilon_0[r_d^2 ln \cdot r_d/r_j - (r_d^2 - r_j^2)/2]$....................................(5.8)

Equation 5.7 and 5.8 give the peak-off voltages for the devices with $l_G \sim l_{Ch}$ and $l_G << l_{Ch.}$

Ratio if the two pinch-off voltages in device (A) and device (B) can be established now:

$V_{PO\ (spherical)} / V_{PO\ (parallel)} =$ rd2/ $a^2.\ln r_d/ r_j - (r_d/a)^2. \frac{1}{2}[1-(r_j/r_d)]$

Since at pinch-off, $r_d = a$ and junction depth is very small than r_d so $r_d/ r_j => 1$

Hence $\mathbf{V_{PO(spherical)} > V_{PO(parallel)}}$

Higher pinch-off voltages lead to higher saturation currents which is related to transconductance by the equation-

$I_D = G_0 (1\text{-}h/a) V_{ds}$ where I_D is saturation current and G_0 is transconductance.

or, $G_0 = I_D/ V_{ds}(1\text{-}h/a)\ \alpha\ V_{PO}$

Hence MESFET B is expected to show higher transonductance values than MESFET A. However, despite the disadvantages of lower pinch-off voltages in MESFET A, the small series resistance for gate (due to small regions of gate not in the contact with channel) does not affect the charge velocities and transconductance values are expected to be close to that of the bulk semiconductor material. The devices with small gate length (B) have an induced channel resistance in series with the gate which affects the charge velocities and thus the transconductance values of the devices as well. Image C proposes an architecture of MESFET which combines short gate length effect of higher pinch-off voltages with minimal induced resistance to the gate. In the device schematics, the channel is deposited with small metal gates which would join each other in parallel and add-up the gate capacitances, while maintaining the spherical depletion regions in the channel. The parallel configuration of metal-semiconductor contacts through out the length of the channel also reduces the non-contacted channel portions responsible for series resistance to the gate. This configuration shall provide high performance MESFET with higher pinch-off voltages with little compromise on transconductance values.

(ii) Experimental

Efforts have been made to fabricate high performance nanoscale MESFETs with GaAs [197], CNTs[198] and other materials[199, 200] by downscaling and adjusting the gate-channel length. While a device configuration for maximum transconductance values with rising pinch-off voltages still remains a technological challenge in building high performance MESFET devices with any semiconducting material, real applications for devices made with materials other than GaAs still need to be explored.

Like GaAs, semiconductor NWs can be used for MESFETs. Some research groups have suggested the fabrication of NW based MESFET and proposed their application in different fields[200, 201]. This section discusses the fabrication of ZnO NW based MESFET. Self-assembled ZnO NW transistors as discussed in chapter 3 were used to construct ZnO NW MESFET. ZnO NWs contacted by Ti/Pt source and drain microelctrode electrodes were decorated with gold and palladium NPs using an electrochemical deposition method. The set-up for the electrochemical deposition of metal NPs was earlier discussed in chapter 4 and shown in **figure 4.8**. A mixture of 0.1 M $LiClO_4$ and 2 mM $HAuCl_4$ (10:1) and $Na_2[PdCl_4]$ in water were used for the deposition of gold and palladium NPs respectively [202]. $LiClO_4$ here worked as supporting electrolyte in the solution. Typically a voltage of -1.1 V versus Pt was applied for 12 seconds for carrying out the electrodeposition. Figure **5.5 A** and **B** show SEM images of a device before and after carrying out the electrodeposition and illustrate the selective deposition of metal NPs on ZnO NWs. The average size of NPs was found to be 50 nm as inferred from AFM profiles. The metal NPs formed Schottky contacts on the NWs and worked as gate in liquid medium where gate voltage was applied using an Ag/AgCl refrence electrode.

(iii) Device characteristics

The operation of liquid gated ZnO NW MESFETs is discussed in this section. **Figure 5.4** illustrates the design of ZnO NW based liquid gated MESFET. An electrochemical gate set-up was used to characterize ZnO NW MESFETs as described in the previous chapter. **Figure 5.5 C** shows the dependence of conductance on liquid gate for a typical MESFET before (black curve) and after (red curve) NPs deposition. The ZnO NW MESFET shows an *n*-type transistor characteristic. The transistor conductance in liquid gate as plotted in the black curve can be modulated up to 2 orders of magnitude at gate voltages from -1 to +1 V.

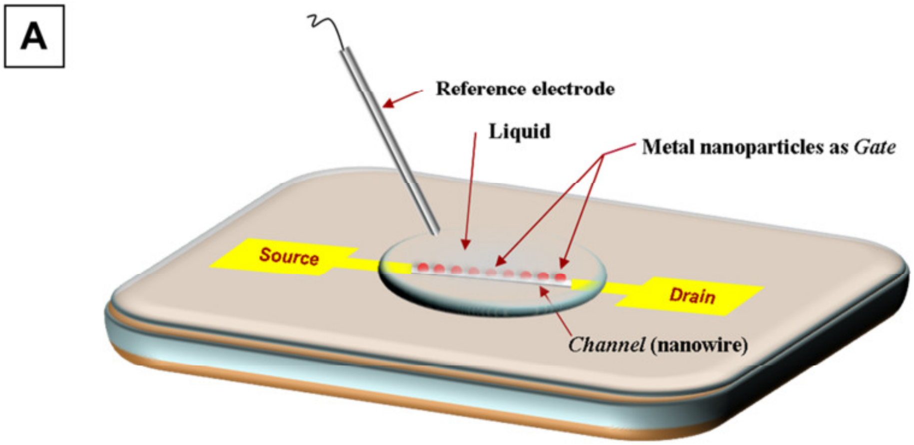

Figure 5.4: Model of NW based liquid gated MESFET (A) an electrochemical gate set-up (B) Schematic representation of device architecture showing nanoparticle metal gates parallel to electrochemical gating.

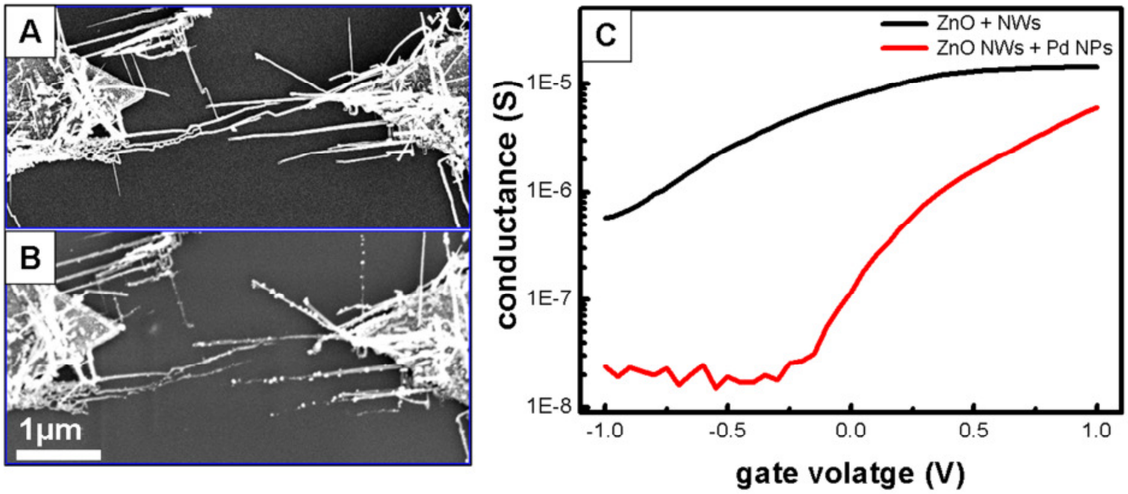

Figure 5.5: (A) and (B) represent SEM images of a typical ZnO NW device before and after electrochemical deposition of metal NPs. (C) Liquid gate dependence of conductance before and after NPs deposition.

When using metal NPs as gate, the conductance could be modulated more than 4 orders of magnitude for the same devices. The enhanced gating effect can be attributed to the electrochemical gate and metal-nanoparticle gate adding to each other in parallel as suggested in the theoretical discussion and showed in figure 5.4 B.

5.5 Chemical sensing

The use of metal NPs as gate thus improves the transistor performance and makes ZnO NW MESFETs as potential candidate to employ as liquid gated transistors. In addition to this, the use of metal NPs as gate gives an opportunity to tune the performance by varying their size and density. Moreover it is also possible to control the chemistry on nanoparticle surfaces. NPs can be selectively functionalized by organic and inorganic molecules in order to render MESFETs sensitivity to specific analytes present in the surroundings. Metal NPs have also been demonstrated to selectively bind with enzymes and proteins which is again useful to perform label-free electrical biosensing with such transistors. This section presents a discussion of the modification of ZnO NW MESFET to attain a chemical sensor operating in liquid environment.

The ZnO NW MESFET with palladium NPs as gate was functionalized with p-aminothiophenol (p-ATP) and p-hydroxythiophenol (p-HTP). At neutral pH, p-ATP contains a positively charged amino group while p-HTP a negatively charge hydroxyl group. P-ATP and p-HTP can be selectively bound to the metal NPs on ZnO NWs by their thiol end groups. After functionalization with p-ATP field-effect behavior of the devices was characterized in in phosphate buffer @ pH 8.0. The gate dependence of conductance before and after p-ATP functionalization is plotted as black and red curves in **figure 6.6A**. The transistor shows conductance modulation of up to 5 orders of magnitude while applying a gate voltage from -0.5 to + 0.5 Volts. It is apparent that the threshold voltage of transistor shifts towards positive gate voltages when functionalized with protonated p-ATP molecules. On the other hand, functionalizing the same device with a molecule which tends to get deprotonated shifts the threshold voltage towards the negative gate voltages. This is in accordance with the fact that increasing the positive charges on a metal nanoparticle gate would require applying a more positive bias to switch-on a transistor and vice-versa. ZnO NW MESFETs discussed in this chapter report lD MESFETs operation in liquid medium for the first time. High performance devices demonstrated as chemical sensor opens up opportunities for their application in biological sensing.

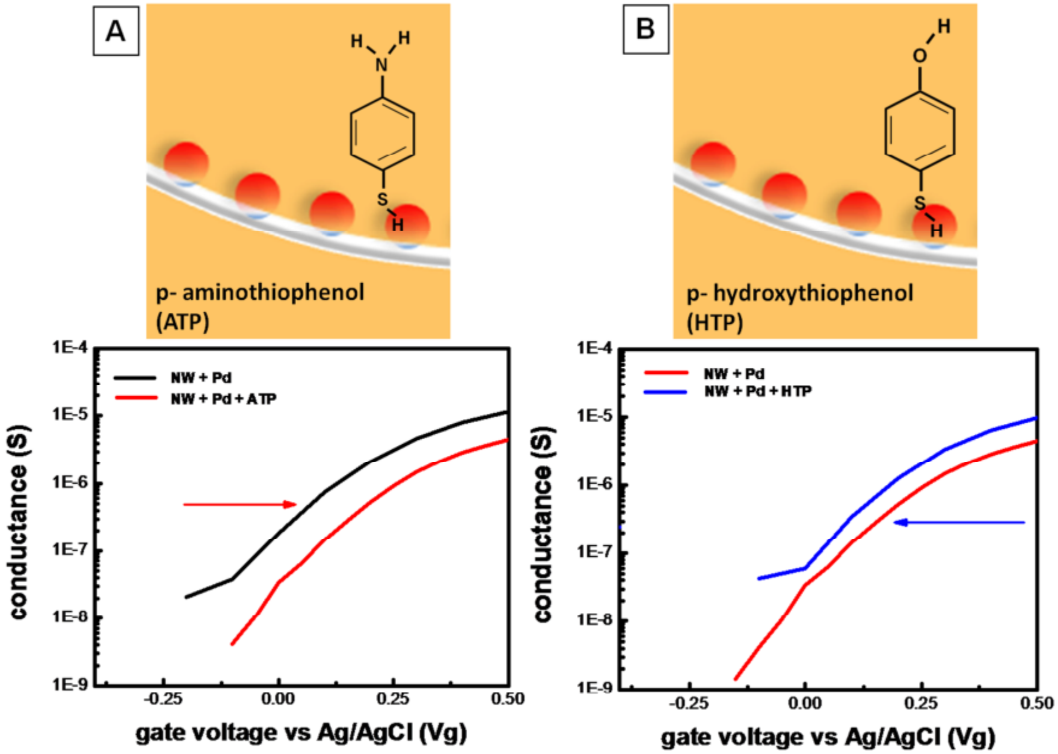

Figure 5.6: Schematic representation of Pd nanoparticle metal gate on ZnO NW MESFET selectively functionalized with p-amonithiophenol and p-hydroxythiophenol (A and B respectively). The transport characteristic in both plots corresponds to the same device. (A) Liquid gate dependence of conductance of MESFET when functionalized with p-ATP and (B) when functionalized with p-HTP.

Chapter 6

Summary and Outlook

This thesis presented the fabrication of FETs based on ZnO NWs and their use is demonstrated for electrical sensing applications. An aqueous solution based chemical bath deposition (CBD) method was devised and optimized for the synthesis of hierarchical ZnO nanostructures. The CBD method was also optimized for the site-specific growth of ZnO NWs. This technique was utilized for the fabrication of ZnO NW transistors. The NWs were selectively grown on prewritten microelectrodes working as source and drain. This is the first report of site-specific self-assembled transistors fabricated using a simple solution based growth method.

The CBD based method to grow ZnO NWs site-specifically was further employed for the scalable fabrication of transistors on flexible substrates. Kapton polyimide foils were used as flexible substrates to photolithographically write Cr/Pt electrodes working as source and drain. A chemical method for surface optimization of kapton foils before photolithography was devised which provided robust adhesion of microelectrodes to the surface. The Kapton foils written with microelectrodes were used for scalable self-assembled growth of ZnO NW transistors. The experiments demonstrated over 80 percent yield of fabrication on a 80×80 mm foil with a density of 120 microelectrode pairs.

The self-assembled ZnO NWs were used for all the experiments related with liquid based sensing trials. It is the first time where ZnO NW based transistors were characterized using an electrochemical gate and demonstrated as pH sensors. The NW transistors showed field-effect characteristic in liquids with 4-6 orders of magnitude current modulation at gate voltages ± 2 Volts. The liquid-gated ZnO NW transistors exhibited field-effect mobilities up to 1.85 cm2/Vs and sub-threshold slopes around 105 mV/decade.

ZnO NW transistors fabricated on silicon and kapton foils were integrated with open and closed microfluidics in order to facilitate liquid handling for sensing experiments. An open microfluidic system based on silicon nitride or PDMS and a closed microfluidic system based entirely on PDMS were assembled for microfluidic integration of ZnO NW transistors. Using the latter system, the thesis demonstrated a novel approach for self-assembled fabrication of

ZnO NW transistors and other nanostructures inside microfluidic channels.

Liquid-gated ZnO NW transistors were subsequently deployed as biosensors. An enzyme-based electrical sensing method is realized for the sensing of urea molecules in buffer. The enzyme urease was functionalized on the ZnO NW surface in order to construct enzyme-FETs.

In addition to the application of ZnO NW devices for biosensing applications, the thesis demonstrated a novel architecture for improving the field-effect characteristics of nanoscale FETs. ZnO NWs FETs chosen as example were electrochemically decorated with metal NPs. The metal NPs deposited on NW surface forming Schottky contacts were used as metal gates while applying gate voltage through the liquids. The transistors operating as metal-semiconductor FETs (MESFETs) in liquid showed 2-3 times improvement in field-effect characteristics. This is the first demonstration of ZnO NW based metal-semiconductor FETs working in liquid medium. The MESFETs were also deployed as chemical sensors by functionalizing metal NPs with charge sensitive receptors.

The work carried out for this thesis excels in the realization of a novel scalable fabrication method for ZnO NW transistors. The method which avoids use of conventionally used techniques such as e-beam lithography etc. for transistor fabrication is expected to provide immense opportunities for low cost production of electrical devices for different applications. The successful realization of transistors in a site-specific self-assembled manner on flexile substrates advocates the potential of this novel fabrication approach for future applications in flexible electronics, photovoltaics and electrical sensors.

The understanding gained in the formation of 2D and 3D hierarchical nanostructures using a solution based method can be further utilized for other material systems like organic polymer crystals to create 3D architecture of materials. The synthesis of nanomaterials with 3D architecture also attracts more interest for applications in biology and photonics. *In situ* growth of nanostructures inside microfluidic channels as performed in this thesis can be further explored for site-specific positioning of nanostructures and localized growth of nanomaterials.

Liquid gated ZnO NW FETs acting as high performance chemical and biosensors invite opportunities for their use in real applications in environmental sensing and other diagnostic purposes. Future investigations will focus on their deployment in biomolecule sensing in blood serum and urine samples. The mechanics of molecular binding on the receptors can be studied using such electrical platform in order to gain understanding in molecular interactions in biology.

Overall, this thesis introduces the idea to integrate simple nanomaterial growth methods to device fabrication techniques which till now are far from fully explored. The fabrication of fully functional electrical sensors based on ZnO NW operating in liquid medium and their use in sensing shows promise for their future application in biosensing and the viability of such fabrication techniques. The novel method to further improve the filed-effect characteristics of liquid-gated transistors by using a metal nanoparticle gate system soars promise to yield opportunities in fabrication of FETs with much higher performances. The higher performance of FETs is expected to yield high sensitivities of electrical sensors and low voltage operation which are the fundamental concerns in developing electrical biosensors. Moreover, the devices present a novel system to study the metal-semiconductor gating effect in liquid medium for the first time and can be exploited for some fundamental studies related to the catalytic activity of NPs with other chemical and biological species. The conjugation of NPs as a gate in the devices may also be studied further for optoelectronic properties of devices in air and liquid medium.

Bibliography

1. Roy, S. and Z. Gao, *Nanostructure-based electrical biosensors.* Nano Today, 2009. **4**(4): p. 318.
2. Wang, J., *Carbon-Nanotube Based Electrochemical Biosensors: A Review.* Electroanalysis, 2005. **17**(1): p. 7.
3. Fan, X., et al., *Sensitive optical biosensors for unlabeled targets: A review.* Analytica Chimica Acta, 2008. **620**(1-2): p. 8.
4. Erickson, D., et al., *Nanobiosensors: optofluidic, electrical and mechanical approaches to biomolecular detection at the nanoscale.* Microfluidics and Nanofluidics, 2008. **4**(1): p. 33.
5. Rajesh, T. Ahuja, and D. Kumar, *Recent progress in the development of nano-structured conducting polymers/nanocomposites for sensor applications.* Sensors and Actuators B: Chemical, 2009. **136**(1): p. 275.
6. Cui, Y., et al., *NW Nanosensors for Highly Sensitive and Selective Detection of Biological and Chemical Species.* Science, 2001. **293**(5533): p. 1289.
7. T. Kurkina, A.V., A. Ahmad, K. Kern, K. Balasubramanian, *Label-free detection of few copies of DNA using carbon nanotube impedance biosensors.* Angvandte Chemie Int., 2011.
8. Besteman, K., et al., *Enzyme-Coated Carbon Nanotubes as Single-Molecule Biosensors.* Nano Letters, 2003. **3**(6): p. 727.
9. Vlandas, A., et al., *Enzyme-Free Sugar Sensing in Microfluidic Channels with an Affinity-Based Single-Wall Carbon Nanotube Sensor.* Analytical Chemistry. **82**(14): p. 6090.
10. Vo-Dinh, T. and B. Cullum, *Biosensors and biochips: advances in biological and medical diagnostics.* Fresenius' Journal of Analytical Chemistry, 2000. **366**(6): p. 540.
11. Cheng, M.M.-C., et al., *Nanotechnologies for biomolecular detection and medical diagnostics.* Current Opinion in Chemical Biology, 2006. **10**(1): p. 11.
12. Walt, D.R., *Miniature Analytical Methods for Medical Diagnostics.* Science, 2005. **308**(5719): p. 217.
13. S. M. Sze, K.K.N., *Physics of semiconductor devices*. 2007: John Wiley and Sons.
14. Wang, D., et al., *Germanium NW field-effect transistors with SiO[sub 2] and high-kappa HfO[sub 2] gate dielectrics.* Applied Physics Letters, 2003. **83**(12): p. 2432.
15. Cha, S.N., et al., *High performance ZnO NW field effect transistor using self-aligned nanogap gate electrodes.* Applied Physics Letters, 2006. **89**(26): p. 263102.
16. Keem, K., et al., *Fabrication and Device Characterization of Omega-Shaped-Gate ZnO NW Field-Effect Transistors.* Nano Letters, 2006. **6**(7): p. 1454.

17. Josowicz, M. and J. Janata, *Suspended gate field effect transistors modified with polypyrrole as alcohol sensor.* Analytical Chemistry, 1986. **58**(3): p. 514.

18. Yang, M.H., et al., *Advantages of top-gate, high-k dielectric carbon nanotube field-effect transistors.* Applied Physics Letters, 2006. **88**(11): p. 113507.

19. Schwierz, F., *Graphene transistors.* Nat Nano. **5**(7): p. 487.

20. Wang, J., G. Liu, and M.R. Jan, *Ultrasensitive Electrical Biosensing of Proteins and DNA:â€‰ Carbon-Nanotube Derived Amplification of the Recognition and Transduction Events.* Journal of the American Chemical Society, 2004. **126**(10): p. 3010.

21. Qi, P., et al., *Toward Large Arrays of Multiplex Functionalized Carbon Nanotube Sensors for Highly Sensitive and Selective Molecular Detection.* Nano Letters, 2003. **3**(3): p. 347.

22. Tang, X., et al., *Carbon Nanotube DNA Sensor and Sensing Mechanism.* Nano Letters, 2006. **6**(8): p. 1632.

23. Daniel, S., et al., *A review of DNA functionalized/grafted carbon nanotubes and their characterization.* Sensors and Actuators B: Chemical, 2007. **122**(2): p. 672.

24. Zheng, G., et al., *Multiplexed electrical detection of cancer markers with NW sensor arrays.* Nat Biotech, 2005. **23**(10): p. 1294.

25. Liu, H., et al., *Polymeric NW Chemical Sensor.* Nano Letters, 2004. **4**(4): p. 671.

26. Ramanathan, K., et al., *Bioaffinity Sensing Using Biologically Functionalized Conducting-Polymer NW.* Journal of the American Chemical Society, 2004. **127**(2): p. 496.

27. Patolsky, F. and C.M. Lieber, *NW nanosensors.* Materials Today, 2005. **8**(4): p. 20.

28. Wanekaya, A.K., et al., *NW-Based Electrochemical Biosensors.* Electroanalysis, 2006. **18**(6): p. 533.

29. Kolmakov, A., et al., *Enhanced Gas Sensing by Individual SnO_2 NWs and Nanobelts Functionalized with Pd Catalyst Particles.* Nano Letters, 2005. **5**(4): p. 667.

30. Wang, Z.L., *FUNCTIONAL OXIDE NANOBELTS: Materials, Properties and Potential Applications in Nanosystems and Biotechnology.* Annual Review of Physical Chemistry, 2004. **55**(1): p. 159-196.

31. H. Kind, H.Y., B. Messer, M. Law, P. Yang, *Low-temperature orientation-selective growth and ultraviolet emission of single-crystal ZnO NWs*, Appl. Phys. Lett., 2004. **84**: p. 3358.

32. O. Harnack, C.P., H. Weller, A. Yasuda and J.M.Wessels, *Rectifying behavior of Electrically aligned ZnO nanorods*, NanoLetters, 2003. **3** (8): p. 1097-1101.

33. Wang, Z.L., *Self-assembled nanoarchitectures of polar nanobelts/NWs*, J. Mater. Chem., 2005. **15**: p. 1021.

34. Wang, Z.L., *ZnO nanostructures: growth, properties and applications*, J. Phys.: Condens. Mater., 2004. **16**: p. R829.

35. J.B.K. Law, J.T.L. Thong, *Improving the NH3 gas sensitivity of ZnO NW sensors by reducing the carrier concentration*, Nanotechnol., 2007. **18**: p. 055601.

36. S.H. Ko, I.P., H. Pan, N. Misra, M.S. Rogers, C.P. Grigoropoulos, A.P. Pisano, ZnO NW network transistor fabrication on a polymer substrate by low-temperature, all-inorganic nanoparticle solution process, Appl. Phys. Lett., 2008. **92**: p. 154102.

37. Wang, Z.L., *ZnO nanostructures: growth, properties and applications* , J. Phys.: Condens. Mater., 2004. **16**(R829): p. 1-18.

38. Wagner, R.S., *Whisker Technology*, ed. A.P. Levitt. 1970, New York: Wiley. 15.

39. C. Hulteen, J. and C.R. Martin, *A general template-based method for the preparation of nanomaterials.* Journal of Materials Chemistry, 1997. **7**(7): p. 1075.

40. Lee, S.T., N. Wang, and C.S. Lee, *Semiconductor NWs: synthesis, structure and properties.* Materials Science and Engineering A, 2000. **286**(1): p. 16.

41. M.H. Wong, A.b., X Qi, M.J. Kappers, Z.H. Barber, B. Illy, Z. Lockman, M.P. Ryan, and JL MacManus-Driscoll, IoP Nanotechnology, 2003. **14**: p. 968-973.

42. Wang, J. and L. Gao, *Hydrothermal synthesis and photoluminescence properties of ZnO NWs.* Solid State Communications, 2004. **132**(3-4): p. 269.

43. H.J. Fan, P. Werner., M. Zacharias, *Semiconductor NWs: From Self-Organization to Patterned Growth*, Small, 2006. **2**: p. 700.

44. k Bradley, J.C.P.-G., M. Briman, A. Star, G. Gruner, *Charge transfer from Ammonia physisorbed on nanotubes*, Phys. Rev. Lett., 2003. **91**: p. 218301.

45. A. Maroto, K.Balasubramanian, M. Burghard, K. Kern, *Functionalized metallic Carbon nanotube devices for pH sensing*, Chem. Phys. Chem., 2007. **8**: p. 220.

46. K. Balasubramanian, E.J.H. Lee, R.T. Weitz, M. Burghard, K. Kern, *Carbon nanotube transistors - chemical functionalization and device characterization*, Phys. Stat. Sol. A, 2008. **205**: p. 633.

47. F. Patolsky, G.Z., C.M. Lieber, *Fabrication of silicon NW devices for ultra-sensitive, label-free, real-time detection of biological and chemical species*, Nature Protocols, 2006. **1**: p. 1711.

48. Kim, D.R. and X. Zheng, *Numerical Characterization and Optimization of the Microfluidics for NW Biosensors.* Nano Letters, 2008. **8**(10): p. 3233.

49. Patolsky, F., G. Zheng, and C.M. Lieber, *Fabrication of silicon NW devices for ultrasensitive, label-free, real-time detection of biological and chemical species.* Nat. Protocols, 2006. **1**(4): p. 1711.

50. Gao, Z., et al., *Silicon NW Arrays for Label-Free Detection of DNA.* Analytical Chemistry, 2007. **79**(9): p. 3291.

51. Bergveld, P., *Development of an ion-sensitive solid-state device for neurophysiological measurements.* IEEE Trans. Biomed. Eng., 1970. **17**: p. 70.

52. Sandy Curtis C. Johnson, K.S.D.M., Jiri A. Janata, *Selective chemical sensitive FET transducers*, U.S. Patents, Editor. 1977.

53. Chen, Y., et al., *Silicon-based nanoelectronic field-effect pH sensor with local gate control.* Applied Physics Letters, 2006. **89**(22): p. 223512.

54. *Surface Modification of Oxide NWs by Nitrogen Plasma.* Electrochemical and Solid-State Letters. **14**(5): p. H218.

55. Park, W.I., et al., *Fabrication and electrical characteristics of high-performance ZnO nanorod field-effect transistors.* Applied Physics Letters, 2004. **85**(21): p. 5052.

56. Walton H. Marsh, B.F., and Henry Miller, *Automated and Manual Direct Methods for the Determination of Blood Urea.* Clinical Chemistry, 1965. **11**: p. 624-627.

57. Gentzkow, C.J. and M.M. With the assistance of John, *AN ACCURATE METHOD FOR THE DETERMINATION OF BLOOD UREA NITROGEN BY DIRECT NESSLERIZATION.* Journal of Biological Chemistry, 1942. **143**(2): p. 531-544.

58. Tanzer, M.L. and C. Gilvarg, *Creatine and Creatine Kinase Measurement.* Journal of Biological Chemistry, 1959. **234**(12): p. 3201-3204.

59. Hadis Morkoç, Ü.Ö., *Zinc Oxide: Fundamentals, Materials and Device Technology*. 2009: Wiley-VCH.

60. Huang, M.H., et al., *Catalytic Growth of Zinc Oxide NWs by Vapor Transport.* Advanced Materials, 2001. **13**(2): p. 113.

61. Wang, Z.L., *Nanostructures of zinc oxide.* Materials Today, 2004. **7**(6): p. 26.

62. Wang, Y.W., et al., *Catalytic growth of semiconducting zinc oxide NWs and their photoluminescence properties.* Journal of Crystal Growth, 2002. **234**(1): p. 171.

63. Dutta, A. and S. Basu, *Modified CVD growth and characterization of ZnO thin films.* Materials Chemistry and Physics, 1993. **34**(1): p. 41.

64. J. Wang and L. Gao, *Hydrothermal synthesis and photoluminescence properties of ZnO NWs*, Solid State Communications, 2004. **132**: p. 269-271.

65. H. Hu, X.H., C. Deng, X. Chen and Y. Qian, *Hydrothermal synthesis of ZnO NWs and nanobelts on a large scale*, Materials Chemistry and Physics, 2007. **106**: p. 58-62.

66. Lai, M. and D.J. Riley, *Templated Electrosynthesis of Zinc Oxide Nanorods.* Chemistry of Materials, 2006. **18**(9): p. 2233.

67. Choi, K.-S., et al., *Electrochemical Synthesis of Nanostructured ZnO Films Utilizing Self-Assembly of Surfactant Molecules at Solidâˆ'Liquid Interfaces.* Journal of the American Chemical Society, 2002. **124**(42): p. 12402.

68. B. Cao, W.C., G. Duan, Y. Li, Q. Zhao and D. Yu, *A template-free electrochemical deposition route to ZnO nanoneedle arrays and their optical and field emission properties*, IoP Nanotechnology, 2005. 16: p. 2567-2574.

69. A. chatterjee and J. Foord,*electrochemical deposition of nanocystalline zinc oxide at conductive diamond electrodes*, Diamond and related materials, 2006. **15**: p. 664-667.

70. B. Cao, X.Teng, S.H. Heo, Y. Li, S.O. Cho, G. Li and U Cai, *Different ZnO nanostructures fabricated by seed layer assisted electrochemical route and field emission properties,* J. Phys. Chem C, 2007. **111**: p. 2470-2476.

71. J. Yang, G. Liu, J. Lu, Y. Qiu and S. Yang, *electrochemical route to the synthesis of ultrathin Zno nanorod/nanobelt arays on zinc substrate*, Applied Physics Letters, 2007. **90**: p. 103-109.

72. M.A. Verges, A. Mifsud and C. J. Serna, *Formation of rod-like zinc oxide microcrystals in homogeneous solutions*, Journal of Chemical Society: Faraday Transactions, 1990. **86**(6): p. 859-963.

73. Wilkinson, A.D.M.a.A., *IUPAC. Compendium of Chemical Terminology (the "Gold Book") XML on-line corrected version*. 2 ed. 1997, Oxford: Blackwell Scientific Publications.

74. Baes, C.F.M., R.E., *The Hydrolysis of Cations*. 1976, New York: Wiley.

75. Wang, Z.L., J. Phys.: Condens. Matter, 2004. **16**: p. R829-858.

76. Jürn Schmelzer, J.W.P.S., *Nucleation Theory and Applications.* 2005.

77. Bahnemann, D.W., C. Kormann, and M.R. Hoffmann, *Preparation and characterization of quantum size zinc oxide: a detailed spectroscopic study.* The Journal of Physical Chemistry, 1987. **91**(14): p. 3789.

78. J. Turkevich, P.C.a.J.H., *A study of the nucleation and growth processes in the synthesis of colloidal gold.* Discuss. Faraday Soc., 1951. **11**: p. 55.

79. A. Sugunan, H.C.W., M. Boman and J. Dutta, Jour. of Sol-Gel Science Tech., 2006. **39**: p. 49-56.

80. Look, P.C., Material Science and Engineering B, 2001. **80**: p. 383-387.

81. Lee, C.J., et al., *Field emission from well-aligned zinc oxide NWs grown at low temperature.* Applied Physics Letters, 2002. **81**(19): p. 3648.

82. Geng, C., et al., *Well-Aligned ZnO NW Arrays Fabricated on Silicon Substrates.* Advanced Functional Materials, 2004. **14**(6): p. 589.

83. B. Liu and H. C. Zeng, *Room temperature solution synthesis of monodispersed single crystalline ZnO nanorods and derived hierarchical nanostructures*, Langmuir, 2004. **20**(10): p. 4196-4204.

84. M. Raula, M.H. Rashid, T.K. Paira, E. Dinda and T.K. Mandal, *Ascorbate assisted growth of hierarchical zno nanostructures: sphere, spindle, flower and their catalytic properties*, Langmuir, 2010. **26** (11).

85. Z. Zhang, S. Liu, S. Chow and M.Y. Han,*Modulation of the morphology of Zno nanostructures via aminolytic reaction: from nanorods to nanosquamas*, Langmuir, 2006. **22**(14): p. 6335-6340.

86. V. Pachauri, C. Subramaniam and T. Pradeep, Novel ZnO nanostructures over gold and silver nanoparticle assemblies, Chemical Physics Letters, 2006(1-3): p. 240-246.

87. Z. Wang, Q.F.Qian, J. Yin and Z.K. Zhu, *Large-Scale fabrication of tower-like, flower-like, and tube like ZnO arrays by a simple chemical solution route*, Langmuir, 2004. **20**(8): p. 3441-3448.

88. S. Cho, S.K., B.R. Lee and K.H. Lee, *Facile and fast synthesis of single-crystalline fractal zinc structures through a solution phase reaction and their conversation to zinc oxide*, Langmuir, 2009. **25**(17): p. 10223-10229.

89. D. Wang, F.Q., C. Yang, Z.H. Zhang and C.M. Leiber, *Rational growth of branched and hyperbranched NW structures*, NanoLetters, 2004. **4**: p. 871-874.

90. A. Narayanswamy, H.F.X., N. Pradhan and X.G. Peng, *Crystalline nanoflowers with different chemical compositions and physical properties grown by limited ligand protection*, Angwandte Chemie Int. Edi., 2006. **118**: p. 5487-5490.

91. A. Umar, M.M. Rahman, A. al-Hajry and Y.B. Han, *Highly sensitive cholesterol biosensor based on well-crystallized flower-shaped ZnO nanostructures*, Talanta, 2009. **78**: p. 284-289.

92. Y. Chen, C.L. Zhu, G. Xiao, *Reduced-temperature ethanol sensing characteristics of flower-like ZnO nanorods synthesized by a sonochemical method*, IoP Nanotechnology, 2006. **17**: p. 4537-4541.

93. Q. Wu, X.C., P. Zhang, Y. Han, X. Chen, Y. Yan and S. Li, *Amnio acid-assisted synthesis of ZnO hierarchical architechtures and their novel photocatalytic activities*, Crystal Growth and Design, 2008. **8**(8): p. 3010-3018.

94. Y. Wu, H. Yan and P. Yang, *Semiconductor NW array: potential substrates for photocatalysis and photovoltaics*, Topics in Catalysis, 2002. **19**: p. 197-202.

95. M. Knez, A.M. Bittner, F. Boes, C. Wege, E. Maiss and K. Kern, *Biotemplate synthesis of 3-nm and cobalt NWs*, Nanoletters, 2003. **3**: p. 1079-1082.

96. S. Sotiropoulou, Y.S.-S., S.S. Mark and C.A. Batt, *Biotemplated nanostructures materials*, Chem. Mater., 2008. **20**: p. 821-834.

97. J.Y. Lao, J.G. Wen and Z.F. Ren, *Hierarchical ZnO nanostructures*, Nanoletters, 2002. **2**: p. 1287-1291.

98. L. Xu, Q. Chen, D. Xu, *Hierarchical ZnO nanostructures obtained by electrodeposition*, Journal of Physical Chemistry C, 2007. **111**: p. 11560-11565.

99. V. Pachauri, A.Vlandas, K. Kern and K. Balasubramanian, *Site-specific self-assembled liquid-gated Zno NW transistor for sensing applications*, Small, 2010. **6**(4): p. 589-594.

100. L. Xu, Q. Chen, D. Xu, *Hierarchical ZnO nanostructures obtained by electrodeposition*, Journal of Physical Chemistry C, 2007. **111**: p. 11560-11565.

101. W.J. Li, E.-W.Shi, W-Z. Zhong, Z-W. Yin, *Growth mechanism and growth habit oxide crystals*, Journal of Crystal Growth, 1999. **203**: p. 186-196.

102. Z. L. Wang, Journal of Physics: Condensed Matter, 2006. **6**: p. R829.

103. H.A. Ali, A.A. Iliadis, U. Lee, *study of ZnO nanocluster formation within styrene-acrylic acid and styrene-methacrylic acid diblock copolymers on Si and* SiO_2 *surfaces*, Solid State Electronics, 2004. **48**: p. 2025-2030.

104. G. Zhang, X.L., W.Wang and X. Li, *Facile synthesis of a hierarchical PbTe flower-like nanostructure and its shape evolution process guided by a kinetically controlled regime,* Chemistry of Materials, 2007 **19**: p. 5207-5209.

105. X. Gao, X.Li, W. Yu, *Flower-like Zno nanostructures via hexamethylenetetramine assisted thermolysis of zinc-ethylenediamine complex*, Journal of Physical Chemistry B, 2005. **109**: p. 1155-1161.

106. Y. Li, B.Tan, Y. Wu, *Ammonia evaporation induced synthetic method for metal (cu, Zn, Cd, Ni) hydroxide/oxide nanostructures*, Chem Matter, 2008. **20**: p. 567-576.

107. F. Lu, W.C., Y. Zhang, *ZnO hierarchical micro/nanoarchitectures: Solvothermal synthesis and structurally enhanced photocatalytic performance*, Advanced Functional Materials, 2008. **18**: p. 1047-1056.

108. U.K. Gautam, M.I., C.S. Rout, Y. Bando, X. Fang, B. Dierre, L. Sakharov, A. Govindraj, T. Sekiguchi, D. Goldberg and CNR Rao, *Unipolar assembly of zinc oxide rods manifesting polarity-driven collective luminescence* , PNAS, 2010: p. 13588-13592.

109. D-F. Zhang, L.-D.S., J-L. Yin, C-H. Yan, *Low-temperature fabrication of highly crystalline* SnO_2 *nanorods*, Advanced Materials, 2003. **15**(12): p. 1022-1025.

110. X. Han, G.Wang, L. Zhou, J.G. Hou, *Crystal orientation-ordered ZnO nanorod bundles on hexagonal heads of ZnO microcones: epitaxial growth and self-attraction*, Chem Comm., 2006: p. 212-214.

111. S. Manjunatha, L.S. Panchakarla, K. Biswas and C.N.R. Rao, *Nanorods and nanofilms of ZnO generated at the liquid-liquid interface*, Inorganica Chimica Acta, 2010. **363**: p. 2125-2130.

112. M. C. McAlpine, H. ahmad, D. Wang and J.R. Heath, *Highly ordered NW arrays on plastic substrates for ultrasensitive flexible chemical sensors.* Nat Mater, 2007. **6**(5): p. 379.

113. J.J. Mastrototaro, *Appratus and method for implantation of sensors,* 1994 US Patent.

114. K-W Lee, S.P.Kowalczyk and.J.M. Shaw, *surface modification of PMDA-oxydianiline polyimide. Surface structure-adhesion relationship*, Macromolecules, 1990. **23**: p. 2097.

115. Craighead, H., *Future lab-on-a-chip technologies for interrogating individual molecules.* Nature, 2006. **442**(7101): p. 387.

116. Haeberle, S. and R. Zengerle, *Microfluidic platforms for lab-on-a-chip applications.* Lab on a Chip, 2007. **7**(9): p. 1094.

117. Terry, S.C., J.H. Jerman, and J.B. Angell, *A gas chromatographic air analyzer fabricated on a silicon wafer.* Electron Devices, IEEE Transactions on, 1979. **26**(12): p. 1880.

118. Shoji, S., M. Esashi, and T. Matsuo, *Prototype miniature blood gas analyser fabricated on a silicon wafer.* Sensors and Actuators, 1988. **14**(2): p. 101.

119. Manz, A., et al., *Design of an open-tubular column liquid chromatograph using silicon chip technology.* Sensors and Actuators B: Chemical, 1990. **1**(1-6): p. 249.

120. *Fabrication of a normally-closed microvalve utilizing lithographically defined silicone micro O-rings.* Journal of Micromechanics and Microengineering. **21**(2): p. 025011.

121. *Development of multistage distillation in a microfluidic chip.* Lab on a Chip. **11**(7): p. 1311.

122. Woias, P., *Micropumps--past, progress and future prospects.* Sensors and Actuators B: Chemical, 2005. **105**(1): p. 28.

123. An, M.P. and et al., *In-situ fabrication of polymer microsieves for Î¼TAS by slanted angle holography.* Microfluidics and Nanofluidics.

124. *Roll-to-roll fabricated lab-on-a-chip devices.* Journal of Micromechanics and Microengineering. **21**(3): p. 035006.

125. H.A. Pohl, *The motion and precipitation of suspensoids in divergent electric fields*, Journal of Applied Physics, 1951. **22** (7): p. 869-871.

126. Pohl, H.A., *Dielectrophoresis: The behavior of neutral matter in nonuniform electric fields*. 1978: Cambridge University Press.

127. H. Morgan and N.G. Green, *Dielectrophoretic separation of NPs*, J. Phys. D: Applied Physics, 1997. **30**: p. L41-L84.

128. Pethig, R., *Automation in Biology ed 1*. 1991, Karube Amsterdam: Elsevier. 159-185.

129. F.F. Becker, X.B.W., Y. Huang, R. Pethig, J. Vykoukal, and P.R.C. Gascoyne, *Separation of human breast cancer cell from blood by differential dielectric affinity*, Proc. Natl. Acad. Sci. USA 92, 1995: p. 860-864.

130. M. Stephens, M.S.T., R. Pethig, A.K. Burnett and K.I. Mills, Bone Marrow Transplantations, 1996. **18**: p. 777-782.

131. J.P.H. Burt, R.P., A. Parton and D Dawson. in *Inst. Phys. Conf.* 1995.

132. K. Yamamoto, S.A.a.Y.N., *Orientation and purification of carbon nanotubes using AC electrophoresis*, Journal of Physics D: Applied Physics, 1998. **31**: p. L34-L36.

133. P.A. Smith, C.D. Nordquist, T.N. Jackson, B.R. Martin, J. Mbindyo, T.S. Mayer and T.E. Mallouk, *Electric field assisted assembly and alignment of metallic NWs*, Applied Physics Letters, 2000. **77**(9): p. 1399-1401.

134. L. Dong, J. Bush, V. Chirayos, R. Solanki and J. Jiao, *dielectrophoretically controlled fabrication of single crystal nickel-silicide NW interconnects*, Nanoletters, 2005. **5**(10): p. 2112-2115.

135. L. Dong, V. Chirayos, J. Bush, J. Jiao, V.M. Dublin, R.V. Chebian, Y. Ono, J.F. Conley Jr and B.D. Ulrich, *Floating potential dielectrophoresis controlled fabrication of single CNT transistors and their electrical properties*, J. of Physical Chemistry B, 2005. **109**: p. 13148-13153.

136. R. Kretschmer and W. Fritzsche, *Pearl chain formation of NPs in microelectrode gaps by dielectrophoresis*, Langmuir, 2004. **20** (26): p. 11797-11801.

137. G. Yang, J. Tang, S. Kato, Q. Zhang, L.C. Qin, M. Woodson, J. Liu, J.W. Kim, P.T. Littlehei, C. Park and O. Zhou, *Magnetic NW ased high resolution magnetic force microscope probes*, Applied Physics Letters, 2005. **87**: p. 123507.

138. S. Evoy, N. DiLello, V. Deshpande, A. Narayanan, H. Liu, M. Riegelman, B.R. Martin, B. Hailer, J-C. Bradley, W. Weiss, T.S. Mayer, Y. Gogotsi, H.H. Bau, T.E. Mallouk and S. Raman, *Dielectrophoretic assembly and integration of NW devices with functional CMOS operating circuitry*, Microelectronic Engineering, 2004. **75**(1): p. 31-42.

139. R. Krupke, F. Hennrich, M.M. Kappes and H. v. Loehneysen, *Surface conductance induces dielectrophoresis of semiconducting SW-CNTs*, NanoLetters, 2004. **4** (8): p. 1395-1399.

140. M.S. Arnold, P. Avouris, Z.W. Pan and Z.L. Wang, *Field-effect transistors based on single semiconducting oxide nanobelt*, Journal of Phys. Chem B, 2003. **107** (3): p. 659-663.

141. T.N. Jackson, *Electric Field Assisted Assembly process*, U.S. Patent, Editor. 2003.

142. X. Wang, J.Song and Z.L. Wang, *NW and nanobelt arrays of zinc oxide from synthesis to properties and to novel devices*, Journal of Materials Chemistry, 2007. **17**: p. 711-720.

143. M. A. Zimmler, D. Stichtenoth, C. Ronning, W. Yi, V. Narayanamurti, T. Voss and F. Capasso, NanoLetters, *Scalabole fabrication of NW photonic and electronic circuits using spin-on glass*, 2008. **8**(6): p. 1695-1699.

144. A. Vijayraghavan, S. Blatt, D. Weissenberger, M. Oron-Carl, F. Hennrich, D. Gerthsen, H. Hahn and R. Krupke, *Ultra-large scale directed assembly of single walled carbon nanotube devices*, NanoLetters. 2007, **7**(6): p. 1556-1560.

145. Vanheusden, K., et al., *Mechanisms behind green photoluminescence in ZnO phosphor powders.* Journal of Applied Physics, 1996. **79**(10): p. 7983.

146. van Dijken, A., et al., *Identification of the transition responsible for the visible emission in ZnO using quantum size effects.* Journal of Luminescence, 2000. **90**(3-4): p. 123.

147. Bergveld, P., *Thirty years of ISFETOLOGY - What happend in the past 30 years and what may happen in the next thirty years.* Sens. Actuators, B, 2003. **88**: p. 1.

148. Matsuo, T. and M. Esashi, *Methods of isfet fabrication.* Sensors and Actuators, 1981. **1**: p. 77.

149. Middelhoek, S., *Celebration of the tenth transducers conference: The past, present, and future of transducer research and development.* Sens. Actuators, A, 2000. **82**: p. 2.

150. S.J. Tans, A.R.M. Verschueren and C. Dekker, *Room-temperature transistor based on single CNT*, Nature, 1998. **393**: p. 49.

151. Kong, J.F., N.; Zhou, C.; Chapline, M.; Peng, S.; Cho, K.; Dai, H., *Nanotube molecular wires as chemical sensors*, Science, 2000. **287**: p. 622.

152. Collins, P.G., Bradley, K., Ishigami, M.; Zettl, A., *Extreme oxygensensitivity of electronic properties of CNTs* , Science, 2000. **287**: p. 1801.

153. Krueger, M.B., M. R.; Nussbaumer, T.; Schonenberger, C., *Electrochemical CNT FET*, Appl. Phys. Lett., 2001. **78**: p. 1291.

154. Duan, X.H., Y.; Cui, Y.; Wang, J.; Lieber, C., *Indium phosphide NWs as building blocks for nanoscale electronic and optoelectronic devices*, Nature, 2001. **409**: p. 66.

155. Y. Cui and C. Lieber,*Functional nanoscale electronic devices assembled using silicon NW building blocks*, Science, 2001. **291**: p. 851.

156. Stern, E.; K., J.F. Klemic; Routenberg, D. A.; Wyrembak, P. N.; Turner-Evans, D. B.; Hamilton, A. D.; LaVan, D. A.; Fahmy, T. M.; Reed, M. A., *Label-free immunodetection with CMOS compatible semiconducting NWs*, Nature, 2007. **445**: p. 519.

157. J. Torkel Wallmark, H.J., *Field-effect transistors: physics, technology and applications*. 1966: Prentice-Hall.

158. Deshpande, N.P., *Electronic devices and circuits: principles and applications*. 2008: Tata McGraw-Hill Education.

159. Shimotani, H., et al., *Gate capacitance in electrochemical transistor of single-walled carbon nanotube.* Applied Physics Letters, 2006. **88**(7): p. 073104.

160. Ni, H. and R.C. Amme, *Ion redistribution in an electric double layer.* Journal of Colloid and Interface Science, 2003. **260**(2): p. 344.

161. Gouy, G., Comt. Rend., 1909. **149**: p. 654.

162. Chapman, D.L., Phil.Mag., 1913. **6**(25): p. 475.

163. S. Rosenblatt, Y.Y., J. Park, J. Gore, V. Sazonova and P.L. McEuen, NanoLetters, 2002. **2**(8): p. 869.

164. Rosenblatt, S., et al., *High Performance Electrolyte Gated Carbon Nanotube Transistors.* Nano Letters, 2002. **2**(8): p. 869.

165. Arvind halliyal, M.T.R., kuo-Tug Chang, Nicholas H. Tripsas and Robert B. Ogle, *Use of high-k dielectric materials in modified ONA structure for semiconductor devices*. 2004.

166. Gritsenko, V.A., et al., *A new low voltage fast SONOS memory with high-k dielectric.* Solid-State Electronics, 2003. **47**(10): p. 1651.

167. Javey, A., et al., *High-[kappa] dielectrics for advanced carbon-nanotube transistors and logic gates.* Nat Mater, 2002. **1**(4): p. 241.

168. Ye, P.D., et al., *GaAs metal--oxide--semiconductor field-effect transistor with nanometer-thin dielectric grown by atomic layer deposition.* Applied Physics Letters, 2003. **83**(1): p. 180.

169. Wind, S.J., et al., *Vertical scaling of carbon nanotube field-effect transistors using top gate electrodes.* Applied Physics Letters, 2002. **80**(20): p. 3817.

170. Blackburn, G.F., *Biosensors: Fundamentals and Applications*, ed. I.K. A. P. F. Turner, G. S. Wilson. 1987, Oxford: Oxford Univ. Press. 481Ð530.

171. S.J. Wind, J. Appenzeller, R. Martel, V. Derycke and P. Avouris, Vertical scaling of CNT FETs using top gate electrodes, Appl. Phys. Lett., 2002. **80**: p. 3817.

172. A. Javey, H.K., M. Brink, Q. Wang, A. Ural, J. Gu, P. McIntyre, P.L. McEuen, M. Lundstrom and H. Dai, *High-k dielectrics for advanced CNT transistors and logic gates*, Nature Materials, 2002. **1**: p. 241.

173. J.H. Back and M. Shim, *pH dependent electron transport properties of CNTs*, J. Phys. Chem. B, 2006. **110**: p. 23736.

174. M. Krüger, M.R. B., T. Nussbaumer, C. Schönenberger and L. Forro, *Electrochemical CNT FET*, Applied Physics Letters, 2001. **78**(9): p. 1291.

175. Rosenblatt, Y.Y., J. Park, J. Gore, V. Sazonova and P.L. McEuen, NanoLetters, 2002. **2**(8): p. 869.

176. S. Ju, K.L., M.H. Yoon, A. Facchetti, T.J. Marks, D.B. Janes, *Fabrication of fully transparent NW transistors for transparent and flexible electronics*, Nature Nanotechnol., 2007. **18**: p. 155201.

177. S.N. Cha, J.E.J., Y. Choi, G.A.J. Amaratunga, G.W. Ho, M.E. Welland, D.G. Hasko, D.J. Kang, J.M. Kim, *High performance ZnO NW FET using self-aligned nanogap gate electrodes*, Appl. Phys. Lett., 2006. **89**: p. 263102.

178. W. Park, J.S. Kim, G.C. Yi, M.H. Bae, H.J. Lee, *Fabrication and electrical characteristics of high-performance ZnO nanorod FETs*, Appl. Phys. Lett., 2004. **85**: p. 5052.

179. S. Rosenblatt, Y.Y., J. Park, J. Gore, V. Sazonova, P.L. McEuen, NanoLetters, 2002. **2**: p. 869.

180. J.H. Back, M. Shim, J. Phys. Chem. B, 2006. **110**: p. 23736.

181. W. Park, J.S. K, G.C. Yi, M.H. Bae, H.J. Lee, Appl. Phys. Lett., 2004. **85**: p. 5052.

182. Tietz, N.W., *Clenical guide to laboratory tests.* 1983.

183. Baird, F.J.S. and M. A., Clenic. Chem., 1979. **25**: p. 1721.

184. Tetiana Kurkina, A. Vlandas, A. Ahmad, K. Kern and K. Balasubramanian, *Label free detection of a few copies of DNA using CNT impedance biosensors.* Angwandte Chemie, 2011.

185. K. Balasubramanian and M. Burghard, *Biosensors based on carbon nanotubes.* Anal. Bioanal. Chem., 2006. **385**: p. 452-468.

186. Wanekaya, A.K., Chen, W., Myung, N.V., Mulchandani, A., *NW based electrochemical biosensors.* Electroanalysis, 2006. **18**: p. 533-550.

187. Roy, S., Gao, Z. Nanostructure-based electrical biosensors, Nano Today, 2009. **4**: p. 318-324.

188. Balasubramanian, K., *Challenges in the use of 1D nanostructures for on-chip biosensing and diagnostics: A Review.* Biosens. Bioelectron., 2011.

189. He, B., Morrow, T.J., Keating, C.D., *NW sensors for multiplexed detection of biomolecules.* Curr. Opin. Chem. Biol., 2008. **12**: p. 522-528.

190. Yu, E.H. and K. Sundmacher, *Enzyme Electrodes for Glucose Oxidation Prepared by Electropolymerization of Pyrrole.* Process Safety and Environmental Protection, 2007. **85**(5): p. 489.

191. Vlandas, A., Kurkina, T., Ahmad, A., Kern, K. & Balasubramanian, K., *Enzyme-free sugar sensing in microfluidic channels with an affinity-based single-wall carbon nanotube sensor.* Anal. Chem., 2010. **82**: p. 6090-6097.

192. Roer, T.G.v.s., *Microwave electronic devices*. 1994: Springer.

193. Baechtold, W., et al., *Si and GaAs 0.5 mu m-gate Schottky-barrier field-effect transistors.* Electronics Letters, 1973. **9**(10): p. 232.

194. Baca, A.G., *Fabrication of GaAs Devices*. 2005: IET. 350.

195. Dingle, R., et al., *Electronic properties of the GaAs---AlGaAs interface with applications to multi-interface heterojunction superlattices.* Surface Science, 1980. **98**(1-3): p. 90.

196. Shockley, W. *A Unipolar "Field-Effect" Transistor*. in *Proceedings of the IRE*. 1952.

197. Sun, Y., et al., *Bendable GaAs metal-semiconductor field-effect transistors formed with printed GaAs wire arrays on plastic substrates.* Applied Physics Letters, 2005. **87**(8): p. 083501.

198. Oh, J., et al., *Carbon Nanotube-Based Dual-Mode Biosensor for Electrical and Surface Plasmon Resonance Measurements.* Nano Letters. **10**(8): p. 2755.

199. Ma, R.M., L. Dai, and G.G. Qin, *Enhancement-mode metal-semiconductor field-effect transistors based on single n-CdS NWs.* Applied Physics Letters, 2007. **90**(9): p. 093109.

200. Ma, R.-M., L. Dai, and G.-G. Qin, *High-Performance Nano-Schottky Diodes and Nano-MESFETs Made on Single CdS Nanobelts.* Nano Letters, 2007. **7**(4): p. 868.

201. R. M. Ma, L.D., G. G. Qin, *Enhancement-mode metal-semiconductor field-effect transistors based on single n-CdS NWs.* Applied Physics Letters, 2007. **90**(9): p. 093109.

202. Schlecht, U., et al., *Electrochemically decorated carbon nanotubes for hydrogen sensing.* Applied Surface Science, 2007. **253**(20): p. 8394.

Publications

1. Vivek Pachauri, Alexis Vlandas, Klaus Kern and Kannan Balasubramanian, Site-specific self-assembled liquid-gated ZnO NW transistors for sensing applications, Small 2010, 6, No. 4, 589-594

2. Vivek Pachauri, Klaus Kern and Kannan Balasubramanian, Template-free self-assembly of hierarchical ZnO structures from nanoscale building blocks Chemical Physics Letters 2010, 498, 317-322

Curriculum Vitae

Name:	Vivek Pachauri
Date of Birth:	December 26, 1986
Nationality:	Republic of India
2000-2003:	“Bachalor of Science” in Biology, at Dr. B.R. Ambedkar University Agra, India
2003-2005:	“Master of Science” in Chemistry at Dr. B.R. Ambedkar University Agra, India
2005-2006:	Project Student at Unit on Nanoscience and Technology, Indian Institute of Technology Madras, Chennai India. and Guest lecturer of Chemistry at Dr. B.R. Ambedkar University Agra, India.
2006-2007:	Junior Research Fellow at Department of Chemistry, Indian Institute of Technology Delhi, New Delhi, India.
2007-2011:	Ph.D. Student in the group of Prof. Klaus Kern at Max Planck Institute for Solid State Research Stuttgart, Germany PhD Thesis titled “Self-assembled liquid-gated ZnO NW transistors: Fabrication and sensing operation”

Acknowledgements

I am very grateful to *Prof. Klaus Kern* for giving me the opportunity to work on my Ph.D. at the Max-Planck Institute for Solid State Research Stuttgart, one of the prestigious research institutions in the world and for guiding me through the course of this thesis.

I am indebted to *Dr. Kannan Balasubramanian* for streamlining my thoughts to work in the right direction, for instilling in me dedication towards every aspect of work however small it might be and for having supported me both technically and personally. I sincerely acknowledge him for guiding me in aspects of performing electrical transport measurements, and for an informal and friendly atmosphere in the lab.

I am thankful to *Dr. Alexis Vlandas* for the successful cooperation in the group in matters concerning TEM measurements and microfluidics integration. He always has been a support and helping hand. I would like to thank *Dr. Ashraf Ahmad* for his always hard-hitting and encouraging discussions. I am also grateful to *Dr. Marko Burghard* and *Dr. Alexander Bittner* for helping me with many facilities in the Labs.

I would like to thank *Tanya Kurkina* for bearing it with me in the Lab and otherwise. She has been a constant support second to none.

I acknowledge the help of *Janis Gregoridis* with SEM, *Marion Kelsch* with TEM, *Stephan Schimidt* and *Yvonne Link* with lithography, *Martin Siemers* and *Rafael Chaikevitch* with mechanical setups and electrical instrumentation.

I am indebted to acknowledge the company of my close friends inside the group *Ravi Shankar Sundaram, Adarsh Sagar, Dr. Liza Herrera Diaz, Dr. Eduardo J.H. Lee, Dr. Tilman Assmus, Dr. Alicia Forment, Dr. Christina Gomez-Navarro, Dr. Ivan Brihuega, Dr. Magal´ı Lingenfelder, Dr. Paola Acosta, Dr. Violetta Sessi, Dr. Santosh Padmanaphan, Dr. Sangita Bose, Dr. UdaiRai Singh, Dr. Hadj Mohammed, Nassim Rafeierd, Subramanian Sundaram, Divya Balakrishnan, Dr. Isabella Gierz, Dr. Theressa Lutz, Eberhard Ulrich Stuetzl, Dr. Robin Ohman, Dr. Jens Boettcher, Dr. Jens Doerfmueller, Dr. Jakob Bork, Thomas Dufaux, Eva Carmen Peters, Frederik Ante, Daniel Kaelblein* . .

. . . and my close friends outside the group *Dr. Jaysen Nelayah, Hilton Borbosa de Aguiar, Burac, Burcu, Manish Sultania, Sridhar Neelimaraju,* for bringing in life during my Ph.D. thesis.
I thank my home-zone friends Vishal Gehrana, Vipul Gupta, Rajeev Yadav, Jaikumar and others to keep my spirits high and having supported me always.

And last but the most important, I am grateful to my beloved family- sister, cousins, uncles, my parents and grandparents for being always with me and for taking care of me, no matter what their physical condition and coordinates are.